Doctor of Hungarian Academy of Sciences Thesis

Innovative steel and composite structures

László Dunai

Candidate of Technical Science, PhD

Budapest, 2007

Table of contents

Acknowledgements

Acknowledgements

1. Introduction

1.1 General

In the doctoral thesis I summarize my activities and collect my new results on the research and development of innovative steel and composite (i.e. steel-concrete) structures. This work has been completed in the last ten years and it is still under progress.

The objectives of these activities are always related to the development and/or design of new types of structures or structural details. The innovative nature of the problems required complex research methodologies with experimental and theoretical studies, with a definite purpose of practical application of results.

In this chapter I give an outline about the structural problems and the applied strategy in the research and development work. First, I describe the studied structural fields with a focus on the "innovative" characters in them. Then, I introduce the basic research principle what I worked out and commonly applied for the solution of different structural problems. I consider as a major result of my activities that I could create – by systematic and continuous education – an efficient research team of young students and colleagues, who have been completed their works under my guidance. In the next part of the chapter I introduce the team and give the interpretation of the "new scientific results" of the team members and myself. Finally I summarize the project and co-operation background of the presented work.

1.2 Structural problems

1.2.1 Definition of innovative structure

The innovation in general means "to renew; to introduce new method, custom, device, etc". For steel and composite structures the innovation can be interpreted at different fields:

- material production,
- fabrication technology,
- structural arrangement and design,
- erection technology.

These innovative activities are in close interaction with each other. Typically: the improved material properties can result in fabrication of new profiles what can renew traditional structural systems, leading to modified erection methods, and the whole process requires an improved design methodology.

In this thesis the innovation is interpreted in the "structural arrangement and design" level for the following structural problems:

- cold-formed steel and composite structures,
- steel and composite joints of buildings,
- non-conventional large scale steel structures.

The global aim on each field is to create new structural arrangements for a definite function with improved and well-controlled structural performance. The **"innovative structure"** in this way has a meaning of a **"new type of structure + behaviour + analysis and design"**. The particular characteristics of the different types of structures are summarized in the following subsections.

1.2.2 Cold-formed steel and composite structures

Due to the development in galvanized high strength sheet production and cold-rolling technology the geometrical shape and size of cold-formed profiles significantly extended in the last one and a half decade. The qualitative and quantitative changes of the profiles provide with the opportunity to use them in new structural functions. On the other hand, both the theoretical and standard background to follow the more complex structural behaviour of the cold-formed profiles in the new arrangements is limited or missing.

Major research and development activities have been completed on cold-formed steel and composite structures under my supervision since 1996. The work has been done under the supports of interacting fundamental [P1], applied R&D [P2] and industrial [P3] projects on the cold-formed frames, light-gauge composite beams and Z-purlin and cladding system, as detailed in the followings:

Cold-formed framed structure

Function: primary load bearing structure of industrial buildings (span: 3-13 m) or residential houses (1- or 2-storey).

Arrangement:
- Structural elements: single and double – box-type – cold-formed C-profiles, laterally non, or partially supported.
- Structural joints: self-drilling screwed or bolted connections of beams and columns in web-to-web arrangement.

Behaviour to be studied:
- Interacting stability phenomena of structural elements (local-distortional-global).
- Interaction of connector and element end behaviour.

Light-gauge composite beam

Function: floor beam of residential houses (span: 3-8m) compatible with different constructional modes.

Arrangement:
- Structural elements: cold-formed C-profile – trapezoidal sheeting – concrete slab.
- Composite action: partially drilled self-drilling screw shear connector.

Behaviour to be studied:
- Behaviour modes of individual shear connectors.
- Interaction of connector – cold-formed beam – concrete behaviour.

Cold-formed Z-purlin and cladding

Function: cladding of industrial type buildings.

Arrangement:
- Structural connection between cold-formed Z-profile and sheeting: partial restraints and sliding clip between the components – floating roof arrangement.

Behaviour to be studied:
- Local interaction of Z-purlin and sheeting – lateral and rotational supports.
- Global behaviour of cladding system.

1.2.3 Steel and composite joints of buildings

Significant research has been done on the moment resisting joints of steel and composite building skeletons in the last two decades. The wide range of international studies on different types of joints resulted in a new design and detailing methodology, the so called semi-rigid joint concept. This design principle – and the developed application rules – are implemented in the major design standards in the last decade (Eurocode and the US codes) and can be utilized in the practice.

On the field of seismic design the two recent major earthquakes in the USA and Japan (Northridge 1994 and Kobe 1995) proved that the joints basically determine the seismic behaviour of the moment resisting frames. It is observed that the typically used bolted and welded joints with traditional detailing – designed mainly for strength – exhibited very different cyclic performance, resulting in less ductility and damages in the joint regions. It is concluded that all the cyclic characteristics of the joints – resistance and stiffness degradation, ductility and energy absorption – should be considered and studied together in order to judge the seismic performance and to develop efficient detailing.

In the frame of a fundamental [P4] and two international joint projects with Technical University of Lisbon: [P5] and [P6], we have been completed research works to determine joint details with improved cyclic behaviour, under my supervision (fundamental project) and co-supervision (joint projects) since 1996, on the following structural fields:

Bolted end-plate joints of steel and composite structural elements

Function: seismic resistant beam-to-column and column base joints of steel and composite moment resisting frames.
Arrangement:
- Hot-rolled and welded H-profile steel and steel-concrete composite members.
- High strength bolted end-plate connection.

Behaviour to be studied:
- Cyclic behaviour modes of joints and joint components.
- Interaction phenomena in the cyclic behaviour of connection and element end.
- Local plate buckling phenomenon of slender composite section under load reversal.

1.2.4 Non-conventional large scale steel structures

In the last five years I have been involved in the design and research background development of two large scale steel structures applied for rather classical functions, as cooling tower and bridge. The structures are non-conventional in the sense of the application of new structural arrangements for the large geometrical sizes. The resulted complex structural behaviour cannot be handled directly by the traditional design tools. This is why for the checking of the load-bearing capacities experiment based research was required to support the realization of these structures.

Despite the very different structural function of the investigated structures and the direct practical application purpose of the research, this is on the common platform both in strategy and result with the previous studies which are detailed in sub-sections 1.2.2 and 1.2.3.

Steel cooling tower system – joint of tubular members

A new steel cooling tower system is developed in Hungary by a consortium of industrial and university partners. The R&D activities covered the functional, aesthetic and structural design as well. The structural development had a focus on the new space structure built-up from tubular elements. The three-dimensional (3D) joint of tubular members in the space structure is studied under my supervision. The junction of the tubular members has been solved by a complicated 3D gusset plate and welded, bolted and pinned connections. The arrangement resulted in interacting phenomena in the different connection and element end behaviour. The research work is supported by an applied R&D project [P7].

Dunaújváros Danube bridge – stability of tied arch with box section

The large geometrical sizes of the Dunaújváros Danube bridge – largest span in the world in the tied arch category – and the erection procedure required the validation and extension of the standardized global and local stability design methods. The structural arrangement of the bridge is a basket handle type arch with cable hangers. Its governing global behaviour modes are the in-plane and out-of-plane arch buckling in interaction with the biaxial bending. During the erection of the bridge the local plate buckling of the arches' and the stiffening beams' stiffened panels governs the stability behaviour. In the frame of an industrial project [P8], I supervised a team to create the research background of the design checking of these phenomena.

1.3 Research strategy

The investigation of the wide range and complicated structural behaviour modes requires a complex strategy. The studies should start at the level of physical phenomena and should be finished by the practically applicable design information. Due to these requirements interacting experimental and numerical research tools had to be used. Note that the development of a design philosophy with this aim is supported by a fundamental project [P9].

1.3.1 Experimental studies

I proposed a general research methodology in which experimental studies had a fundamental role and the test data are directly or indirectly transferred to the design of the structures. In Fig. 1.1 these major aspects of the research strategy are illustrated by the starting and ending "columns" of the flowchart. The derivation of design information from the experimental data can be done in different way. I classified the experimental studies according to the purpose what it is applied for, as shown in Fig. 1.1 and detailed in the followings.
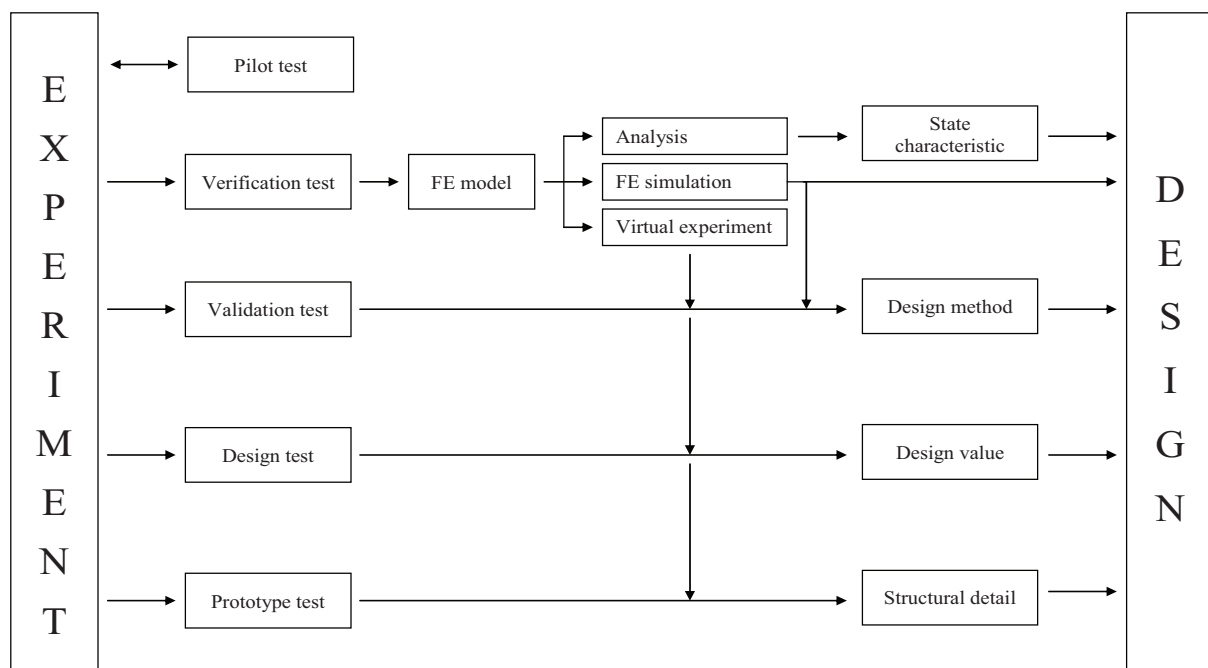
Fig. 1.1: Illustration of the applied R&D strategy – from experiment to design.

Pilot test: this is a preliminary experimental investigation in order to study the fundamental parameters of test specimens and/or arrangement and measurement; by the obtained experiences a detailed testing program can be established.

Verification test: this type of test is used to verify advanced models – in the current research advanced finite element (FE) models – which can be used in the design process in a direct or indirect way, as it is detailed later on.

Validation test: the purpose of this type of test is to prove the applicability of certain design method – in general the traditional application rules of design standards – for a given problem; the result of it is an experimentally validated design procedure for the checking of a targeted phenomenon.

Design test: this type of test is completed usually according to standard recommendations for "design assisted by testing"; from the test results the design values of resistances and rigidities can be derived and directly used in the design checking.

<u>Prototype test:</u> this type of test concentrates on the judgement of a given structural detail on the basis of the observed experimental behaviour; by the results of these tests the structural arrangement of the prototype can be evaluated qualitatively and quantitatively and the favourable behaviour of the improved detail can be proved by repeated test. The prototype test result is an experimentally verified structural detail.

The completed experimental studies on the different structural problems will be characterized by the above categories in the following chapters. Typically the experiments are completed for several functions; it means that the above test categories are overlapping and interacting. For example a prototype test can be used for design resistance determination and/or for FE model verification, as well. It is also typical that the same tests are used for the verification of the numerical model of the analysis and the resistance calculation model.

1.3.2 Numerical studies

In the research methodology the advanced numerical studies are used in an interaction with the experimental tests. In my interpretation the "advanced numerical model" is a finite element model with surface – shell – geometry (note that in some cases finite strip model is also used). The complexity of the geometrical model is very much dependent on the investigated problem, as it will be detailed in the further chapters. In the models the material and/or geometrical nonlinearities are considered according to the requirement of the targeted phenomena and the purpose of the model application. The experimental verification tests are planned such a way that the FE model can be checked in the elastic and/or ultimate range of behaviour (details of test setup and measuring system).

By the verified FE models the design can be supported different way, as shown in Fig. 1.1 and detailed in the followings.

<u>Analysis:</u> applying actions (loads) on the FE model the state characteristics (displacements, stresses, internal forces) can be calculated, at a compatible level with the applied traditional design methods. In this definition the "analysis" means typically linear analysis on the perfect model, where the stability checking is done by the traditional reduction factor based method.

<u>FE simulation:</u> the verified FE model can be the basis of simulation based design where the actions are applied on an imperfect model and both material and geometrical nonlinearities are considered. In this case the strength and stability phenomena can be checked on the basis of a numerical limit point stability analysis, using the equivalent geometrical imperfections, recommended by the pertinent standard (e.g. Eurocode 3). The "equivalent" means, that the different uncertainties in the structure are transferred to initial geometrical deformations. The design resistance can be derived by a standardized way from the numerically determined ultimate load intensity, using the required safety level.

The FE simulation – as an alternative, more accurate design method – can be applied for the verification and/or validation of traditional design procedures which are derived by more simplifications and involve more uncertainties (Fig. 1.1).

<u>Virtual experiment:</u> if the FE simulation is used on a model which includes "real" – measured or assumed in parametric way – imperfections (initial deformed shape, residual stresses), the experimental results can be extended by the results of the FE analyses. I call these studies as "virtually completed experiments" or "virtual experiments". The measurement of the real imperfections in a large number of structures is not possible in general. In this case the results of verification tests can be used to predict the imperfections by a parametric study on the imperfections. This imperfection sensitivity analysis is an efficient way to extend the existing experimental data, and allows the consideration of a wide range of parameters which affect the targeted phenomena. By this way the results of the virtual experiments can be used to support the design similarly to the real experiments, by the previously discussed ways: design method validation, design value derivation, prototype evaluation.

In the following chapters, where the investigated structural problems are discussed in details, I will introduce the level of the applied research strategy with reference to the above principles and I will show the actual process by the actual flowchart shown in Fig. 1.1.

1.4 Research team

1.4.1 Team members

The previously detailed research and development strategy has been completed by a team work. In the last fifteen years I have been continuously and systematically building this research team. I have been working with talented students who have received challenging parts of the research work and have prepared their research reports in the frame of the Research Students Group (TDK). In most of the cases, these works have been extended in their diploma works and the best students have become doctoral students. In the 15-year-period several of them finished – or just finishing their PhD thesis – and became staff members, and in the same time remaining more active member of the research team. Recently, the new TDK students have been connected to the team through these young colleagues. This team has proved the efficiency in both research and educational activities both national and international level.

The research work, discussed in the thesis has been completed by my team of seven PhD students and in average two TDK and three diploma work students per year. The list of the previous and current PhD students of mine who's research is directly connected to the subject of my thesis: Sándor Ádány (PhD degree 2000), Péter Fóti, Nauzika Kovács (2005), Szilvia Erdélyi, Attila László Joó, László Gergely Vigh (2006), Gábor Jakab. I wish to mention the further members of the research team who have been working on different topics, their work, however, are also affected the results of this thesis: Kornél Kiss (2002), Mansour Kachichian, János Néző, Dániel Honfi.

All members of my team executed laboratory tests what is strongly supported by the structural laboratory staff of Budapest University of Technology and Economics, Technical University of Lisbon and Osaka University.

1.4.2 Scientific results of the team

The joint work of me and my PhD students on the research of the above detailed structural problems resulted in new scientific results. Due to the close co-operation between us it is not evident how to distinguish the own result of the student and the supervisor. This is why I wish to state in the beginning of the thesis the way of performing the co-operative work and declaring the new scientific results, as follows.

For all the structural problems presented in the thesis I determined the global research – and in some problems the development – aims, the directions and strategies of the investigation (note that some cases together with co-supervisor or co-operating industrial partner; I will refer to it in the given problem). The specific problems are investigated in details by the PhD students in my team. Both experimental and numerical studies were planned and evaluated together; the practical works were executed by the PhD students. Most of the publications are results of joint work; the PhD theses have been prepared under my guidance and my co-operation in it.

1.5 Research projects

The research and development work of my team have been supported by the following fundamental, R&D and international joint projects.

[P1] OTKA T 035147 NSF research project: "Interaction phenomena of thin-walled steel structures"; supervisor: Dunai, L.; 2001-2004.

[P2] OM ALK 00074/2000 Educational Ministry R&D project: "Lindab light gauge building system"; supervisor: Dunai, L., industrial partner: Lindab Ltd., Kotormán, I.; 2000-2004.

[P3] Industrial R&D projects of BME on "Purlin-sheeting interaction in the Lindab-Butler cladding system" (3 projects); supervisor: Dunai, L., industrial partner: Butler Europe Ltd. and Lindab Butler Ltd., Macdonald, R.; 1998-2002.

[P4] OTKA T 020738 NSF research project: "Cyclic behaviour of steel and steel-concrete joints"; supervisor: Dunai, L.; 1996-1999.

[P5] TÉT P-04/99 Portugal – Hungarian joint project: "Experimental and numerical studies on bolted connections of steel frames under seismic actions"; supervisors: Calado, L., Dunai, L.; 1999-2002.

[P6] TÉT P-11/01 Portugal – Hungarian joint project: "Seismic behaviour of composite column bases"; supervisors: Calado, L., Dunai, L.; 2001-2004.

[P7] NKFP 3/023/2001 Educational Ministry R&D project "Steel cooling tower"; Task within the consortium: "Joint analysis and design"; supervisor: Dunai, L., industrial partner: PiHun Ltd., Cholnoky, P.; 2001-2003.

[P8] Industrial research project of BME on "Analysis and design of the Dunaújváros Danube Bridge"; supervisor: Dunai, L.; industrial partner: Főmterv Co., Horváth, A., Nagy, Zs.; 2004-2006.

[P9] OTKA T 049305 NSF research project: "Virtual experiment based design of steel structures"; supervisor: Dunai, L.; 2005-2008.

2. Cold-formed steel and composite structures

2.1 Introduction

2.1.1 Background

The application of the cold-formed steel structures has been rapidly increased by the development of cold-rolling technology from galvanized steel sheets and strips in the last one and a half decade. Beside the fast production and improved corrosion protection the geometrical shapes and sizes of the cold-formed profiles have been also extended. These qualitative and quantitative changes of the profiles opened the applicability for new – previously not considered – structural functions. The cold-formed steel profiles more and more replacing hot-rolled steel profiles (e.g. in secondary girders, trusses), traditional timber constructions (e.g. building skeletons, roofs) and reinforced concrete structures (e.g. composite floors with trapezoidal sheets). These new application fields require from the theoretical and standard background to follow the more complex structural behaviour in the new arrangements. Due to this fact the research on cold-formed steel structures have been multiplied since the mid 1980's. As a result of these activities new structural analysis and design tools have been developed and built into the national and international standards (Schafer 1998, EN1993-1-3 2005, US Specification 2004).

In Hungary intensive research and development have been done on cold-formed steel and composite structures under my supervision since 1996. These activities have been done under the supports of interacting fundamental, governmental R&D and industrial projects. The work has been concentrated on novel, non-conventional solutions; the resulted behaviour modes have been investigated experimentally and theoretically and finally design rules have been developed in conform to international standards. The research and development have been completed on two major fields: (i) cold-formed building frame system and (ii) cold-formed secondary structural system.

Cold-formed building frame system

Cold-formed structural system is developed for smaller industrial buildings (span: 3-13 m) and for residential houses (1- or 2-storey), as detailed in Dunai and Kotormán (2005). The novel structural solutions are proposed by my team (Lindab patent, 2002), as follows:
- structural elements: single and double – hollow-type – cold-formed C-profiles, laterally not, or partially supported (Jakab and Dunai, 2007);
- structural joints: self-drilling screwed or bolted connections of beams and columns in web-to-web arrangement (Dunai and Fóti, 2005);
- composite floor beams with cold-formed C-profiles and partially drilled self-drilling screw a shear connector (Erdélyi and Dunai, 2007).

My group completed the background research and developed the design method; as a result the structural system has been applied in the constructional practice.

Cold-formed secondary structural system

Cold-formed Z-purlin and cladding system with non-conventional structural solutions – proposed by the industrial partners – are studied by my team, as follows:
- connection between cold-formed Z-profile and sheeting (Kachichian et al. 1999);
- partial restraints and sliding clip between the components in floating roof arrangement (Kachichian and Dunai, 2001);
- compressive resistance of purlins (Dunai et al. 2004);
- strength and stiffness of overlapped joints (Dunai et al. 2007);
- advanced design methodology (Joó and Dunai, 2002).

On the basis of the completed research design values and rules are derived which have been applied in the practical design.

In this chapter I summarize only the research activities on the cold-formed building structure (despite the work cold-formed purlins resulted in new scientific results these are not discussed in the thesis due to the volume limitations). I completed the research work on the building structure with three previous PhD students of mine: Szilvia Erdélyi, Péter Fóti and Gábor Jakab (note that two of them have been preparing the PhD thesis, to be submitted in 2007).

The detailed research results are published by the research team; this chapter gives a general summary on the completed experimental studies, and gives a global view of the achieved results. The application of the results for design model development can be found in the referred publications of the research team.

First the research purposes are defined on the basis of existing structural systems and previous research activities, and then the applied research strategy is outlined. In Section 2.2 a general view about the structural system is presented, detailing the new solutions and the arising problems to be solved. In Sections 2.3, 2.4 and 2.5 the experimental background and results are presented on the cold-formed frame structural elements, on the moment resisting joints and on the composite floor, respectively.

2.1.2 Existing structural systems and previous studies

In the cold-formed residential and industrial type buildings two basic structural systems are used, as (i) panelised and (ii) portal framing systems, with the characteristics as follows:

Panelised system:
This system is developed and applied on the analogy of the timber building skeletons and consist of – generally prefabricated – panels assembled from cold-formed profiles for walls, floors and roofs. The wall panels are load-bearing steel stud walls with heat insulation boards, which provide support and in-plane membrane rigidity. The floor panels consist of cold-formed floor and ceiling joists and deck (dry: load-bearing boards or wet: concrete or composite). The roof panels are rafters or trusses with typically sheeting cladding.
This system is spreading by replacing the timber structures; e.g. in the USA its application is increased exponentially from the beginning of 1990's, and recently they built more than 25 % of the new houses this way. The application is supported by significant background research (Yu, 2000), standards and manuals (AISI, 1997).

Portal framing system:
This system is developed and applied on the analogy of the typical industrial type building skeletons and consist of cold-formed primary frame, secondary columns and beams and cold-formed sheeting cladding; for multi-storey buildings intermediate floor beams are installed. The key elements of this system are (i) the main frame build up from cold-formed sections and (ii) the floor system with compatible structural arrangement with the frame.

In our R&D work this type of building structural system has been developed and studied. In the following part of this section I summarize some of the existing structures of this type and the background research has been completed on them.

Studies on cold-formed portal frames

In the structural arrangement of the cold-formed frames the elements are built from typically open profiles (C and Sigma sections). The advantages of the double symmetrical sections can be utilized by the application of pairs of profiles in battened arrangement. This arrangement, and the galvanised corrosion protection, however, causes difficulties in the joint detailing (mechanical fastening required). Moment resisting rigid beam-to-column – frame corner – and beam-to-beam – apex – joints can be constructed only by using complicated supplementary elements (gussets, brackets). Recently the tendency is to apply simpler detailing, resulting in semi-rigid behaviour of the joints.

One of the first cold-formed portal frames is published by Baigent and Hancock (1982), where the rigid joints are formed by through bolting the steel channel-sections of beams and column, to – rather complicated – hot-rolled stiffened plates. High strength friction grip bolts are used, with low efficiency due to the friction characteristics of the galvanised steel surface.

More advanced rigid jointed frame is introduced by Kirk (1986), by the so called Swagebeam system. The Sigma-section beams and columns are connected in the joints by back-to-back cold-formed special brackets, in which the swages – formed in the brackets – fit to the web stiffeners of the Sigma-profiles. By bolting the structural elements and bracket to each other the swage interlock is activated, providing with rigid solution, with a relatively small number of bolts. The system is innovative, however, require special fabrication due to the non-standard profiles and brackets. Similar Sigma-profile cold-formed frame is published by Makelainen and Kankaanpaa (1996).

De Vos and Van Rensburg (1997) proposed a cold-formed frame with structural elements formed by double C-profiles welded together, forming a hollow section; the rigid joints are formed by on-site welding. Due to the applied welding technology this system cannot be used by galvanised profiles.

The structural solution can be simplified by accepting the semi-rigidity of the joints. Lim and Nethercot (2003a,b) presented a frame with battened double C-profile beams and columns. In the joints the sections are connected only through the webs to a bracket through bolted connections. Chung and Shi (1999) applied similar frame corners with different shapes of connecting bracket plates, such as haunched, rectangular, L-shaped. Same structural solution with haunched bracket is tested under monotonic and cyclic loading (Dubina et al. 2004) and a component method based design procedure is developed (Nagy et al. 2006). These solutions results in partial strength and semi-rigid frame corner and apex joints.

A cold-formed portal frame is developed recently with single C-profiles connected by web-to-web connections, using four bolts (Dundu and Kemp, 2006). The paper emphasizes the simplicity of the system and presents experimental study and shows a simple method to design the bolted connection.

The complexity of the cold-formed beam-column structural element is well-known due to the interacting local-distortional-global stability behaviour, as summarized in details in Yu (2000). If the above joint arrangements are considered, it is evident that in the structural analysis and design the behaviour of the structural elements should be studied in interaction with the joint behaviour. This investigation requires the application of experimental research.

Studies on light-gauge composite floors

The composite floors built-up from cold-formed products have two groups, according to the structural solutions: (i) composite slabs with profiled steel sheeting (composite action between concrete and cold-formed sheet), and (ii) composite beam with cold-formed profile (composite action between concrete deck and cold-formed beam). While the first group of composite floors have been widely studied, supported by standard design rules (EN1994-1-1, 2004) and applied in the constructional industry, the structures in the second group are rather novel, and only limited applications are published. In the current study only the second structural system is studied and called light-gauge composite floor hereinafter.

In general the framing of light-gauge composite floor systems is built by cold formed C- or Z-profile floor joists. The applied height of the joist is determined by the span and total depth of the floor structure and typically ranges from 150 to 250 mm, while the typical distance between them is around 600 mm. The formwork of the concrete deck is plywood or trapezoidal sheeting. The thickness of the concrete deck ranges from 50 to 80 mm. The composite action between the concrete deck and the cold-formed profile is provided by shear connectors which are typically fastened by non-welded, mechanical process to the profile.

Typically modified formation of screws, or special profile elements are used. Most of the research on the existing light-gauge composite floors concentrates on the different arrangement and behaviour of shear connectors.

Mujagic et al. (2001) studied the standoff screw shear connector, a modified self-drilling and self-tapping screw, manufactured with a special, variable length standoff shank that stops the drilling when the adequate embedment in the concrete is reached.

The Metal Stud Crete shear connector is a special, V-profile element with a continuous, longitudinal web strip, and used in the Earl Composite Systems (2001). The longitudinal strip is fastened to the top flange or to the web depending on the structural arrangement. This shear connector can be used for both wall panels and floor decks.

Several other types of profiled shear connectors are presented and investigated by push-out and full-scale beam tests by Hanaor (2000).

Another special solution is the application of special cold-formed joist with deformed top flange along the top edges, as applied in the system of Building Works Inc. (2003). This part of the cold-formed beam embeds in concrete providing the composite action without application of shear connector.

A full-scale experimental study is presented on composite cold-formed C-section beams applying different types of shear connectors in a recent paper of Lakkavalli and Liu (2006). In the structural arrangement on the upper flange of the C-section holes, bent-up tabs and self-drilling screws are used and the whole upper flange is embedded in the concrete deck.

In the behaviour of the light gauge composite floors the complex stability phenomena of the cold-formed beam is combined with the composite actions. This is why the design of this structure should be based on the cold-formed and composite beam theories, supported by experimental research.

Conclusions on the existing systems and previous studies

On the basis of the existing structural systems and the research studies the following conclusions can be drawn:
- Cold-formed portal frames: most difficulties are in the joints between the structural elements; simple detailing is required for fabrication and erection efficiency; the joint and element interaction results in a highly complex behaviour.
- Light-gauge composite floor: key point is the structural solution of the shear connector by a simple constructional detail what is conform to the cold-formed beam, and results in adequate structural performance.

In the investigated literature we did not find:
- structural detailing and behaviour of cold-formed portal frame with eccentrically arranged C-profile beam and column elements and self-drilling screwed web-to-web type of semi-rigid joints;
- structural detailing and behaviour of cold-formed compression elements built-up from two C-profiles, forming hollow section, connected by self-drilling screws, without welding;
- structural detailing and behaviour of composite beams with C-profile cold-formed beams trapezoidal sheeting permanent formwork/deck, fixed by partially drilled self-drilling screw shear connectors.

2.1.3 Purpose and research strategy

The <u>main aim</u> of the current research was to create the background knowledge for the development and design a new type of cold-formed building system.

The <u>particular purposes</u> were defined as follows:
- identification and characterization of new behaviour modes of novel structural solutions by experimental studies:
  - (i)   cold-formed hollow-type column,
  - (ii)   cold-formed frame corner,
  - (iii)   partially drilled self-drilling screw shear connector, and
  - (iv)   cold-formed composite floor beams;
- deriving test based rigidities and resistances for design purposes;
- verification of existing design methods for the new structures;
- developing advanced design methods.

The applied research <u>strategy</u> is illustrated in Fig. 2.1; the solid arrows indicate the completed work, while the dashed arrows show the possible application of the results and the further extension of the research.

In the first phase of the research experimental studies are completed in order to determine the complex structural phenomena. In the lack of preliminary information on testing methods and uncertainties in the detail prototypes "pilot tests" are done and the test programs are planned on these experiences. According to the above detailed purposes the test results are used to define the prototype behaviour ("prototype test"), as qualitative characterization. The measured rigidities and resistances are applied to derive the test based design values for practical design purposes ("design test"), as quantitative characterization. On the basis of test results existing design formulae are verified and new design methods are developed ("validation test"). The results of the executed tests have been used for model verification, ("verification test"). In the current phase of the research finite element and finite strip models have been developed for some of the studied details. The extension for virtual experiments is under progress.

In my thesis the focus is on the experimental research, the applications of the results are available in the design and analysis oriented papers of the research team.
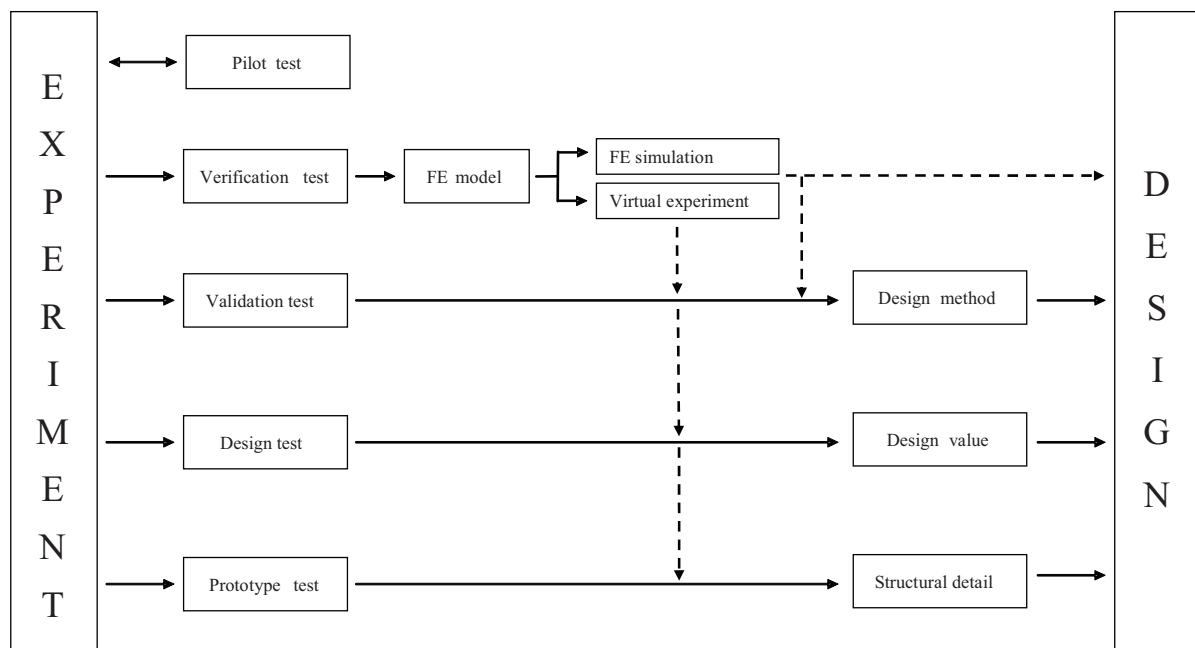
Fig. 2.1: Applied research strategy – cold-formed building structure.

2.2 Cold-formed steel framed building structure

2.2.1 Structural arrangement

The cold-formed structural system is developed on the basis of the fabrication background of Lindab Ltd, the applied erection method of the related steel construction companies and functional needs. Under these restraints the structural development is completed by my team in co-operation with the engineers of Lindab. The developed structural system has a patent (Lindab patent, 2002). In this Section a general view on the arrangements of the building structural system for industrial type and for residential house type applications is presented.

Industrial type building structure

This structural system is developed for simple, double pitched box building which applied for smaller industrial and commercial hall buildings. It is developed in a modular system with the dimension range as follows: 3.0-13.0m width, 3.0-20.0m length, 2.5-4.0m eave height, 18° roof slope. The structural set-up follows the classical metal hall buildings; it consists of primaries, secondaries and roof/wall cladding, as shown in Fig. 2.2. The main frame distance is the base module size: M=1.0m.

The primary portal frame can be seen in Fig. 2.3. The elements of the two-hinged planar frames are made of single C-profiles. All the frame connections (anchoring, frame corner, apex) are eccentric web-to-web types, screwed or bolted on site. Means that the plane of the frame is not the symmetry plane of the beam and column elements. In the static model the frame corner and the apex are considered as moment-resisting semi-rigid joints.
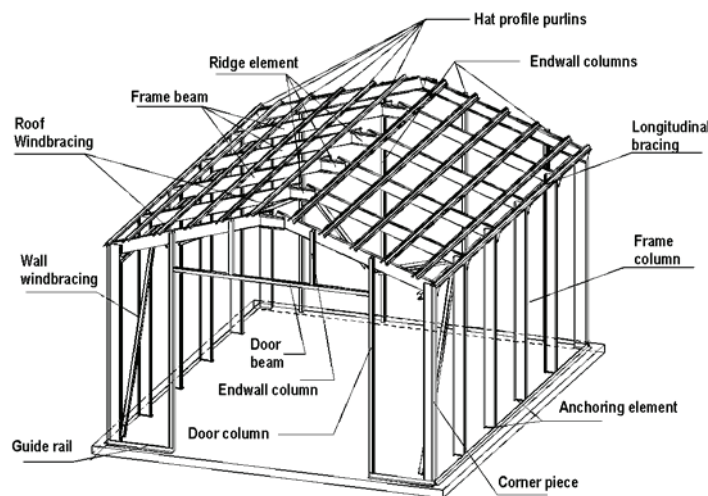
Fig. 2.2: Industrial type building structure.
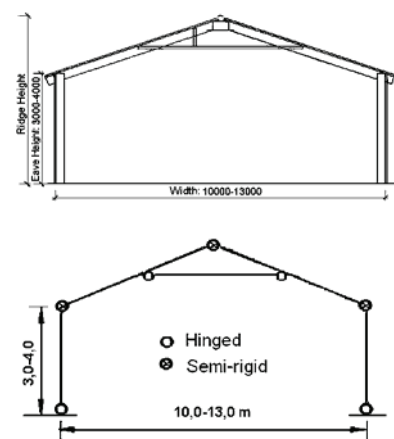
Fig. 2.3: Primary frame and statical model.

The secondary load-bearing elements – roof purlins, end wall columns – are also made of cold-formed profiles (hat- and C-sections). The roof and wall cladding is made of coated trapezoidal/corrugated sheets, fixing by self-drilling screws. The structural system supports the required functional requirements (openings, ventilation, insulation, etc.) with several standardized solutions.

The spatial bracing of the whole building is provided by additional C-profiled longitudinal bracing rods and diagonals in the roof and wall. The cladding trapezoidal sheeting also has important stabilising effect, it is considered as lateral support for the primary columns (on one or both flanges), and also as bracing component with its in-plane shear stiffness (diaphragm effect).

Residential house type building structure

This structural sub-system is developed on the bases of the basic industrial type structure. The base unit of the building is also a double pitched box volume in modular system, but with different values: base module size M=1.275m, width 3M-7M, length up to 15M, frame distance 1M. This building system has two different versions: vs. #1 means single-storey, and vs. #2 refers to two-storey building units; the roof slope and the eave height depend on the version. The box-like units can be attached to each other in different forms ("L", "T" or "U" shaped plans), as illustrated in Fig. 2.4.

The primary frames in the single-storey version are made of the same components as in the industrial type structure. The two-storey frame (vs. #2), however, is significantly expanded. It has an intermediate load-bearing floor beam made of single C-profile and, as a consequence of the higher loads, strengthened external frame columns from double C-section (hollow section arrangement), and over 4M span of floor beam, a C-profiled intermediate column, as shown in Fig. 2.5. The connections of the elements are also generally eccentric, screwed together directly on their webs/flanges or using gusset plates. The frame corner and apex joints are considered semi-rigid, all the other joints are pinned.
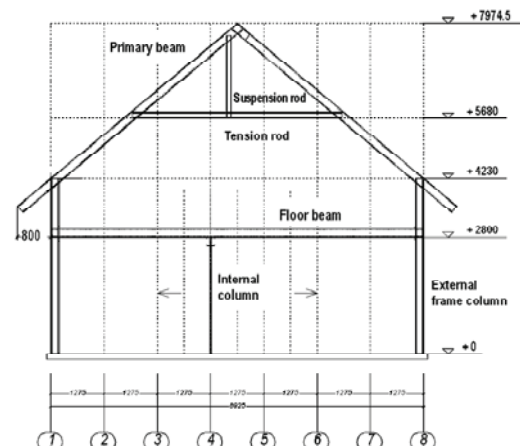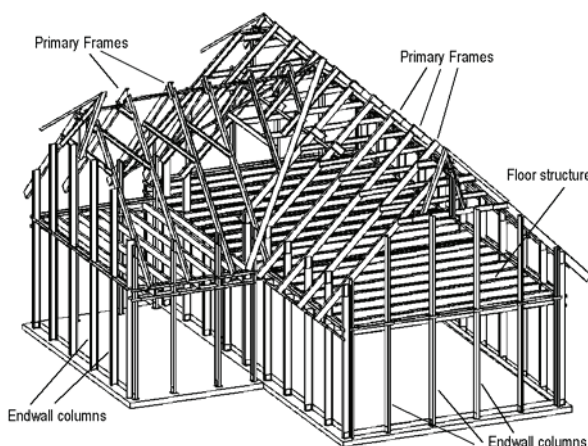
Fig. 2.4: Residential house type building structure   Fig. 2.5: Primary portal frame of vs. #2

The intermediate floor structure is formed by simply supported cold-formed composite beams with a 50mm thick concrete deck. The concrete is supported during the erection by permanent trapezoidal sheeting formwork. The composite action is provided by partially drilled self-drilling screws shear connectors. The floor beams are spaced to 0.5M, therefore beside the ones in the primary frames, additional composite C-beams are built between the frames, and these are supported by longitudinal ring beams made of double built-up C-profiles. The connections are hinged and formed by sheared screws. The lower flanges of the C-beams are supported laterally by secondary hat-profiled beams and gypsum boards.

The secondary load-bearing structure consists of the roof purlins and wall girts made of hat-profiles. There are several types of roof and wall cladding variants tailoring to the functional needs (steel sheeting roof, wall claddings made of mortar or brick facade wall). Special system details are used to realise unique features often required for residential houses, i.e. different wall openings (windows, doors, gates), floor opening (for stairs), roof hipping etc.

The spatial bracing is the same as for the industrial type structure.

The fire resistance of the structure is ensured by the internal gypsum board cladding, designed with a thickness to fulfil the actual requirements.

14

2.2.2 Behaviour and design characteristics

As a consequence of the applied novel solutions in the developed building structure system, several uncertainties raised in the structural behaviour and in the design. In the followings these behaviour characteristics, the applied investigation and design philosophy are briefly summarized, with a focus on the primary framing.

Structural elements

The structural elements of the frame are under compression and biaxial bending, with different lateral and end supporting conditions (beam-columns). The governing phenomena are the interacting local plate buckling, distortional buckling and global lateral torsional buckling. For a separated element the resistance under such behaviour can be calculated by standard recommendations (EN 1993-1-3, 2005). The determination of the critical load factors, however, requires advanced numerical analyses (finite element and finite strip methods) due to the different conditions of lateral supports. The governing behaviour of a single C-profile, continuously supported on both flanges, is always the interaction of bending and in-plane buckling. When a single C-profile is laterally supported only on one flange, the member resistance is concerning to the interaction of flexural-torsional and lateral-torsional buckling about the restrained axis. When a hollow section is formed by two C-profiles by pushing the two members into each other, the hollow type behaviour is uncertain due to the conditional restraints between the two profiles. Further problems are raised by the local effect at the element ends, close to the joints (frame corner and column base). These complex phenomena are investigated by the compression member tests (Section 2.3).

Structural joints

The moment resisting joints are formed by screwed and bolted web-to-web connections between the structural elements. This connection arrangement in addition to the interaction of the element ends and connection, results in a complex moment – rotation behaviour of the joints, including: element end deformation and buckling, connecting element slipping and tilting, interlocking between the webs. Due to this complexity of phenomena and uncertainties in the arrangement experimental studies are applied to define the behaviour modes and the design characteristics of the semi-rigid and partial strength joints (Section 2.4).

In the structure several hinged connections are constructed, directly between the structural elements or through gusset plates, by single sheared screws (e.g. tension rod-to-beam connection, column base). The behaviour of one self-drilling screw, depending on the screw type and the thickness of connected sheets, is investigated by experiments and the design values for shear resistance are derived from the relevant experimental test results. The separated screw test results are also used in the evaluation of moment resisting joint results.

Composite floor

The light-gauge composite floor represents also an innovative solution. The global behaviour is combined from the cold-formed steel beam having composite action by flexible shear connectors. The tilting of the self-drilling screw connection in interaction with the concrete supporting effect is the phenomenon that should be adjusted to achieve a reliable composite action. This could be done only by experimental studies on push-out type basic specimens. Having identified and characterized the favourable behaviour modes of the connectors, and the partial composite connection principle of the Eurocode 4 standard (EN 1994-1-1, 2005), a design procedure is derived. The complexity of the cold-formed composite beam behaviour, however, required further verification of the behaviour and the design method by full-scale experiments on beam specimens. The overall view of the experimental studies can be found in Section 2.5.

2.3 Cold-formed compression members

2.3.1 Research program

The C-profile structural members of the cold-formed frame introduced in Section 2.2 are studied by compression tests with different cross-sections and end and lateral supporting conditions. The purpose of the tests was to determine the complex stability phenomena and to derive the test-based design resistances of the cold-formed members under conditions and arrangements that are not covered by standard calculation methods.

In the experimental study 37 laboratory tests are completed, as detailed in Dunai et al. (2004). In this Section the results of selected specimens will be presented (laterally unsupported 28 specimens, with web b/t ratios of 100, 150 and 200). The first type of specimens is a single C-profile with ball support at the ends, resulting nominally axial uniform compression (hereinafter "compressed C" specimen). The second type of specimens is a single C-profile member that is loaded by compression in its web using a gusset plate, resulting compression and bending (hereinafter "simple C" specimen). The third type of specimens is made by stucking two C-sections into each other – forming a "closed" section – and connecting them at their flanges using self-drilling screws, as shown in Fig. 2.6 (hereinafter "double C" specimen). Similarly to the simple C, gusset plates are used to apply the load in the web for both C-profiles. Hence, the load in this case is nominally axial compression for the "closed" section and eccentric compression for the two C-profile components.

The results of the laboratory tests are evaluated by describing and comparing the observed stability behaviour, failure modes and ultimate loads. In parallel with the tests Eurocode-based calculations are completed using different assumptions. The experimental and standard-based resistances are compared and evaluated. A proposal for the prediction of design resistance of double C members is done.

2.3.2 Experimental investigation

<u>Design of specimens</u>

The specimens' cross-sections and lengths are designed with the aim to be able to observe the coupled failure modes that can occur in these cold-formed members. An extended finite strip buckling analysis is used as background of the design (Schafer, 1998). The completed parametric study showed the different failure modes and their coupling under the different loading and supporting conditions. The applied CUFSM program provided the bifurcation points of the stability path of the members for the defined buckling lengths, and the buckled shape of the members. The results of the finite strip analysis are illustrated in Fig. 2.7: the local plate buckling, the distortional buckling and the global flexural torsional buckling can be seen for the different length of compression members. Based on these results the failure mode can be estimated in function of the buckling length, and the EC3-based design resistance of the member can be evaluated (Jakab, 2003).

As a result of the parametric study three lengths – 800 mm, 2000 mm, 3600 mm – and three C-sections with web heights of 150 and 200mm, thicknesses 1 and 2 mm are chosen for the tests, as detailed in Table 2.1. The arrangement of the double C-section is shown in Fig. 2.6.

Profile	web	small flange	large flange	lip	thickness
C150/1	150	41	47	16.2	1.0
C200/1	200	66	74	19.7	1.0
C200/2	200	66	74	22.8	2.0
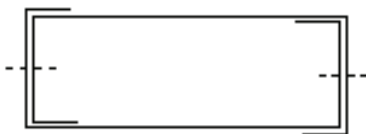
Figure 2.6: Double C-section.   Table 2.1: Geometry of the cross-sections.
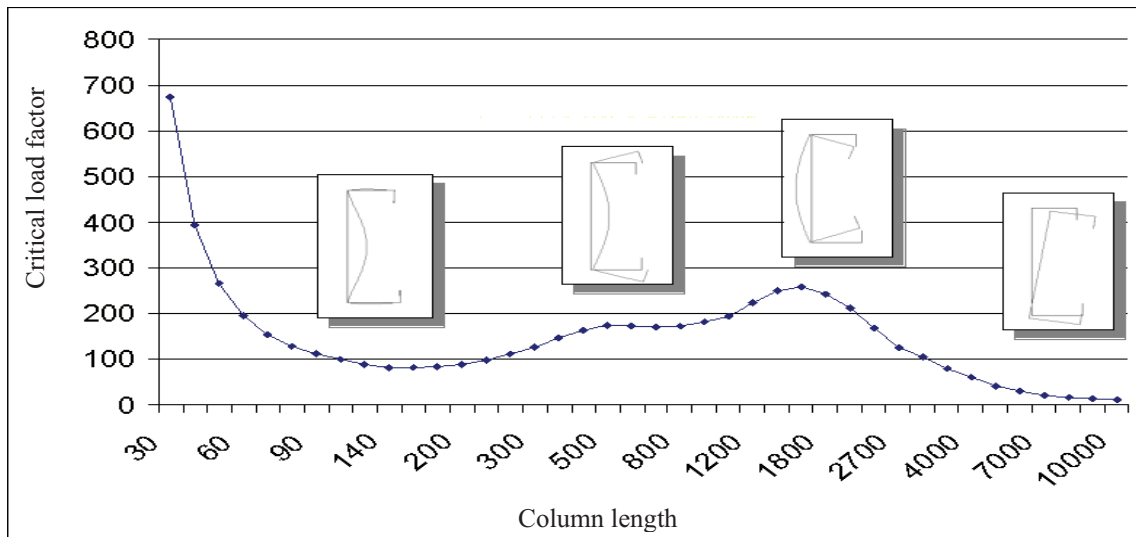
Figure 2.7: Buckling shapes of C-profile specimens.

Test arrangement

The specimen are tested in vertical position in a loading frame as shown in Fig. 3,a. The load is applied at the lower end of the specimen using a hydraulic jack. The load is introduced into the section by means of end-plate or gusset plate, as shown in Fig. 3,b. The measurement system consists of eight displacement transducers at the edges of the middle cross-section of the specimen, as shown in Fig. 3,c, and one to measure the shortening of the column. A load cell is applied to measure the load.
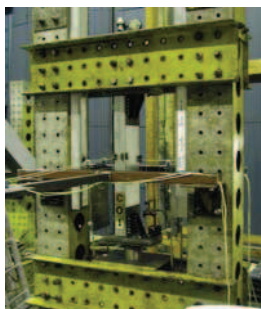
(a) loading frame   (b) load application   (c) displacement measuring
Figure 2.8: Test setup.
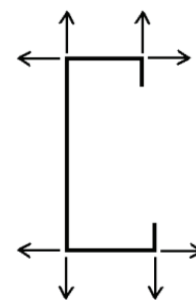
In the tests the uniform compression on the purely compressed C-specimen is provided by a ball support in the centroid of the cross-section and thick plates to distribute the load to the whole cross-section (Fig 2.9,a). In the case of simple C- and double C-specimens the load is introduced in the web of the sections using gusset plates connected to the specimen using self-drilling screws (Figs. 2.9,b and 2.9,c). The double C-specimen is in most tests connected to each other at their flanges using self-drilling screws at certain distances (as detailed later on).

(a) compressed C   (b) simple C   (c): double C
Figure 2.9: Supports.
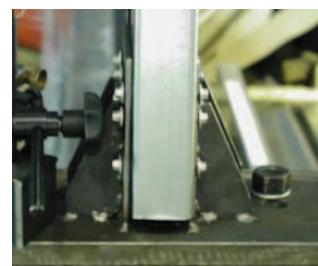
17

Tests results of compressed C specimens

Altogether 6 specimens are tested in compressed C arrangement. The specimen properties as well as the observed behaviour, the obtained failure modes and the measured ultimate load are detailed in Table 2.2. Although different failure modes are observed for the different specimen lengths, in all tests a common characteristic phenomenon is experienced, the elastic local buckling of the web.

In the case of the shortest specimen (800 mm) global stability phenomenon is not observed, the failure occurred always near to the end-plates because of the web crushing, as shown in Fig. 2.10,a.

Both specimens with the length of 2000 mm showed a distortional type of stability phenomenon in the elastic range, as shown in Fig. 2.10,b. In one of these tests the final failure is caused by flexural buckling about the minor axis: the relative large global deformations eliminated the distortional behaviour and a local yield mechanism formed in the middle of the column. The other specimen failed similarly to the shortest ones, due to the significant local initial imperfections.

In both tests with the length of 3600 mm a flexural buckling-type of behaviour and a final failure caused by local yield mechanism at the middle of the column is obtained, as shown in Fig. 2.10,c. In case of the specimen with the profile C200/1 torsion of the middle cross section is also observed.

Table 2.2: Test results of compressed C specimens.

Profile	Length [mm]	Observed behaviour and failure mode	Ultimate load [kN]
C200/2	800	crushing of the web and flange; failure near to the lower end	133.57
C200/1		crushing of the web and flange; failure near to the upper end	35.91
C200/2	2000	combination of distortional and flexural buckling; failure in the middle	104.34
C200/1		crushing of the web and flange; failure near to the lower end (specimen with initial defects)	25.62
C200/2	3600	combination of local buckling and flexural buckling; failure in the middle	53.16
C200/1		combination of local buckling and torsional-flexural buckling; failure in the middle	24.65

(a) end crushing   (b) plate and flexural buckling   (c) yield mechanism
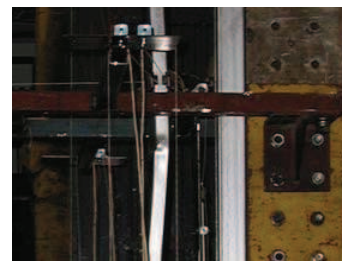
Figure 2.10: Failure modes.

Tests results of simple C specimens

Altogether 10 specimens are tested in single C arrangement. The specimen properties as well as the observed behaviour, the obtained failure modes and the measured ultimate load can be found in Table 2.3.

In this arrangement the specimens are subject to compression and bending about the minor axis due to the eccentricity of the load-drive-in.

Similarly to the tests on compressed C specimens, elastic local buckling of the web is observed in all tests. Due to the bending moment about the minor axis, at failure relative large – the greater the slenderness of the specimen the larger – displacement of the middle cross-section and rotation at the gusset plates is observed in the tests.

The failure in the case of the shortest specimens occurred by the crushing of the web at the gusset plate. In all cases large rotation of the self-drilling screws is observed. In these tests the failure mode is a coupled failure of the connection at the load introduction at the end of specimen and the crushing of the web, as shown in Fig. 2.11,a.

In the case of all the specimens with the length of 2000 mm and 3600 mm the observed stability behaviour is flexural buckling about the minor axis with relatively large elastic deformations, as shown in Fig. 2.11,b. The failure is caused by forming a local yield mechanism near to the middle of the specimen, as shown in Fig. 2.11,c. The exact position of the mechanism depends on the position of the plate buckling waves in the web. As in these arrangements the specimens are subject to compression and bending, this local yield mechanism is practically an interactive hinge (Iványi, 1983).

Table 2.3: Test results of simple C specimens.

Profile	Length [mm]	Observed behaviour and failure mode	Ultimate load [kN]
C200/2	800	local buckling of the web; failure: crushing of the web at the screwed connection at the gusset plate	85.92
C200/1			21.86
C150/1			18.05
C200/2	2000	combination of local buckling (web) and flexural buckling; failure in the middle of the column	71.11
C200/1			24.16
C150/1			12.50
C200/2	3600		46.77
C200/1			17.24
C150/1			9.47
C200/2			46.67
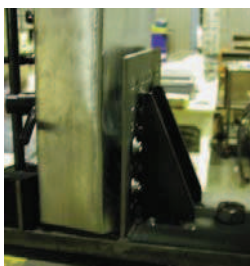
(a) web crushing
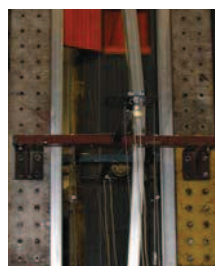
(b) bending deformations
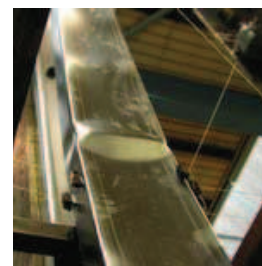
(c) yield mechanism

Figure 2.11: Failure modes.

Tests results of double C specimens

Altogether 12 specimens are tested in double C arrangement. The specimen properties as well as the observed behaviour, the obtained failure modes and the measured ultimate load can be found in Table 2.4. Similarly to the previous tests, elastic local buckling of the web is observed in all tests.

In the tests of the short (800 mm) and in two tests of the specimen with length of 2000 mm the failure occurred near the gusset plate by crushing, forming local yield mechanism. Besides this crushing of the web large rotations of the self-drilling screws and large deformations of the column ends are observed. In these tests the failure mode is a coupled failure of the connection at the load introduction at the end of specimen as shown in Fig. 2.12,a.

In the other seven tests global failure, flexural buckling about the minor axis is obtained. The rotation of the self-drilling screws at the gusset plate is observed in these cases as well, but it did not have effect on the global behaviour of the specimen. During the loading process the C-sections worked together by giving each other lateral support, regardless of the number of the screws in the flanges. This phenomenon is illustrated also by the solid cross-section type bending: as the lateral displacement is increased the "compression" and "tension" side can be clearly recognized, as shown in Fig. 2.12,b. A distortional type of behaviour is observed in all cases as the lip (and the pertinent flange) at the middle cross-section of the column on the compression side opened, as shown in Fig. 2.12,c. The final failure is caused by a local yield mechanism near the failed lip.

Table 2.4: Test results of double C specimens

Profile	Length [mm]	Screw dist. in flanges [mm]	Observed behaviour and failure mode	Ultimate load [kN]
C200/2	800	500	local buckling of the web; failure: crushing of the web at the screwed connection at the gusset plate, or cross-section crushing close to the end	200.78
C200/1	800	500		55.27
C150/1	800	500		47.28
C200/2	2000	500		219.02
C150/1	2000	500		45.78
C200/1	2000	500	combination of local (web), distortional and flexural buckling (minor axis); failure in the middle of the column	58.66
C200/2	3600	500		150.87
C200/1	3600	500		58.00
C150/1	3600	500		26.04
C200/1	3600	no screws		56.17
C200/2	3600	no screws		140.44
C200/2	3600	1000		180.67
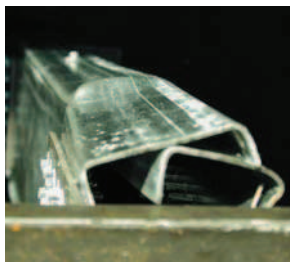
(a) end support failure   (b) tension and compression sides   (c) distortional buckling
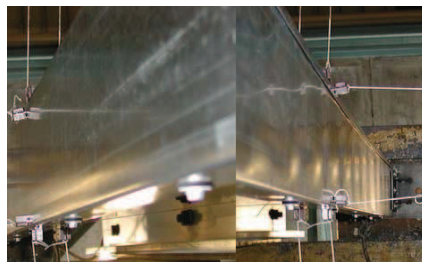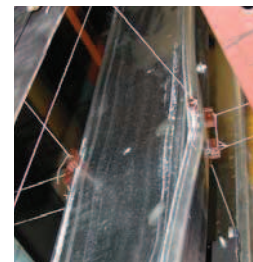
Figure 2.12: Failure modes.

2.3.3 Evaluation of test results

Behaviour modes

Plate buckling: in the elastic range of the experimental behaviour local elastic web buckling is obtained in all the tests, as it is expected due to the applied b/t plate ratios (Figs. 2.10,b; 2.12,b; 2.13,c). Without mentioning, this phenomenon is always coupled with the other stability behaviour.

Crushing at the end of the specimens: in the case of the specimens with the length of 800 mm this failure is obtained for all three types of specimen. The different end arrangement resulted in different phenomena: web and flange crushing (compressed C, Fig. 2.10,a); web crushing (simple C, Fig. 2.11,a); web crushing with constrained deformation of the cross-section (double C, Fig. 2.12,a).

Flexural buckling: this "pure" stability type failure is observed in the case of the specimens with the length of 3600 mm and simple or double sections with axial loading (compressed C). Due to the imperfections, naturally this failure always showed the combination of flexural buckling and bending, as typical beam-column limit point type stability behaviour. This type of phenomenon is observed clearly for the eccentrically loaded simple C specimens with the length of 3600 mm. Note, that in one compressed C specimen (C200/1, 3600) flexural-torsional buckling is also observed.

Distortional buckling is always experienced in an interaction with other behaviour modes, as follows:
- combination of distortional and flexural buckling for compressed C specimens (C200/2, 2000, Fig. 2.13,c),
- combination of distortional and flexural buckling for double C specimens (Figs. 2.12,c and 2.13,a).

The final failure is caused always by local yield mechanisms in various positions of the specimens, as follows:
- end crushing, at the connection or in the supporting zone (as discussed under the crushing behaviour);
- compression type yield mechanism close to the end of the specimen (Fig. 2.13,b shows the phenomenon of the double section specimen near to the lower end);
- bending type yield mechanism of single section (Figs. 2.10,c; 2.11,c);
- bending type yield mechanism of double section (Figs. 2.12,c; 2.13,a).

(a)   (b)   (c)
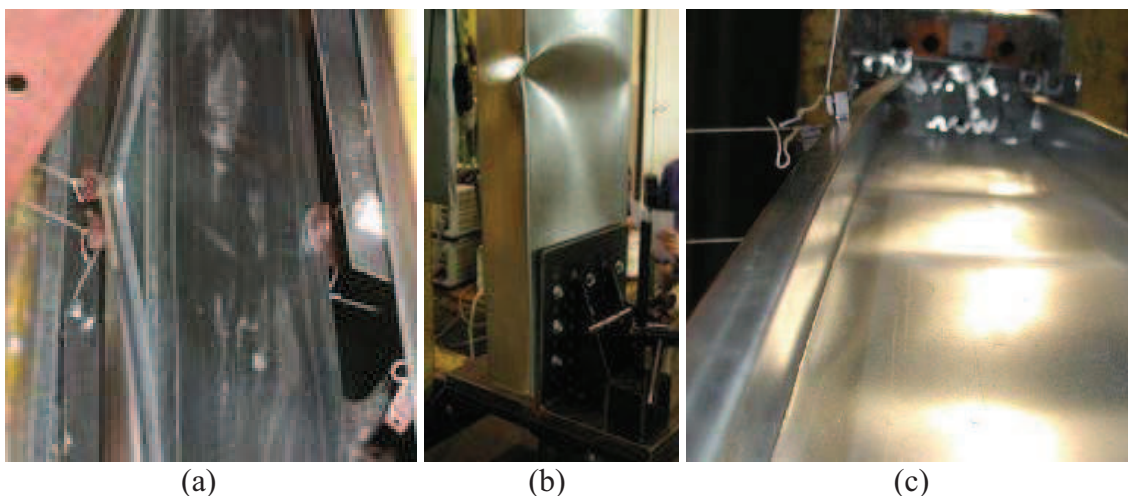
Figure 2.13: (a) Bending type yield mechanism of double C; (b) compression type yield mechanism of double C; (c) combination of local-distortional buckling of compressed C.

Six typical behaviour modes are illustrated in Fig. 2.14 by the load – lateral displacement curves, as follows:
- flexural buckling type behaviour: simple C specimens: C12 (C200/2, 2000) and C23 (C200/2, 3600),
- combination of distortional and flexural buckling of compressed C specimen: C13 (C200/2, 2000),
- combination of distortional and flexural buckling of double C specimen: C31 (C200/2, 3600) specimen (Fig. 2.12,c).
- end crushing failure of simple C specimen: C01 (C200/2, 2000).
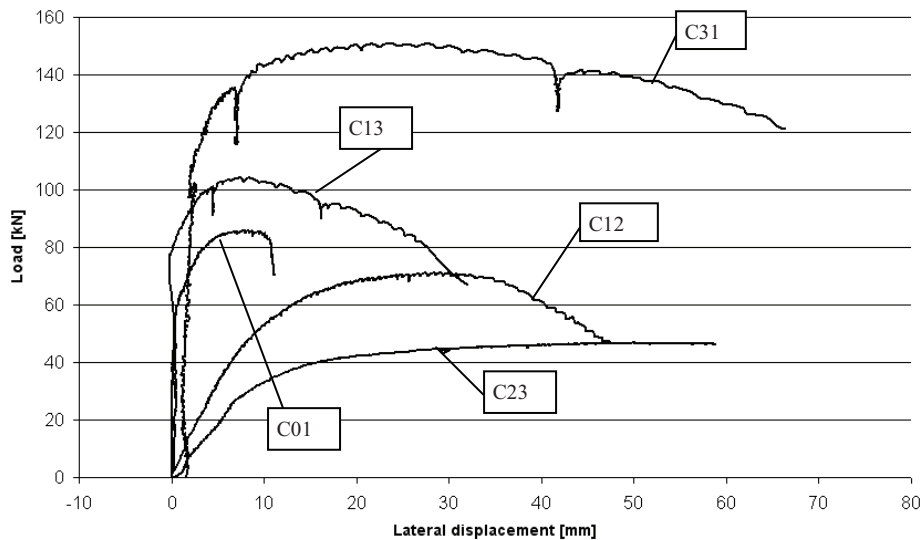
Figure 2.14: Load – lateral displacement relationships.

Ultimate loads

The measured ultimate loads compressed C, simple C and double C specimens are shown in Fig. 2.15. The tendencies clearly show (i) the effect of crushing type element end failure and (ii) the efficiency of the double C-profile application. The hollow type sections of double C-profile have more than double compressive resistances in the cases of all the observed local and global behaviour modes, due to the section type and the higher efficiency of the applied gusset plate support (prototype test).
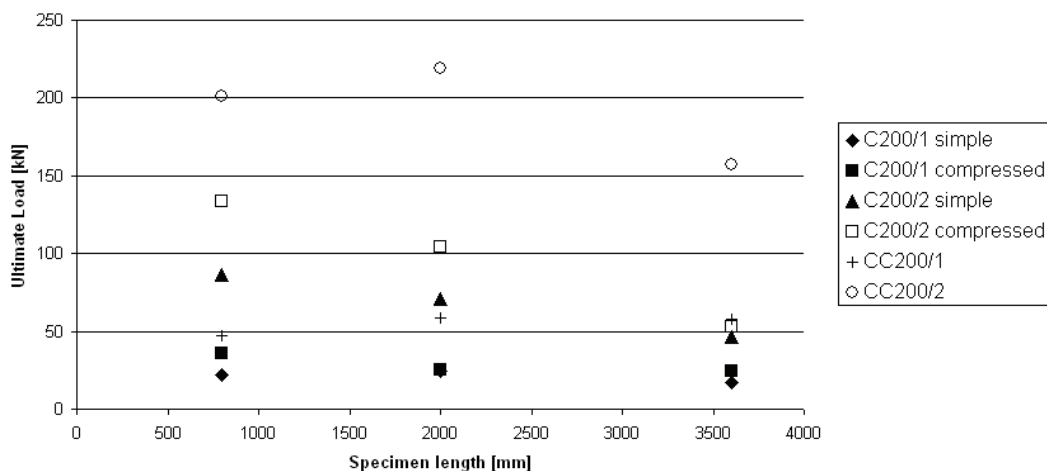
Figure 2.15: Measured ultimate loads.

22

2.3.4 Design resistances and application proposals

From the results of the experimental study the test based design resistances are calculated on the bases of the Eurocode 3 (previous draft of EN 1993-1-3, 2005) recommendations (design tests). The calculation details and the resistances can be found in Jakab (2003). These results can be used directly in the practical design, for the given cases. In order to extend the experimental findings for practical design purposes a comparison study is completed on the test and EC3 standardized resistances (validation tests), as detailed in Jakab and Dunai (2007).

The EC3-based design buckling resistances are calculated for compressed C and simple C specimens, without using safety factors and using material properties derived from tensile tests and using the cross-sectional properties determined by ColdForm (2000) program. Notes: (i) in the case of short columns the cross-section resistances are calculated, assuming local plate buckling failure; the crushing resistance by can be calculated by improved design model, on the basis of observed yield mechanisms from extended experimental study; (ii) for simple C specimens the buckling resistance includes the eccentricity. The test and calculated results are presented in Table 2.5.

In the case of the compressed C specimen the EC3-based resistances in general overestimate the test results. It can be explained by the un-avoided eccentricity of the supports during the tests. The differences are smaller in the range of higher slenderness, as it is expected. In the case of the simple C specimens with a profile C200/2 the standard based resistances are very close to the test results. For the 1 mm thickness, however, higher differences and scatter of the results is experienced. For C200/1 the EC3 results significantly underestimate the test resistances. It can be explained by the relatively bigger end rigidity comparing to the bending stiffness of the member.

profile	length [mm]	compressed C		simple C	
		test	EC3	test	EC3
C200/1	800	35.9	39.6	21.9	17.8
C200/2		133.6	163.4	85.9	91.2
C200/1	2000	25.6	34.2	24.2	15.1
C200/2		104.3	121.4	71.1	72.8
C200/1	3600	24.7	23.6	17.2	12.7
C200/2		53.2	59.5	46.7	44.8

Table 2.5: Measured and calculated resistances in [kN] – simple and compressed C specimens.

By the experimental studies the practical design application of the EC3 recommendations are proved for the applied column size range (over 3000 mm) – validation test. In the interaction formula of EC3 the minor axis bending, caused by the column base eccentricity can be considered by the buckling resistance. The major axis bending causes lateral torsional and/or distortional buckling, what can be investigated by the previously mentioned finite strip bifurcation analysis. From the critical factors and the relevant buckling shapes the slenderness ratio and the buckling moment resistance can be calculated.

The design resistances of double C specimens are predicted using three approaches. According to the first one the resistance of a double C specimen is twice of the resistance of a simple C specimen with the same length and profile. In the second approach the resistances of the compressed C sections is doubled. The third approach models the double C section as a hollow section with uniform plate thickness under uniform compression.

The measured and predicted resistances of double C specimens are presented in Table 2.6.

profile	length [mm]	2 x compressed C		2 x simple C		EC3 hollow	double C test
		test	EC3	test	EC3		
C200/1	800	71.8	79.2	43.7	35.6	55.3	103.6
C200/2		267.1	326.8	171.8	182.3	200.8	335.9
C200/1	2000	51.2	68.4	48.3	30.3	58.7	88.3
C200/2		208.7	242.8	142.2	145.6	219.0	258.9
C200/1	3600	49.3	47.2	34.5	25.5	56.2	58.5
C200/2		106.3	119.0	93.4	89.7	140.4	134.6

Table 2.6: Measured and predicted resistances in [kN] – double C specimens.

By comparing the calculated resistances to the load-bearing capacity obtained from the test in the table, the following conclusions can be drawn:

- By doubling the test ultimate load or the design resistance of the simple C specimens the results are always on the safe side, regardless of the length of the specimen, leading to a very conservative design.

- By doubling the load-bearing capacities obtained from the tests and resistances calculated according to EC3 of the compressed C specimen, it is found that with the increasing specimen length the double C to doubled compressed C ratio values are getting lower. For 2000 and 3600 mm lengths of specimens the doubled compressed C calculated results are 23-29% (b/t=200) and 7-13% (b/t=100) smaller than the double C test results.

- By calculating the design resistances according to the hollow section analogy, the comparison between the double C test results show bigger scatter. Even smaller overestimation of the resistances is experienced (C200/2, 3600mm).

- On the basis of the obtained results and the supplementary parametric studies using the different design approaches it is concluded that in practical design of double C members (the length is over 3000mm and b/t smaller or equal to 150), the compressed C section based design approach can be applied.

An alternative way to calculate the EC3-based design resistances for such cold-formed members is based on FE simulation. Despite in the EN 1993-1-3 (2005) equivalent imperfections are not included for cold-formed section, the executed tests provides with verification background for model development (verification tests). By the verified models virtual experiments can be completed to derive the test based resistances. This approach is used in the Z-purlin research of my team (Joó and Dunai, 2004). The achieved results can be directly used for the C-profile beam-column structural elements, too.

2.4 Cold-formed steel frame corner joints

2.4.1 Research program

The single or double C-profile structural members of the cold-formed frame are connected to each other in a web-to-web arrangement in the frame corner. Similar arrangement is used in the apex joint, applying a C-profile connecting element. The connection is solved by self-drilling screws or bolts. This structural detailing results in semi-rigid and partial strength joint. An extended experimental study is completed on the frame corner joint and the separated connecting elements with the purpose to determine the complex joint – element end and connection – behaviour, to calculate the test-based design stiffness and resistances of the joint and to derive practically applicable semi-empirical joint models.

In the two experimental programs 56 frame corner joint and 38 self-drilling screw connection laboratory tests are completed, as detailed in Dunai et al. (2000), Dunai et al. (2001). The frame corner tests are completed in a column-cantilever beam arrangement under dominant bending. Both single and double C-profile columns are investigated (according to the detailing discussed in Section 2.2 and 2.3); the beams are always single C-profile elements. The self-drilling screw connecting elements are tested under shear.

The results of the laboratory tests are evaluated by describing and comparing the observed behaviour and failure modes. On this basis the frame corner prototypes are selected and for these joints the test based design stiffness and resistance values are calculated. In parallel the experimental results are used to develop semi-empirical joint model for the prediction of the moment-rotation relationship. The frame corner joint results are extended for the apex joint design.

Note, that in this Section the only the results of screwed joints (38 tests) are presented; the bolted connections are not discussed. A pilot study is also completed on screwed-bonded connections (Tuza, 2005); this is also out of the scope of this Section.

2.4.2 Experimental program

Frame corner joint tests

Altogether 38 experiments are performed and the investigated parameters are as follows:
- size of the fasteners: 5.5 and 6.3 mm diameters,
- arrangement – number and placing – of fasteners: 5-22 pieces of self-drilling connectors,
- height and thickness of connected C-profiles: 150-300 and 1.0–3.0 mm,
- types of column: single or double (hollow) C-profile.

Two types of test setups are used in the experiment. Figure 2.16,a shows test setup A including a typical joint. The lengths of the column and beam elements are 1.0 and 1.5 – 2.0 meters, respectively in the arrangement. The concentrated load is applied on 1.0 – 1.5 meters arms for different profile heights. Lateral bracings are applied on the top flange by hat profiles (purlins) and a C-profile (bracing) on the compression side of the joint.

Figure 2.16,b shows test setup B. The setup is designed for residential frame system, using a 1.0 m long double C-profile column element and a 2.5 m long beam. The beam is connected to one of the C-profiles of the column by self-drilling screws. Lateral bracing is solved by two pairs of hot rolled columns keeping the beam in the plane of the frame by fork supports.

The main purpose of the experiments was to obtain the moment-rotation relationships of the joints. The rotations are measured in three points of the joint region by rotation measurement devices: on the column under the connection and on the beam both sides of the connection, as shown by the numbered boxes in Fig. 2.16,a. The displacements are measured in four places: vertically under the force and in the middle of the beam; horizontally, transverse direction in the joint; and horizontally, lateral direction in the joint. Strains are also measured; strain gauges are placed on the flanges of the beam near to the joint.
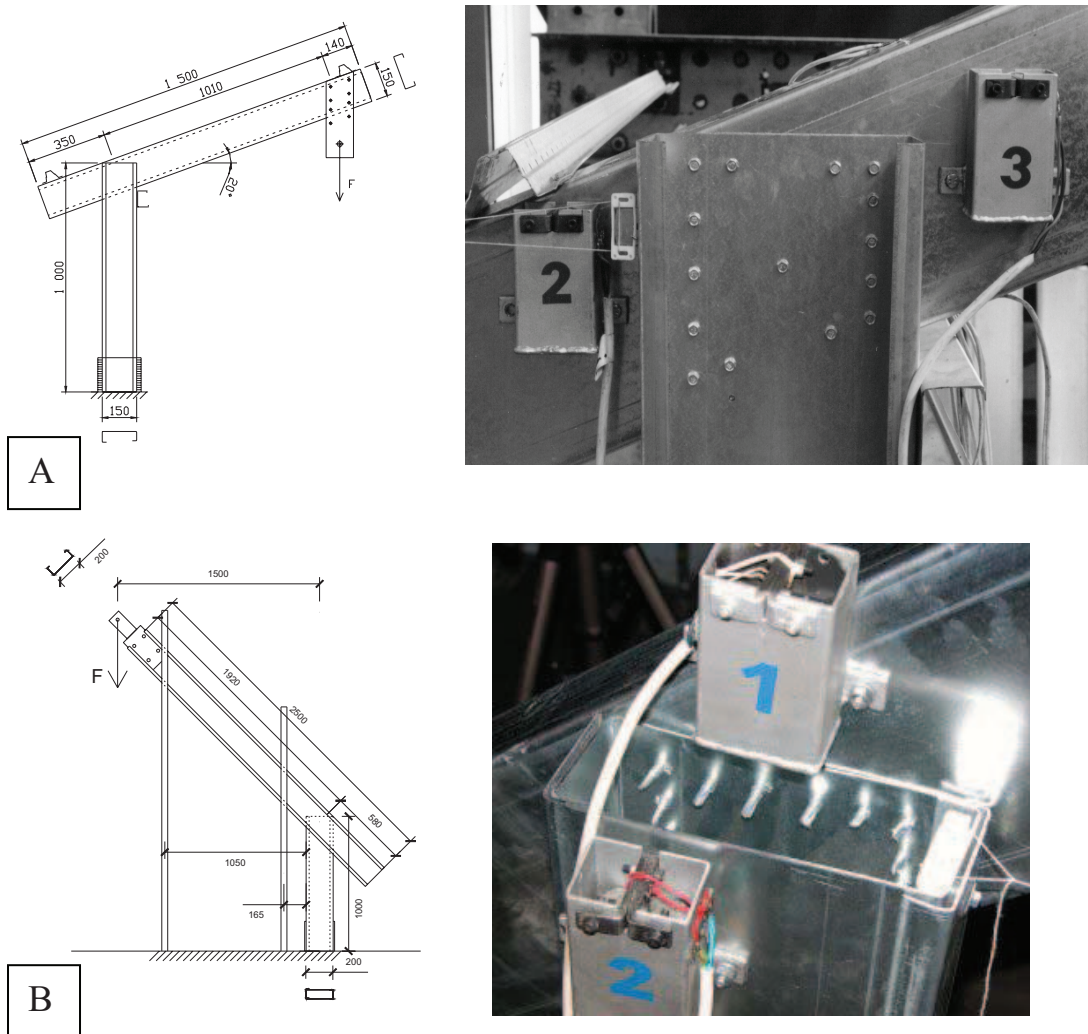
Figure 2.16: Frame corner test arrangements A and B.

Self-drilling screw connection tests

Self-drilling screws of the frame corner joints are tested under shear, in single overlapped condition in the "local" experiments. The screw types and sizes are the same as applied in the "global" tests. The plates of the specimens are partly cut out from the global specimens and partly obtained from base material of the C-profiles. Cold-formed steel strips of nominal yield strength of 350 MPa and ultimate tensile strength of 420 MPa, with thickness 1.0 – 3.0 mm are used. In the program one, two and three screwed specimens are tested, as shown in Fig. 2.17. In the tests the force-displacement relationship of the specimens are measured.
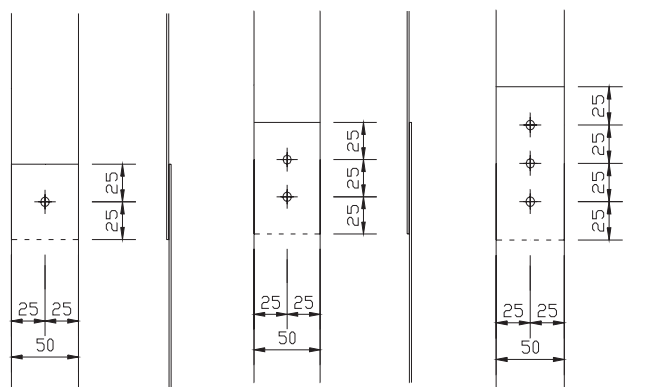
Figure 2.17: Self-drilling screw specimens.

2.4.3 Method of test result evaluation

The test results of the "global" joint and "local" screw tests are evaluated and presented in Dunai et al. (2000b), Fóti and Dunai (2000), and Dunai et al. (2000a), Fóti (2002), respectively. In the followings the two types of tests are combined and presented with the purpose to obtain correlation between the connector component and the joint behaviour. This background is required to develop a component based design method for the joint as it is presented by Fóti and Dunai (2002).

In the traditional approach a bolted connection under shear is designed by separating it into connector and base material, and checked on the bases of the "independent" failure by the application rules of the given standard. The results are connector resistances, from which the number of connectors can be determined.

In the investigated details the joint is assumed as a multi-component structure. The interaction in the element and connector behaviour requires another level of design methodology. The connector and its region are considered as a unit. The difference between the separations is similar to the difference between the meanings of connection and joint. This approach follows the philosophy that is used in the moment resisting end-plate joint design of Eurocode 3.

If the screw is separated with its region, the interactive failure modes that are affected by both screw and material properties can be followed. These possible interactive failure modes are obtained from the tests, as follows:
- tilting and pull-out,
- tilting and bearing,
- tilting and shear and
- tilting and tension failure of fastener.

It means, that only two failure modes: pure bearing failure (not experienced) and pure screw shear failure are non-interactive (independent modes). In all other cases the properties of the screws and the base material affect the behaviour of each other.

To connect the joint and reference local tests, the similarities and the differences of the conditions should be analyzed first.

Main similarities between the conditions of built-in and separated screw testing:
- same steel properties,
- same screw types,
- same steel plate thickness,
- mainly pure shear acts on the screws,
- single overlapped arrangements.

Main differences between the conditions of built-in and separated screw testing:
- different number and arrangement of screws,
- stiffening effect of the group of screws (less chance for pull-out in built-in screws),
- more in-plane bending due to the eccentricities (more chance for pull-out of built-in screws),
- local buckling and distortional buckling creates tension force in built-in screws,
- combined plastic deformations.

In the followings the combined (local and global) test results are presented and discussed for typical joint failure modes.

2.4.4 Behaviour modes

Joint failure mode #1: shearing

This failure mode is occurred when a relatively small number of screws are applied in relatively thick profiles. In this case the tilting and pull-out of fasteners cannot take place. The failure is observed in two ways, as shown in the moment-rotation diagrams of Fig. 2.18.

The first mode is illustrated in Fig. 18,a: the dominant screw is sheared suddenly, the downward steps over the top equals to the shearing resistance of the screws, one by one. By the hydraulic loading system the remaining load bearing capacity could be followed due to the active remaining screws. In the second mode at the maximum level of the moment the shearing failure is occurred in practically all screws at the same time and it resulted in a sudden collapse of the whole joint, as shown in Fig. 2.18,b.
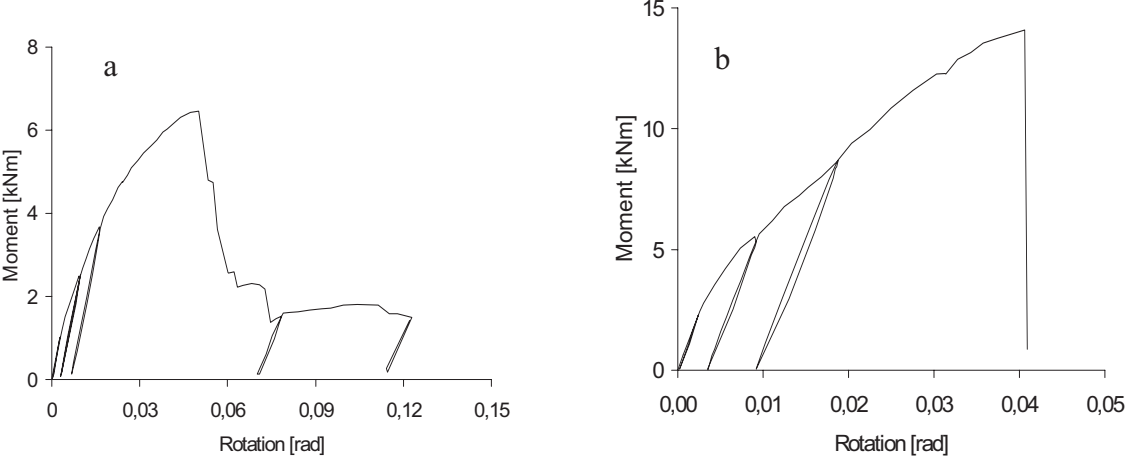
Figure 2.18: Joint shearing failure.

Figure 2.19 shows the force-displacement relationship of the reference local screw test using the same thickness of plates, failed by tilting and shearing mode. It is a two-screwed specimen. The plateau refers to tilting of the screws. After significant tilting one screw is sheared and the other is worked under reduced load bearing capacity; this screw is sheared after another plastic-like state, caused by further tilting. The phenomenon is illustrated in Fig. 2.20.
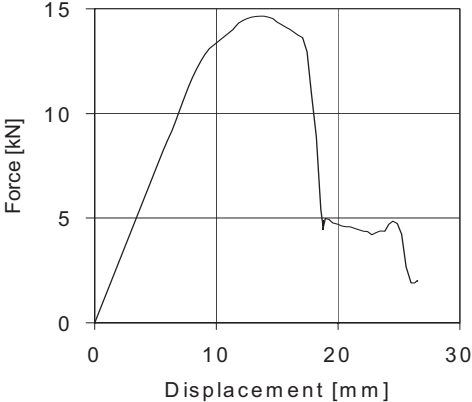
Figure 2.19: Screw tilting and shearing failure.

Figure 2.20: Illustration of shearing failures.

28

<u>Joint failure mode #2: pull-out</u>

This failure mode is experienced when a relatively small number of screws are applied in a relatively thin profile. The typical moment–rotation diagram can be seen in Fig. 2.21.
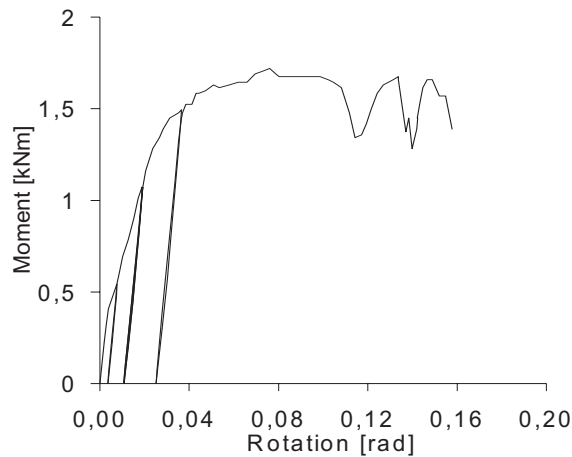
Figure 2.21: Joint pull-out failure.

At the ultimate level having large rotations of the screws' axes (over 60 degrees), the screws started to be pulled out from the section. On the curve it can be seen as the sudden reduction of the moment when one thread of the screw is jumped out. When it is stopped on the next thread the moment capacity is reached again. Then the phenomenon is continued and a series of jumping are appeared on the curve. This phenomenon results in a ductile behaviour. Plastic damages of the profiles are localized under the screws. In the case of specimen with more screws the beam finally is failed by local buckling as an interactive behaviour of element and connection, and classified as buckling type failure in the next section.

Figure 2.22 shows the force-displacement relationship of the reference local screw tests using the same thickness of plates, failed by tilting and pull-out mode. The failure mode is illustrated by the photo. As it can be seen the jumping phenomenon of the screw behaviour is inherited in the global joint behaviour.
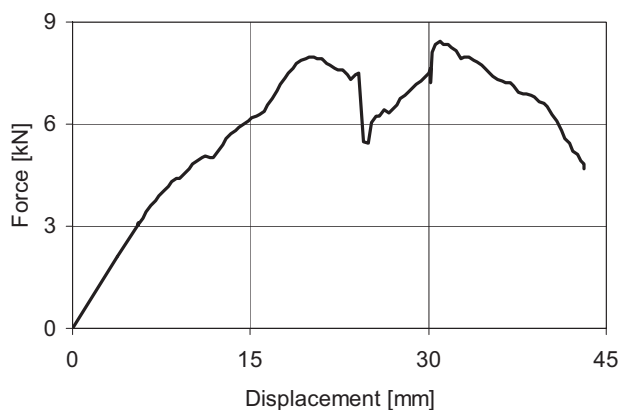
Figure 2.22: Screw tilting and pulling-out failure.

<u>Joint failure mode #3: buckling</u>

This phenomenon may appear in the column or in the beam, or in both of them. In all of these cases, the connectors are strong enough to avoid the failure but due to tilting and/or bearing the behaviour is combined. The place where local buckling appears is determined basically by the arrangement of the connectors. Using spread screws the profile's failure is experienced in three places: next to the joint in the beam (Fig. 2.23), just bellow the fasteners in the column (Fig. 2.24), and near to the joint in the column.
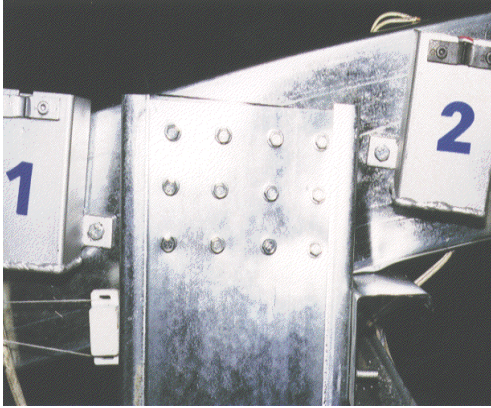
Figure 2.23: Buckling in the beam.

Figure 2.24: Buckling in the column.

Interaction of tilting/bearing and buckling:

This failure mode is obtained when strong enough connection is applied in thinner plates and the dominant behaviour is appeared in the element by plate buckling. Typically obtained in case of four groups of self-drilling screws (Fig. 2.24). Figure 2.25 shows that the initial part of the moment–rotation curve is nearly linear then the stiffness is gradually decreasing due to plastic deformation of the components and tilting of screws. In the ultimate behaviour under the screw group in the compression side of the joint local buckling is experienced, by an interaction of screw deformations.
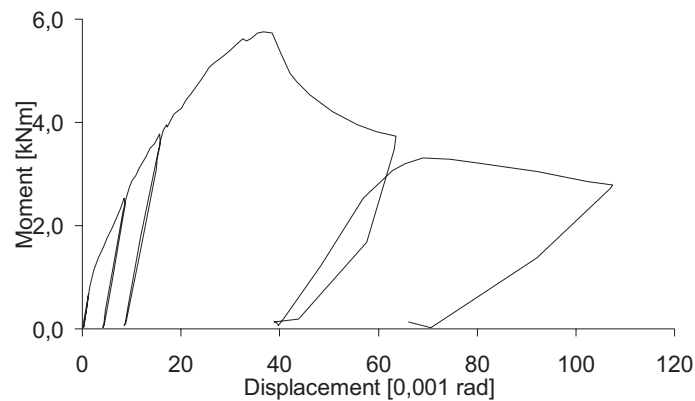
Figure 2.25: Interaction of tilting/bearing and buckling.

The reference screw local behaviour is shown in Fig. 2.26. The force-displacement diagram starts with a linear part, followed by plastic-like behaviour, caused by the interaction of tilting and bearing. A jump on the diagram shows a pull-out effect, followed by bearing failure.
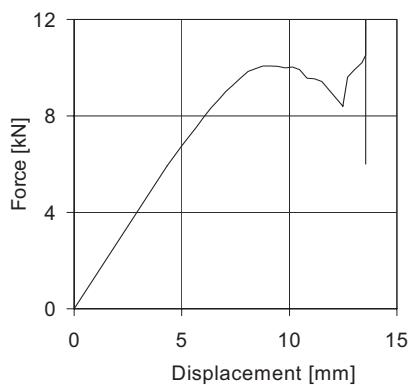
Figure 2.26: Screw tilting and bearing failure.

Interaction of tilting/pull-out and buckling

This failure mode is experienced when the tilting/pull-out resistance of the connection and the buckling resistance of the element are close to each other. It is typical when spread of self-drilling screws is used and in the behaviour the most effected screw (farthest from the centroid of the screw arrangement) is dominant. Due to the large deformation capacity of the screws by tilting, a long plateau of the moment-rotation curve at the ultimate level is obtained, as it is shown in Fig. 2.27. After significant plastic deformation, local buckling appeared in the beam due to the concentrated bolt force effect on the compression side of the profile. Due to the increased rotations of the joint in the dominant screws pull-out phenomenon is experienced. The reference local screw experiment is the same as it is shown in the case of failure mode #2 of the joint (see Fig. 2.22).
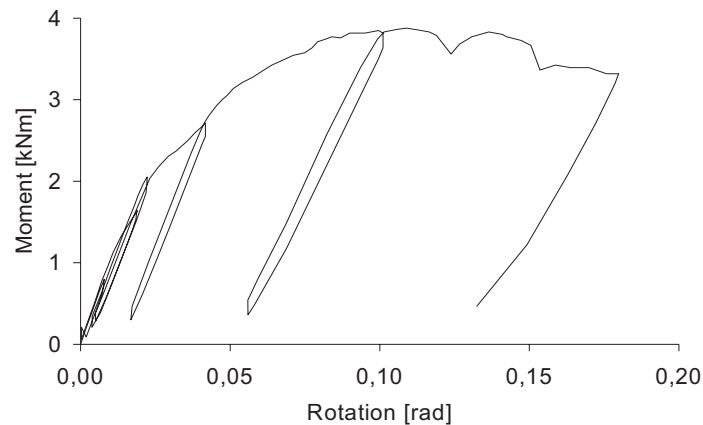
Figure 2.27: Interaction of tilting/pull-out and buckling.

Joint failure mode #4: distortion

Distortion of the column's web is typically appeared in specimens of test setup B when the connectors are strong enough to avoid shearing failure Fig. 2.28). This type failure mode is in certain correlation with the buckling resistance, but also greatly effected by the eccentricity of the setup. The phenomenon is the following: the web of the beam moves out from the initial plane first, from that point this plate should carry load as a bended plate and it causes decrease in the bending stiffness of the whole section, as it is shown in Fig. 2.29, with huge plastic deformations. On this load level a dominant tilting of the screws appears, the jumps refer to pull-out of screws. The reference screw local behaviour is illustrated in Fig. 2.22.

Figure 2.28: Illustration of distortion.   Figure 2.29: Distortion failure.
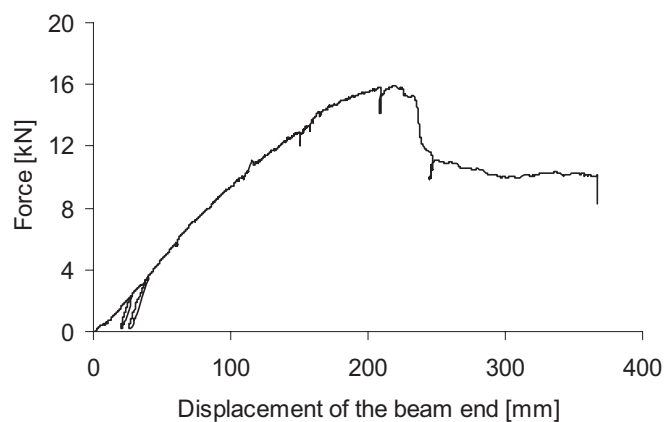
2.4.5 Application of experimental results

Prototype selection

The experimental findings show the advantages of the arrangements resulting buckling type failure modes. This results in similar type behaviour such as the cold-formed section and elements in the joint region ("uniformity of behaviour"). The initial stiffness and the resistance are reduced comparing to the section values due to the web-to-web connection (flanges are not connected), producing semi-rigid and partial strength joints. The observed level of semi-rigidity of the studied joints can create the required frame rigidity.

Accordingly the target phenomenon is the buckling behaviour mode, to be reached in the practical application. The detailing for the prototypes of the practical range of the frame corners is completed on the bases of the test experiences (prototype test), by the extrapolation from the joint and connection test results, using semi-empirical joint models. The new prototypes are tested in the same arrangement, for verification and design value determination (design test).

Design stiffness and resistances

From the test results of the joints and sheared screws the design resistances and stiffness are derived using the standardized test based design method of Eurocode 3 (previous version of EN 1993-1-3, 2005). The calculated stiffness values are built into the frame model; by the structural analysis using this model (i) the deflections of the frame are checked (serviceability limit state); (ii) the internal force distribution is obtained and (iii) the frame stability is investigated. The test based joint resistances are used in the ultimate limit state checking of the joint.

Joint model development

The combined screw and joint test results are used to derive design model for this type of joints (validation test); the model is detailed in Fóti and Dunai (2002).

The semi-empirical model uses the results of separated screw tests. The joint is handled as a rigid plate body, with spring point supports (with k_n stiffness) in the application points of the screws, as it can be seen in Fig. 2.30. The load-distribution is calculated using the force-displacement relationship as the spring characteristics (appears in k_n). The model is used with elastic, elastic-plastic and nonlinear springs to predict the initial rotational stiffness, the moment resistance and the whole moment-rotation diagram (rotational capacity).

The development of a more advanced FE model is started to be developed (Mihálffy, 2004). In the numerical study several modelling problems are solved, and showed the difficulties of the consideration of the complex phenomena (self-drilling screw deformation, restrained plate bending and buckling, friction, etc.).
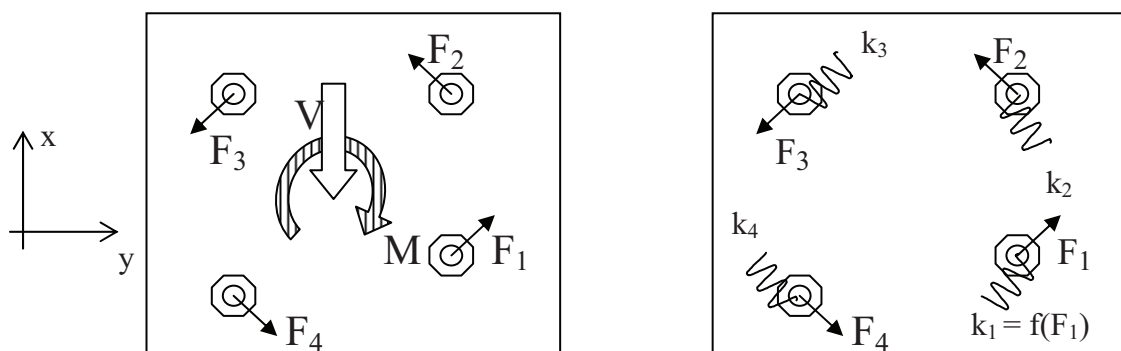
Figure 2.30: Joint model.

2.5 Cold-formed composite beam

2.5.1 Research program

The light-gauge composite floor is developed from cold formed C-profiles, and the concrete deck is installed on trapezoidal sheeting as a formwork. The composite action is provided by a modified formation of the generally used self-drilling screw beam-to-sheet connection. The first phase of the research focused on the behaviour of this novel composite connection with the purpose to determine the behaviour modes and the efficiency of the different structural detailing. On the basis of the pilot test results (Erdélyi and Dunai, 2002) a proper connection type is chosen for the application and additional tests are done with further parameters (Erdélyi and Dunai, 2004). A total of 42 specimens are investigated.

In the next phase from the push-out test results the design values of the connections (stiffness, resistance and ductility) are determined (Erdélyi and Dunai, 2004). By the consideration of the behaviour and design aspects of thin-walled structures and the measured stiffness of the composite connection, a design procedure is developed for the cold-formed composite beam using the partial shear connection method (Dunai et al. 2003/a), according to the recommendations of the previous versions of Eurocode 3, (EN 1993-1-3, 2005) and the Eurocode 4 (EN 1994-1-1, 2004). By the developed procedure design tables are determined for practical application (Dunai et al. 2003/b).

In the following phase six full-scale cold-formed composite beams are tested with the purpose of prototype verification and design model validation. The structural arrangement of the beams is equivalent of the developed floor system. The global geometry of the floor beams are the same, the effect of the thickness of the C-profile, the arrangement of the trapezoidal sheeting and different connection forms – in accordance with the results of the push-out tests – are investigated. The stiffness, the ultimate behaviour and the composite action of the beams are studied. The test results are compared with the resistance values of the proposed design method (Dunai and Erdélyi, 2005).

In this Section the experimental studies and their main results are presented emphasizing the observed structural behaviour. The main assumptions and the compared results of the design method are shown.

2.5.2 Push-out test program on shear connectors

The applied standard push-out specimens are shown in Fig. 2.31. In the experimental program altogether 42 specimens are tested; 12 specimens are investigated in parallel with the full-scale beam tests.

The global parameters of the specimens are the same: C-profile with 200 mm height, concrete deck of 50 mm thickness with normal quality (C16/20). The following local parameters are changed (see Fig. 2.31):

- fastening mode of screw,
- type and size of screw,
- embedment length,
- type and size of trapezoidal sheeting,
- placing mode of trapezoidal sheeting,
- thickness of C-section,
- concrete deck reinforcement.

Three types of fastening mode are used: two specimens are formed by normal fastening, when the self-drilling screw is drilled in standard way, fully into the sheets and the flange of the C-profile. Further two specimens are completed with the so-called inverse fastening, when the screw is drilled from inside of the flange then only the threaded part of the screw is embedded in the concrete. Most of the specimens (38) are formed by the partially drilling mode, when a part of the screw and the head are embedded in concrete with length ranges from 30 to 60 mm.

Four types of self-drilling screws are used: three different products of standard self-drilling screw (SFS SD6-6.3, HS-6.3, EJOT-JT2-6.3) and a special product (SFS SXC5-5.5) which is applied for sandwich panels.

Two types of trapezoidal sheets are applied: Lindab LTP45 and LTP20 of 0,5 and 0,7 mm thickness. The placing type is changed: in the positive arrangement the concrete fills the larger, and in negative arrangement the smaller rib. Most of the specimens (38) are formed by LTP20 trapezoidal sheeting.

A normal quality concrete (C16/20) deck of 50 mm thickness is applied above the rib in every specimen. 30 specimens are formed without reinforcement and in 12 specimens a minimal reinforcement ($\phi3,6/100$) is installed (same as in the tested composite beams).
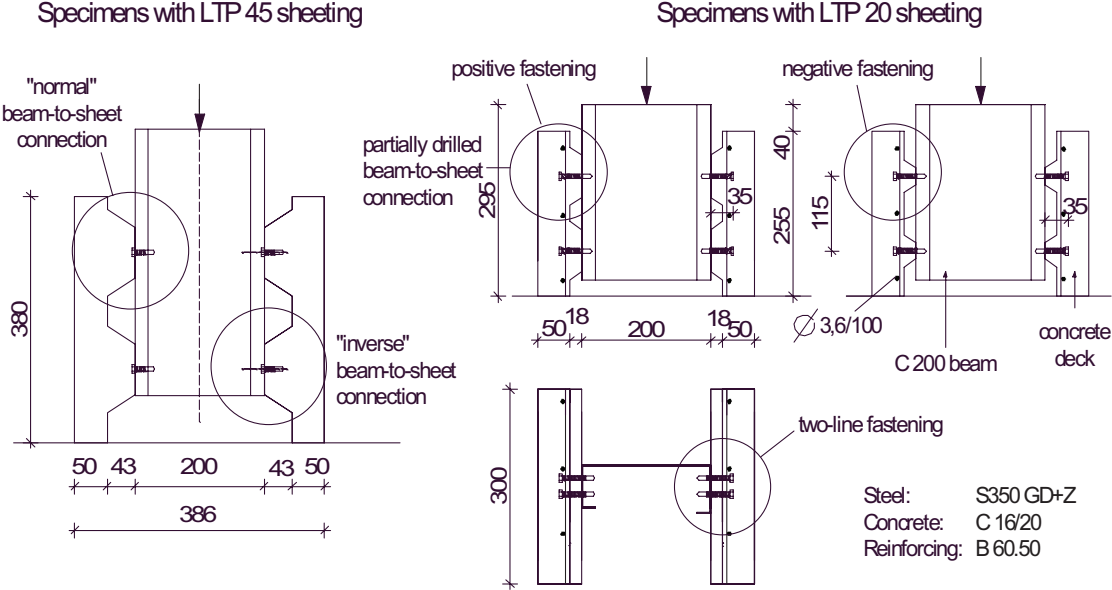
Figure 2.31: Push-out specimens.

In the tests the load is applied on the top end of the C-profile by hydraulic jack and the relative displacement is measured between the flanges and the base plate (the longitudinal deformation of the concrete deck is neglected). The measured load and displacement data are collected and monitored by the computer measurement system.

2.5.3 Behaviour of shear connectors

On the bases of the push-out test results the behaviour of the different types of composite connections are characterized by the different failure modes, as follows:

1. Pull-out failures
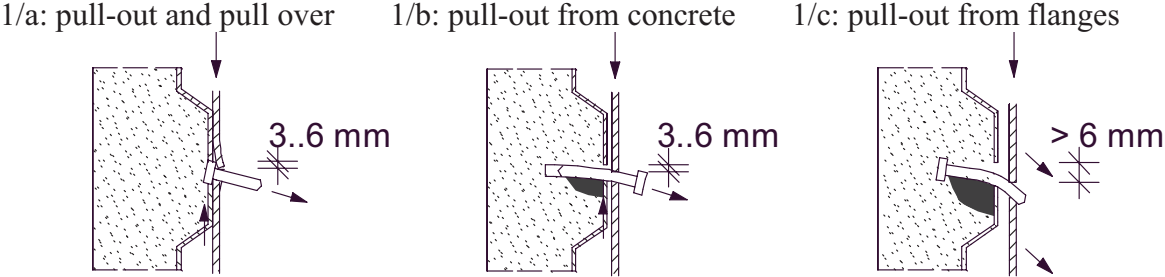
Figure 2.32: Pull-out failure modes.

In the tests three basically different types of pull-out failure modes are observed, as shown in Fig. 2.32. Pull-out and pull-over failure (1/a) occurs when the common beam-to-sheet connection is applied. Since only the head of the screw is embedded, under relatively low

force level the head pulls out from concrete. The stiffness is relatively low and the ultimate strength is approximately equivalent to the ultimate shear force of the beam-to-sheet connection without concrete. The dominancy of the steel components appears in the descending branch of the behaviour: after the ultimate load level is reached, a plastic zone appears in plates and the pull over failure occurs.

The importance of the test with the common beam-to-sheet connection is the studying of the composite effect of only the beam-to-sheet connection without concrete – for example in light-gauge floors with dry system – what is generally neglected. The experimentally determined stiffness and resistance of this connection provides with the basis for the further comparisons. More information about this connection is presented in Erdélyi and Dunai (2002).

Pull-out of the screw from the concrete (1/b) is observed when the strength of the concrete is sufficient but the embedment is not effective. It is experienced in case of the "inverse" fastening, when the bolt of the screw pulls out from concrete (Erdélyi and Dunai, 2002).

The third type of the pull-out failures is when the fastener pulls out from the flanges (1/c). When the screw has sufficient ductility, the relative displacement between the concrete deck and the flanges can be increased. Due to this the screw rotates and becomes more and more tensioned. If the displacement capacity of the screw is high enough, the screw can pull out from the flanges before the failure of either component.

2. Screw failures

2/a: dominant shear   2/b: shear and tension   2/c: dominant tension

< 3 mm   3..6 mm   > 6 mm
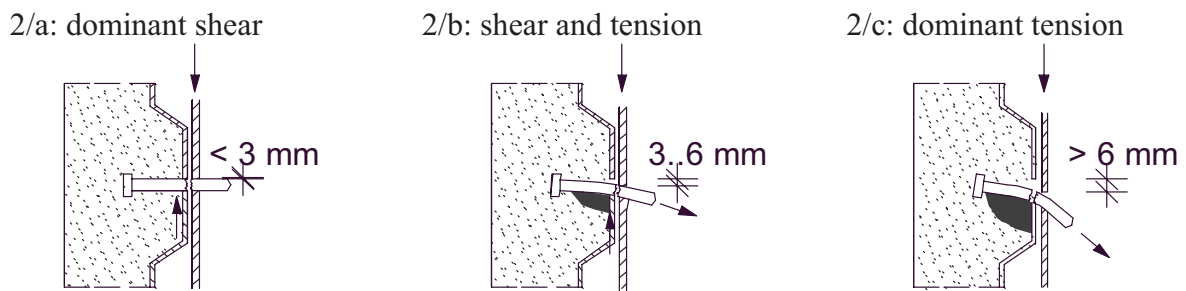
Figure 2.33: Screw failure modes.

Screw failure occurs when the embedment is effective and the strength of the concrete is relatively higher than the strength of the screw, as illustrated in Fig. 2.33. Two types of this failure mode are experienced depending on the displacement capacity of the screw. If it is relatively low the ultimate failure is the dominant screw shear (2/a).

If the displacement capacity of the screw is relatively high the rotation of the screw can be occurred and the screw becomes tensioned. Depending on the displacement capacity of the screw the final failure due to the combination of shear and tension (2/b), or dominant tension (2/c).

3. Concrete failure

Concrete failure occurs when the strength of the screw is relatively higher than the strength of the concrete, as shown in Fig. 2.34. Depending on the direction of the transmitted force from the connection, shear or tension type failures are observed. If the relative displacement capacity is relatively low the concrete deck fails by the effect of shear forces (3/a), with concrete cone failure surface and/or with a longitudinal shear crack.

If the displacement capacity of the screw is relatively high the screw and also the concrete becomes tensioned and the final failure is the tension failure of the concrete deck (3/b). The failure surface is also a crack cone similar to the shear failure. This behaviour results in the largest displacement capacity, similar to the dominant tension failure of the screw (2/c).

3/a: shear failure   3/b: tension failure
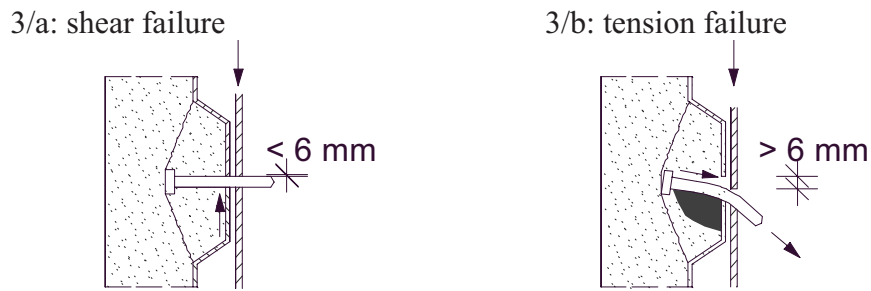
Figure 2.34: Concrete failure modes.

The dimension of the crack cone highly depends on the geometry of the rib. Narrow crack cone is observed when LTP20 trapezoidal sheeting with positive fastening mode is applied. Due to the relatively large dimensions of the rib the behaviour is similar to a deck without rib. The failed deck can be seen in Fig. 2.35,a. In case of negative fastening, the crack surface is a common cone with app. 45 degrees, as shown in Fig. 2.35,b. It has relatively large extension when two-line fastening is applied. In Fig. 2.35,c a combined failure mode is shown: the upper connection fails by the pull-out of the screws from the flanges (1/c) and the lower connection fails by the tension of the concrete (3/b).
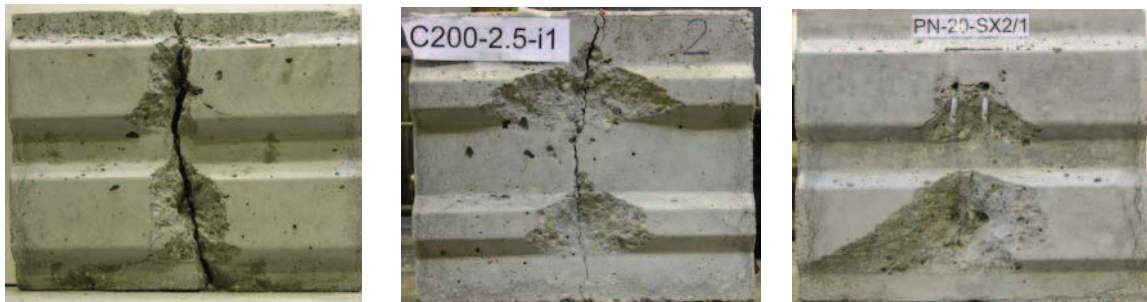
Figure 2.35: Different failure surfaces of the concrete deck.

The observed behaviour modes are illustrated by the shear force/screw – relative displacements diagrams in Fig. 2.36.
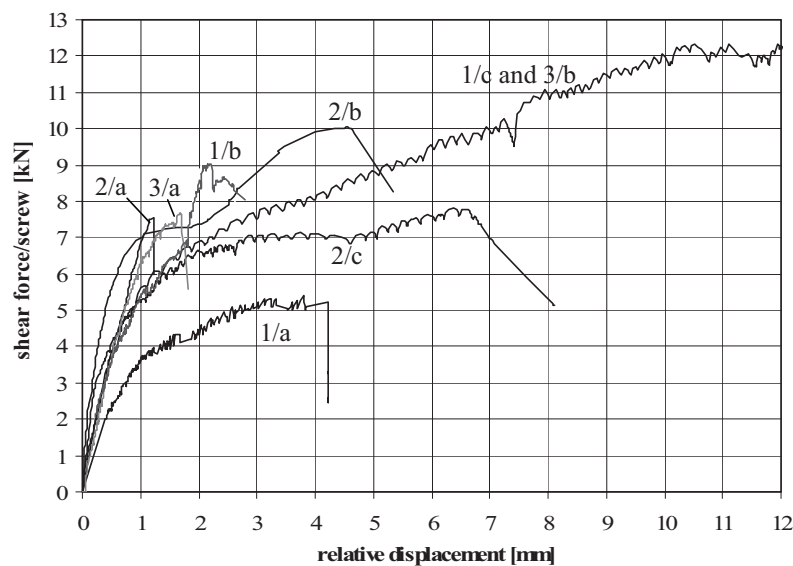
Figure 2.36: Typical load-displacement diagrams of different failure modes.

2.5.4 Design characteristics of shear connectors

Based on the measured load-displacement diagrams the design characteristics of the composite connections are determined. The derivation of the design values of the stiffness and resistance is generally based on the Eurocode 4, (EN 1994-1-1, 2004) recommendations; its interpretation and details can be found in Erdélyi and Dunai (2004).

In Table 2.7 a summary is presented about the geometry, the design values and the failure modes of the selected 25 specimens. The specimens are grouped by the screw type, the fastening mode and the thickness of the C-profile. On the basis of the experimental observations and the determined design values the following evaluation can be done.

Stiffness

In general it can be stated that the stiffness values show large scatter. The stiffness of the connection increases when the thickness of the profile increases, but the other connection parameters (connector type, embedment, rib form, existence of reinforcing) have no significant influence on it. Important observation that the highest stiffness values are found in case of connections with such small displacement capacities what do not allow the application in practical design. Note that the measured average stiffness of the studied composite connections about 5% of the stiffness of the generally used headed stud connectors in hot rolled composite beams.

It can be concluded that the consideration of the connection flexibility is essential in the serviceability limit state design of the cold-formed composite beam.

	GEOMETRY						DESIGN VALUES				
	screw type-fast-line	t_{beam} [mm]	fast. mode	sheet type	h_{emb} [mm]	Rein-forc.	$P_{failure}$ [kN]	P_{Rd} [kN]	stiffness [kN/m]	max. displ. [mm]	failure mode
1.	SD-n-1	1,5	pos	LTP45-0.5	0	no	5,307	3,184	4500	3,3	1/a
2.	SD-i-1	1,5	pos	LTP45-0.7	30	no	9,107	5,464	7400	2,2	1/b
3.	SD-i-2	1,5	pos	LTP45-0.7	30	no	12,517	7,510	7400	2	3/a
4.	HS-p-1	1,5	pos	LTP45-0.5	30	no	7,546	4,528	7700	1,2	2/a
5.	HS-p-2	1,5	pos	LTP45-0.5	30	no	12,45	7,470	16400	1	2/a
6.	HS-p-2	1,5	pos	LTP45-0.5	60	no	16,494	9,896	16200	3,2	2/b
7.	**EJ-p-1**	**1,5**	**pos**	**LTP20-0.5**	**35**	**no**	**6,489**	**3,894**	**7200**	**6**	**3/a**
8.	**EJ-p-1**	**1,5**	**pos**	**LTP20-0.5**	**35**	**yes**	**7,614**	**4,568**	**3000**	**5,8**	**2/b**
9.	EJ-p-1	1,5	neg	LTP20-0.5	35	no	4,882	2,930	5100	1,7	3/a
10.	EJ-p-2	1,5	pos	LTP20-0.5	35	no	11,472	6,883	8800	2,2	2/b
11.	EJ-p-2	1,5	neg	LTP20-0.5	35	no	8,235	4,941	8600	1,1	3/a
12.	EJ-p-1	2,0	pos	LTP20-0.5	35	no	6,614	3,969	6500	2,5	3/a
13.	**EJ-p-1**	**2,0**	**pos**	**LTP20-0.5**	**35**	**yes**	**9,912**	**5,947**	**5200**	**6**	**2/b**
14.	EJ-p-1	2,0	neg	LTP20-0.5	35	no	6,584	3,950	6300	4,2	3/a
15.	**EJ-p-1**	**2,0**	**neg**	**LTP20-0.5**	**35**	**yes**	**6,702**	**4,021**	**11000**	**7**	**2/c**
16.	EJ-p-2	2,0	pos	LTP20-0.5	35	no	11,054	6,632	n.a.		3/a
17.	EJ-p-2	2,0	neg	LTP20-0.5	35	no	7,993	4,796	6000	1,2	3/a
18.	EJ-p-1	2,5	pos	LTP20-0.5	35	no	8,075	4,845	5200	3,2	3/a
19.	**EJ-p-1**	**2,5**	**pos**	**LTP20-0.5**	**35**	**yes**	**13,008**	**7,805**	**10000**	**7**	**3/b**
20.	EJ-p-1	2,5	neg	LTP20-0.5	35	no	7,403	4,442	7400	4,5	3/a
21.	EJ-p-2	2,5	pos	LTP20-0.5	35	no	13,361	8,017	5300	1,5	3/a
22.	EJ-p-2	2,5	neg	LTP20-0.5	35	no	8,429	5,057	5700	1,3	3/a
23.	SXC-p-1	1,5	pos	LTP45-0.5	45	no	10,053	6,032	14600	4,54	2/b
24.	**SXC-p-1**	**2,0**	**pos**	**LTP20-0.5**	**35**	**yes**	**12,21**	**7,326**	**6000**	**10**	**1/c and 3/b**
25.	**SXC-p-2**	**2,0**	**pos**	**LTP20-0.5**	**35**	**yes**	**19,056**	**11,434**	**11000**	**8**	**1/c and 3/b**

Table 2.7: Geometry and design characteristics of the selected specimens.

Resistance

In general it can be stated that the experienced ultimate load highly depends on the geometry of the connection and it has strong relationship with the observed failure modes.

Significant increase of resistance can be reached by the increasing of the thickness of the flanges, due to the more efficient clamping of the cantilever. The measure of growth ranges from 2 to 31%. In case of two-line connections the effect of the thickness is relatively lower.

Concerning to the concrete rib dimensions when positive fastening with LTP20 trapezoidal sheeting is used, the ultimate load is higher in most cases than in case of inverse fastening due to bigger sizes of the ribs.

When reinforcement is used in the deck the resistance is significantly increased (from 17 to 61%, as it is illustrated in Fig. 2.37 *a* and *b* curves).

The applied screw type highly influences the resistance. As it is described in the behaviour modes when a screw with large displacement capacity is applied, a favourable failure mode occurs with higher resistance. This effect is in the curves of Fig. 2.37: the difference between the equivalent connections with different screw type is 23 % (*b* and *d* curves). In the first case (curve *b*) the combination of screw shear and tension (2,b), and in the second case (curve *d*) concrete tension (3,b) and screw pull-out from flanges (1,c) are occurred.

According to the range of the experimentally determined design resistances it can be concluded, that in the ultimate limit state design the partial shear connection method to be used in the practical design (the longitudinal shear force cannot produce the full moment capacity of the composite cross-section in the case on the practically applied shear lengths).
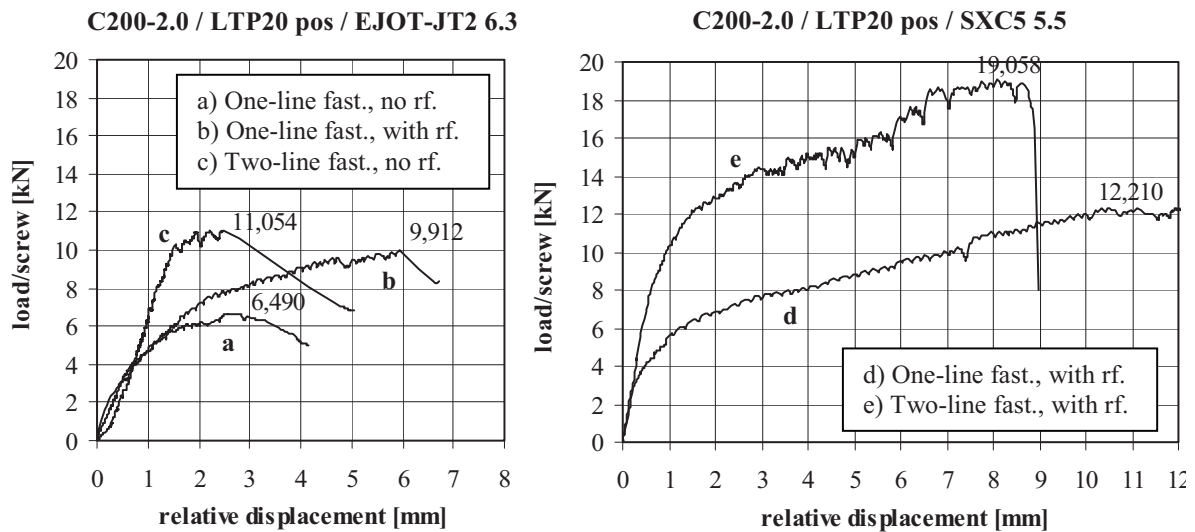
Figure 2.37: Load-displacement curves of specimens with 2.0 mm flange thickness.

Ductility

In the experimental programme a strong relationship is observed between the relative displacement capacity and the failure mode. The displacement capacities belonging to each failure modes are shown in Figs. 2.32-2.34.

When pull-out and pull-over (1/a) or pull-out from concrete (1/b) failures occur the connection shows medium relative displacement capacity (between 3 and 6 mm): the rotation of the screw is allowed, but the resistance of the components (1/a) or the anchorage length (1/b) is not effective.

In case of shear failure of the screw (2/a) or the concrete (3/a), the relative displacement capacity of the connection is low (under 3 mm). When the displacement capacity of the screw

38

allows the rotation to some degree, the combination of shear and tension of the screw (2/b) failure occurs which increase the displacement capacity.

The specimens that fail by dominant tension failure (1/c, 2/c, 3/b) have high relative displacement capacities. This favourable phenomenon is well illustrated by the deformed shape of the fasteners and pertinent load – displacement curves in Fig. 2.38.

In accordance with Eurocode 4 proposal the relative displacement of the connection should be over 6 mm in order to apply the plastic design formulas. The connectors which have high relative displacement capacities satisfy to this requirement, so these can be used in the practical design.
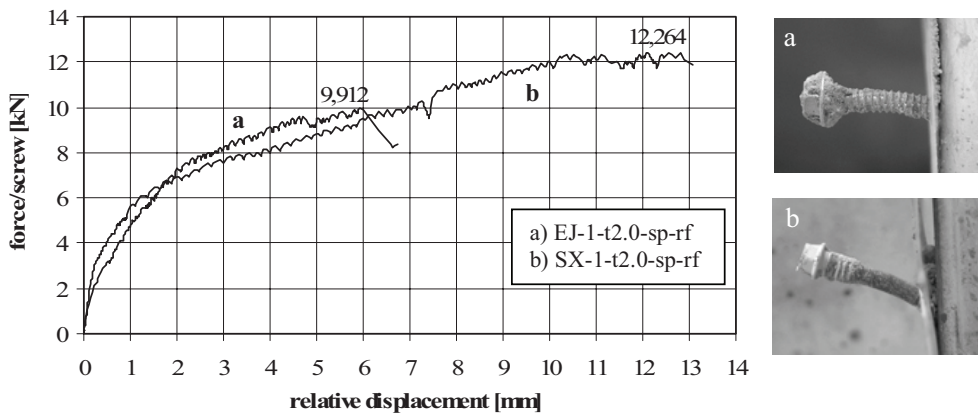
Figure 2.38: Illustration of high relative displacement capacity.

Practical application

On the bases of the experimental observations, derived design values (design test) and standard recommendations the practically applicable composite connections are defined. The specimens with favourable behaviour are selected (these are bolds in Table 2.7). These arrangements are used in the full-scale beam tests (prototype test), detailed in the next Section and in the practical design (Section 2.5.7).

2.5.5 Cold-formed composite beam tests

Six full-scale beam specimens are investigated with the same global parameters as follows: C-profile with 200 mm height, LTP20 trapezoidal sheeting, and concrete deck of 50 mm thickness above the rib, with normal quality (C16/20). The following parameters are modified: the thickness of the C-profile, the type and the formation of the composite connection, and the arrangement of the trapezoidal sheet (positive and negative), as shown in Fig. 2.39 and detailed in Table 2.8.

	L	d_{beam}	C-profile	Sheet	screw type	emb. length	line
Specimen	[mm]	[mm]	height-thickn.	height-th.-arr		[mm]	
1. FN-15-EJ			C200-1.5	LTP20-0.5 pos.	EJOT JT2-6.3	35	1
2. FN-20-EJ			C200-2.0	LTP20-0.5 pos.	EJOT JT2-6.3	35	1
3. FI-20-EJ			C200-2.0	LTP20-0.5 neg	EJOT JT2-6.3	35	1
4. FN-25-EJ	5980	600	C200-2.5	LTP20-0.5 pos.	EJOT JT2-6.3	35	1
5. FN-20-SX1			C200-2.0	LTP20-0.5 pos.	SXC5-5.5	45	1
6. FN-20-SX2			C200-2.0	LTP20-0.5 pos.	SXC5-5.5	45	2

Table 2.8: Geometrical parameters of the composite beam specimens.

The applied span (5980 mm in every case) is given by the multiple of the distance between the screws that is determined by the distance of the rib (115 mm). The relatively large span is required to investigate the full composite action.

The specimens are built by two C-profiles (with 600 mm distance) and the attached concrete deck (with 1200 mm width), as shown in Fig. 2.39. This arrangement provides the uniform load distribution between the beams, and ensures the parallel measuring in the beams.

In the tests two concentrated loads are applied by a hydraulic jack, as shown in the experimental arrangement in Fig. 2.39. The concentrated forces are relatively close to each other: the distance is 800 mm, resulting in a long longitudinal shear transfer.

To prevent the lateral distortion of the lower flange a bracing system is used: the bottom flanges are joined by hat profiles and transverse trusses are applied in three cross-sections along the beam.

The measured values are the load, the vertical displacements, the relative displacement between the top flange of the C-profile and the concrete deck, and the stress distribution in the C-profiles in the mid-span. These values measured and in parallel monitored for both C-sections. The loading and the measuring system can be seen in Fig. 2.39.

Figure 2.39: Composite beam specimen and test arrangement.

2.5.6 Behaviour of cold-formed composite beams

Behaviour under service load level

The initial stiffness and the elastic behaviour are investigated by the structural response under 1 kN load/beam level. The measured displacement $e_{1kN.test}$ ranges from 1,03 to 1,56 mm, as shown in Table 2.9. The measured values are compared to the calculated mid-span deflections $e_{1kN.calc}$, using ideal cross-section rigid composite connections. The comparison of the values shows the effect of semi-rigid composite connections: the ratio of the calculated (rigid) and the measured deflections ranges from 0,91 to 0,95 that means relatively high initial stiffness, and relatively low difference between the connections in the initial state.

In the next step the load level belongs to the L/300 deflection limit (19,93 mm) is determined. The calculated loads in case of rigid connections ($F_{L/300.calc}$) and the measured loads ($F_{L/300.test}$) are detailed in Table 2.9. The ratio of the two values ranges from 0,69 to 0,77; the observed scattering is larger and the results show the nonlinearity of the composite connection behaviour under service load, inherited from the nonlinearity of the composite connection behaviour in this range of load (as shown in the load – displacement diagrams of the previous Section).

40

specimen	1 kN load			Service load		
	$e_{1kN.calc}$ full interaction	$e_{1kN.test}$	$e_{1kN.calc}/$ $e_{1kN.test}$	$F_{L/300.calc}$ full interaction	$F_{L/300.test}$	$F_{L/300.calc}/$ $F_{L/300.test}$
	[mm]	[mm]		[kN]	[kN]	
1. FN-15-EJ	1,415	1,56	0,91	14,089	9,760	0,69
2. FN-20-EJ	1,126	1,19	0,95	17,710	13,650	0,77
3. FI-20-EJ	1,131	1,22	0,93	17,630	13,000	0,74
4. FN-25-EJ	0,946	1,03	0,92	21,067	15,804	0,75
5. FN-20-SX1	1,126	1,19	0,95	17,710	12,450	0,70
6. FN-20-SX2	1,126	1,19	0,95	17,710	13,530	0,76

Table 2.9: Deflections of composite beam specimens.

Ultimate behaviour

Figure 2.40 shows the load – deflection relationship of the composite beam specimens: Fig. 2.40,a for specimens EJOT-JT2-6.3 screws and Fig. 2.40,b for specimens with SXC5-5.5 screws. Two different types of ultimate behaviour are observed: the failure of the screw connector (longitudinal shear failure), and the plastic bending failure of the composite beam.

The longitudinal shear failure is observed in the case of composite connection with smaller ductility, in the specimens with EJOT screws (curves *a*, *b*, *c* and *d* in Fig. 2.40). The rotation of the screw due to the relative displacement and the separation of the concrete deck from the sheet can be seen in the Fig. 2.41,a and b. The failure is occurred by the unzipping phenomenon. Figure 2.41,c shows the behaviour of FI-20-EJ specimen after the failure of the connection; as it is shown after the total load is transmitted to the C-sections the buckling of the compressed zone is occurred.

In the cases of specimens FN-20-SXC1 and FN-20-SXC2 plastic bending failure is observed. In the cross-sections of the concentrated loads plastic hinges are developed. First, due to the eccentric loading of the C-profile, significant distortion of the cross-sections is experienced in the nonlinear range, as shown in Fig. 2.41,e. Then the yielding is started and developed in the whole C-profile, as it can be seen in Fig. 2.42. When the ultimate strain is reached the fracture of the bottom flange is occurred in the net cross-section at the fastened hat profile (lateral bracing), as shown in Fig. 2.41,e. The contraction of the steel flange can be clearly seen in the figure due to yielding before the fracture, and the deformation of the hat profile due to the torsion of the cross-section. Figure 2.41,f shows the cracked concrete deck at the ultimate load level, as a secondary effect of the large displacement the bottom side of the thin concrete deck becomes tensioned and results in the cracks.
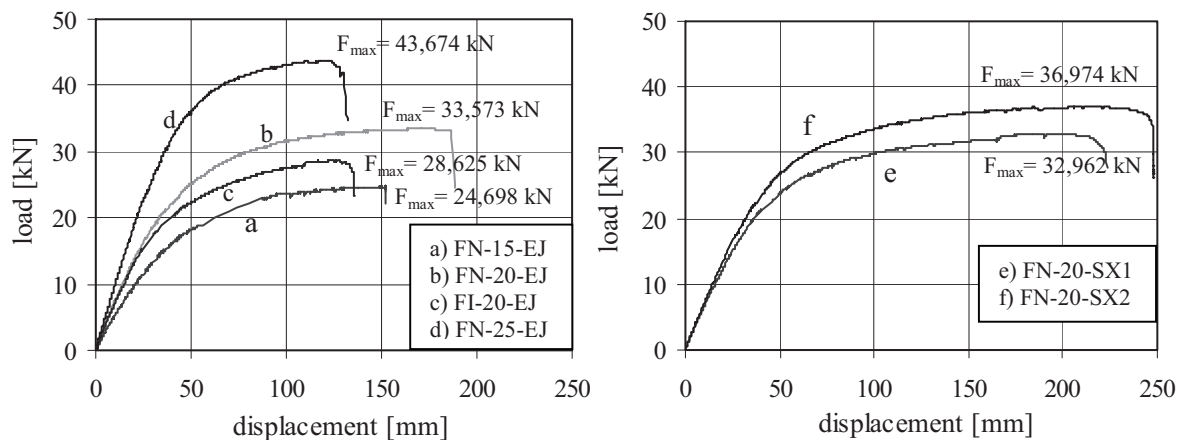

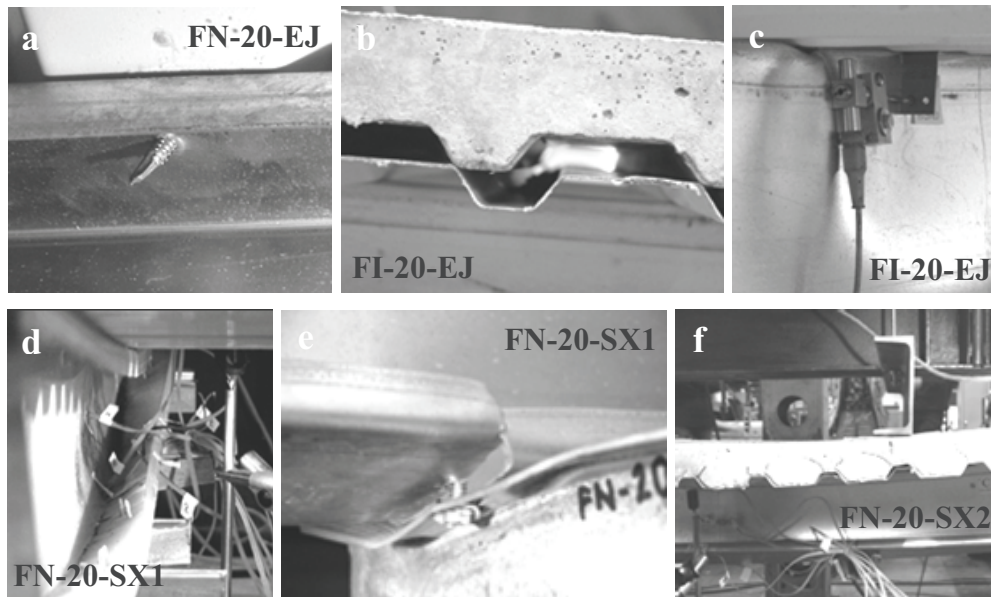Figure 2.40: Load – deflection diagrams of composite beam specimens.

Figure 2.41: Ultimate behaviour: a) rotation of screw b) separation of sheet and concrete deck
c) local buckling d) distortion e) tension failure f) concrete cracks.

The specimens FN-20-EJ, FN-20-SX1 and FN-20-SX2 show the most favourable plastic behaviour and the largest deformation capacity. The other specimens show lower but reasonable plastic performance. The maximum displacement ranges from 150 to 240 mm (L/46...L/24).

The maximum loads are between 24,70 kN and 43,67 kN; the maximum load to SLS load ratio ranges from 2,20 to 2,76 (load related to L/300 deflection). The ratio of the highest and lowest maximum load value is 1,77. The behaviour of the specimen with positive sheet fastening is favourable: the difference between the equivalent specimens with positive and negative sheet fastening is 17% in the maximum load, and 38% in the maximum displacement (curves b and c in Fig. 2.40). The effect of one- or two-line-connector is not significant in the case of ductile connectors: the resistance of the FN-20-SX2 specimen (curve f) is only 12% higher than the resistance of FN-20-SX2 specimen (curve e).

Composite action

The composite action is studied by measuring the relative displacement between the top flange of the C-profile and the concrete deck and by the stress distribution in the mid-span.

The relative displacement is measured in four cross-sections of the shear zone, as shown in the test arrangement in Fig. 2.39. Figure 2.42 shows the load – relative displacement diagrams of FN-20-SX1 specimen in three measured cross-sections (c2, c3, c4). The diagrams well illustrate the behaviour of the connection in accordance with the results of the push-out tests. In the ultimate state the connections show plastic behaviour with sufficient ductility. The rotation of the screws can be seen on the right hand side of the figure.

In Fig. 2.42 well illustrated the high initial stiffness and the significantly decreased secant stiffness at the service load level (app. 50% of the ultimate load). This fact explains the experiences on the global rigidity under the 1 kN and the service load levels.

 The stress distribution is studied by measuring the strains in the middle cross-section on both sides of the web and in the bottom flange, as shown in Fig 2.39. Figure 2.43 shows the changing of the strains along the cross-section in case of FN-20-SX1 specimen.
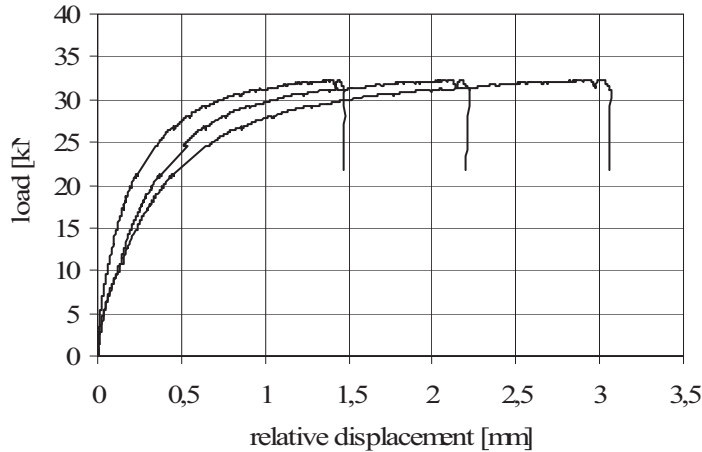
Figure 2.42: Load – relative displacement diagrams – FN-20-SX1 spec., c2, c3, c4 sections.

The whole C-section is under tension that shows the composite behaviour, by developing the plastic moment. The plastic strain increases toward the bottom side of the web and the difference between the strains in the lower side of the web and in the bottom flange shows the effect of cross-section distortion. The stress distribution results are very similar for all the specimens; the full steel section of the five specimens with normal sheet fastening is tensioned, in the case of FI-20-EJ specimen with negative sheet fastening, the top flange is compressed through the loading process. The compression in the top flange results in buckling in ultimate range.

The experimental program on cold-formed composite beams proved the applicability of plastic design in which the longitudinal shear is considered by the partial shear connection method of the Eurocode 4 standard.
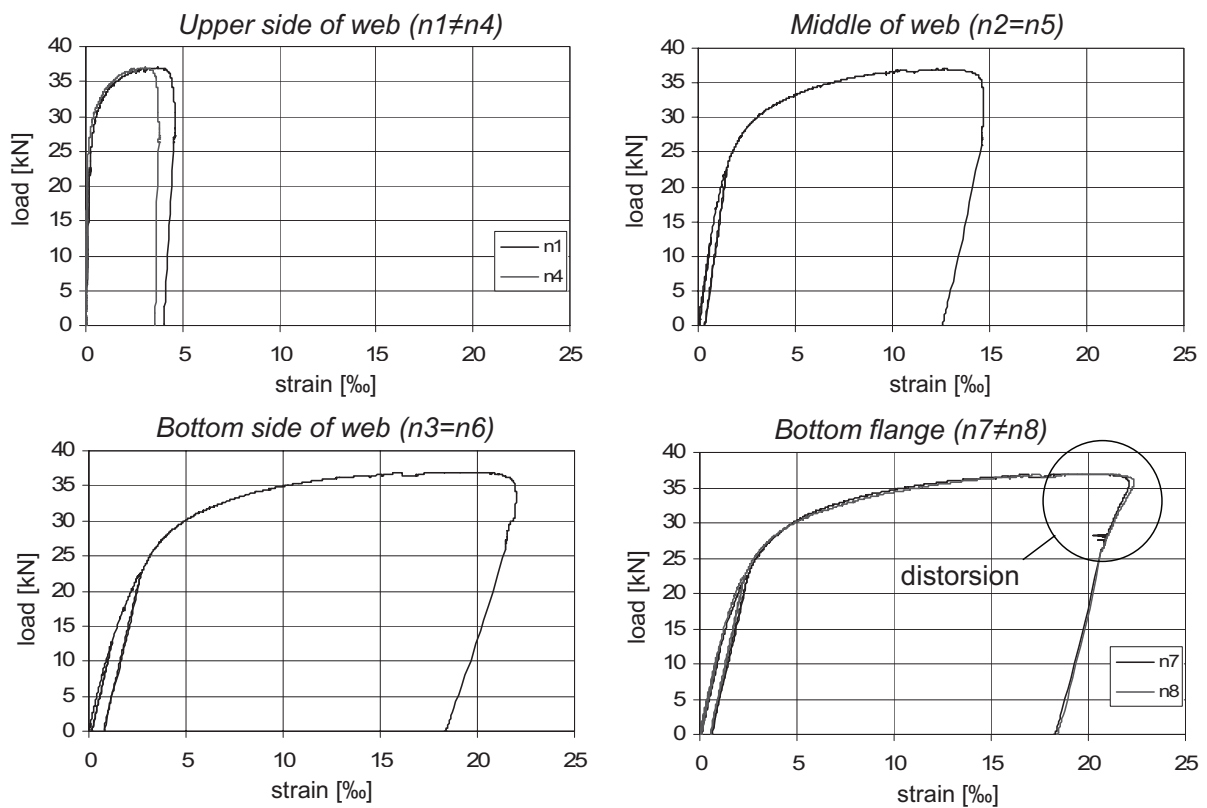

Figure 2.43: Stress distribution in the mid-span – FN-20-SX1 specimen.

2.5.7 Design method for cold-formed composite beams

In the research and development work design models are developed for both ultimate and serviceability limit state checking.

The ULS design model concentrates on the moment resistance calculation considering (i) the specialities of the cold-formed section using the Eurocode 3 rules (EN 1993-1-3, 2005) and (ii) the partial shear connector method of the Eurocode 4 (EN 1994-1-1, 2004). The Eurocode models are extended, and the proposed model is based on the plastic resistance of the composite cross-section, assuming elastic-plastic stress-strain distribution, considering the local buckling of the cold-formed section and the effects of the partial shear connectors. The main features of the design model are summarized in the followings, more details can be found in Dunai et al. (2003/a).

In Eurocode 4 the bending and the longitudinal shear resistances can be checked in a combined way on the basis of the moment resistance diagram. This diagram defines the moment resistance of any cross-section of the beam on the basis of the longitudinal shear length and the full moment capacity of the composite cross-section (assuming full composite action). At the end of the composite beam the longitudinal shear is zero, and the moment resistance is equal to the moment resistance of the steel cross-section part. In the cross-sections, with a suitable distance from the end – in which the longitudinal shear can create the required compressive force in the compressed part of the section for full plasticity – the moment capacity equals to the full plastic resistance. In between the partial moment resistance can be calculated on the basis of the compressive force produced by the longitudinal shear on the actual longitudinal shear length. Once the moment capacity at any cross-section is known, the design can be carried out by comparing the actual bending moment and the moment resistance.

The full plastic resistance can be calculated by assuming the normal stress is equal to the yield stress at any point of the cross-section. In the cold-formed section, however, the local buckling should be taken into account, so elastic stress distribution must be considered in the compressed zone, while plastic or elastic-plastic stress distribution is still allowed in the tensioned zone. In addition, the effect of local buckling must be considered by using effective width approach in the compressed plane elements. The stress distribution satisfy to this requirement is shown in Fig. 2.44.
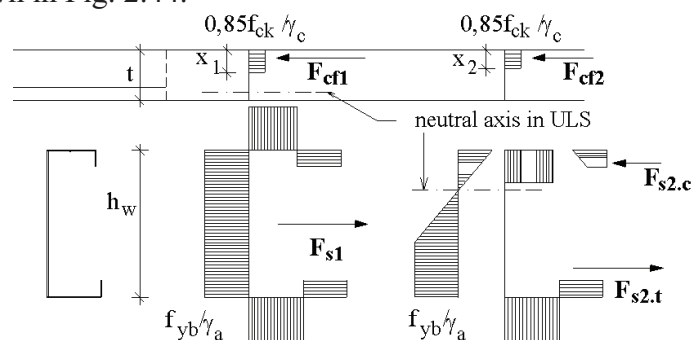
Figure 2.44: Assumed stress distribution in ULS.

The longitudinal shear forces can be calculated by the assumption of plastic distribution of the forces between the individual shear connectors, so it is equal with the sum of the forces belong to the "yielding" of the shear connectors from the end to the given cross-section. The shear resistance of the composite connection is determined by the push-out tests. The stress resultant of the concrete part of a given cross-section is equal to this longitudinal shear force. On the basis of this normal force equilibrium and compatibility requirements the partial moment resistance of the given cross-section can be calculated by an iterative way.

The design model and the developed procedure are applied to derive the design resistance of the composite beam test specimens. Table 2.10 summarizes the experimental results and the pertinent design resistances. The resistance of the load per a beam, F_{Rd} is calculated based on the design values of the material properties and the test based design resistance of the shear connection, determined by push-out tests.

The table shows the comparison at different load levels: the ratio of the calculated design load (F_{Rd}) and measured ultimate load ($F_{max.test}$), and the ratio of the load level belong to the serviceability limit value of L/300 deflection ($F_{L/300.test}$) and design load.

It is found that the design load is 55 to 71% of the maximum load and the serviceability limit state value (belongs to L/300 deflection) is 47 to 67% of the design load level.

The results show that the design model follows the observed behaviour and prove the safety in the ultimate limit state level (ratio of failure and design loads are between 1,4 and 1,8).

Specimen	$F_{max.test}$	F_{Rd}	$F_{L/300.test}$	$F_{Rd}/$ $F_{max.test}$	$F_{L/300.test}/$ $F_{Rd.nom}$	$e_{1kN.test}$	$e_{max.test}$	Failure mode
	[kN]	[kN]	[kN]			[mm]	[mm]	
1. FN-15-EJ	24,7	15,74	9,76	64%	62%	1,56	150	screw failure
2. FN-20-EJ	33,57	21,34	13,65	64%	64%	1,19	180	screw failure
3. FI-20-EJ	28,63	19,35	13,00	68%	67%	1,22	130	screw failure
4. FN-25-EJ	43,67	24,14	15,80	55%	66%	1,03	125	screw failure
5. FN-20-SX1	32,96	23,50	12,45	71%	53%	1,19	220	plastic bending failure
6. FN-20-SX2	36,97	29,12	13,53	79%	47%	1,19	240	plastic bending failure

Table 2.10: Comparison of calculated and measured results.

The SLS design model is an advanced finite element model; the cold-formed beams are modelled by beam elements, the concrete deck is shell and the shear connectors are springs in between. The spring characteristics are the design values of the measured secant stiffness at the SLS load level. The whole floor panels with different aspect ratios are modelled and analysed for different load cases. The SLS load resistances are derived on the basis of the different deflection criteria.

2.5.8 Application of results

The completed experimental research continuously supported the development of the light-gauge floor system.

The experimental tests are applied as:
- design test: for test based design characteristics derivation of the novel shear connectors;
- prototype test: for (i) determination of the applicable shear connector arrangement, and for (ii) confirmation the composite beam prototype's behaviour;
- validation test: for design model verification;
- verification test: for advanced finite element model verification and application for virtual experiments (Erdélyi, 2005).

The developed design models are used to determine the resistances of the composite floor for both serviceability and ultimate limit states. On this basis load-bearing design tables are developed and published (Dunai et al. 2003/b).

3. Steel and composite joints of buildings

3.1 Introduction

3.1.1 Background

In the seismic design of dissipative steel, composite and steel-concrete mixed moment resisting framed structures the cyclic behaviour of joints has important role. The local ductility of joints has a significant effect on the global ductility of the structure. The joint's ductility can be characterized numerically by cyclic parameters, which are derived from the cyclic moment – rotation relationship of the joint by standardized procedures. Cyclic testing of the joint can be done following international standards (e.g., ECCS, 1986) and the cyclic parameters, such as rigidity, resistance, relative ductility and energy absorption ratios, can be determined from these test results.

Intensive experimental research work has been done on the cyclic behaviour of the joints in the last two decades in several research institutes. The starting point of my research activities on this field is the participation in the cyclic analysis of top-and-seat-angle connections of beam-to-column joints at Lehigh University under the supervision of Prof. Le-Wu Lu. The completed experimental tests on full-scale specimens (Chasten et al. 1989) are extended by an analytical study (Dunai and Lu, 1991a/b).

On the basis of these studies I continued the research activities by further investigations. The main purpose of these experimental and numerical studies was to analyze the cyclic behaviour of steel, steel-concrete composites and mixed, steel-to-concrete joints through experiments. The focus is on typical bolted type end-plate joints with new constructional detailing and new cyclic behaviour modes, to obtain generally applicable conclusions. The "joints" are typically in beam-to-column arrangement, most of the research results, however, can be the extended to base-plate type column base joints.

The experimental tests have been completed in the framework of international collaboration through joint projects with Osaka University and the Technical University of Lisbon. At Osaka University I completed cyclic testing on steel-to-concrete mixed joints; the results are summarized in several papers (Dunai et al. 1994, Dunai et al. 1996b). The cyclic experimental studies are continued at the Technical University of Lisbon on steel (Ádány et al. 2001) and steel-concrete composite joints (Kovács et al. 2002).

Parallel numerical modelling and analyses are completed to provide tools to predict the cyclic characteristics of the studied joint types by parametric investigation (Ádány and Dunai, 2004).

I presented the results of the first two phases of these research activities in my CSc thesis (research at Lehigh University and Osaka University, Dunai, 1995). In this chapter I summarize the work and the results, completed after 1995, as the 3rd and 4th phases of the systematic research activities. I completed these work together with two PhD students of mine: Sándor Ádány (2000) and Nauzika Kovács (2005). The experiments are completed by the co-supervising with Prof. Luis Calado at Technical University of Lisbon.

The detailed research results are published by the research group; this chapter gives a general summary on the completed experimental and numerical research studies, and provides a global view of the achieved results.

First the research purposes are defined in the light of the previous studies and the applied research strategy is outlined. In Sections 3.2 and 3.3 the experimental background and results are presented for both steel and steel-concrete composite joints. In the next two Sections 3.4 and 3.5 the numerical modelling and cyclic analysis are detailed. The design and the cyclic prediction models are discussed in Section 3.6. Finally the conclusions and the application of results are given in Section 3.7.

3.1.2 Previous studies

In this section a summary is given on the existing research results on experimental, analytical and numerical approaches and standard based design methods of steel and composite joints.

Experimental studies

The seismic response of the whole joint is a resultant of several complex phenomena includes not only the behaviour of the connecting elements (bolts, plates), but the connecting columns/beams too. The experimental background has primary importance to establish the possible behaviour modes of the studied joint. During the experimental analysis, the attention is usually paid on certain phenomenon (failure of the connecting elements or the behaviour of the column/beam).

The basic tests are performed on T-stub connections to analyze the cyclic behaviour of the connecting elements (plate, bolt, weld), as shown by Bursi et al. (1997) and Xu and Kasai (2003). The cyclic response of the extended end-plate type bolted connection, which is the subject of the current research, is tested in case of steel-to-steel joints, as reported by Calado and Ferreira (1994) and Bernuzzi et al. (1996), with unsymmetrical investigation by Beg and Skuber (2000) or steel-to-concrete joints, as detailed by Fahny et al. (2000). The effect of the different loading history on the joint behaviour has also been studied and concluded by Kasai et al. (2000).

The connecting structural members (beams, columns) are tested under cyclic bending focusing on the cyclic local plate buckling of the steel elements, as it can be found in the publications of Lee and Lee (1994) and Ballio and Castiglioni (1994). The composition of the behaviour of structural member and connecting elements is presented by Azevedo and Calado (1994) and Bernuzzi et al. (1997). The investigation of the composite members can hardly be found in the literature, although the concrete filled steel columns, mainly tubular sections are widely used in bridges and also in building structures. After the major earthquake in Kobe, researchers analyzed partially concrete filled bridge piers to determine the cyclic and dynamic behaviour (Usami et al. 1997).

Analytical and numerical studies

Analytical studies are performed to predict the moment-rotation relationship of the connections. Most of them concerned to the monotonic behaviour and models, which are categorized in Jaspart (2000). The idea of the component-type-model is widely applied to predict the monotonic response of various connection modes, as detailed in Elnashai and Elghazouli (1994), Shi et al. (1996), Simões da Silva and Coelho (2001) and Kishi et al. (2004).

With the background of the knowledge on monotonic behaviour cyclic analytical models can be developed. The research tools could be classified as the different level of mechanical models, like the component models or advanced finite element (FE) models and the phenomenological models, which are semi-empirical models with the aim to simulate the observed behaviour. A classification of the models can be found in Azevedo and Calado (1994).

The finite element models are mainly used for monotonic loadings due to the difficulties of cyclic loading conditions, as presented by Choi and Chung (1996), Gebbeken et al. (1994), Nemati and Le Houedec (1996) and Maggi et al. (2003). These numerical models generally result in a complicated computational solution technique, which is the major obstacle of the practical application. This is the reason that, despite several models are introduced for monotonic loading analysis, only some of these models are extended and applied in the cyclic analysis of joints.

The other level of the mechanical models contain set of elastic or rigid parts connected to a deformable module representing the behaviour of the component, adopted experimentally or theoretically investigated constitutive law. This type of the models can be found in Ballio et al. (1987), Calado (1989), Shi et al. (1996) and Shen and Astaneh (2000).

The simplified analytical models, which predict the cyclic response by observing and characterizing the phenomenon, are the most common used approaches (Mazzolani, 1988). They require experimental experiences on the field of the characterizing behaviour and parameters, as the resistance, stiffness etc. and apply empirical parameters for the approximation. They have computational simplicity, but this simple approach leads to the limited applicability, since they are specialized to describe for specified behaviour of certain elements. This approach is used in Bernuzzi (1998) introducing the Eurocode 3 design formulas by extending its component method to determine the cyclic relationship. In Kukreti and Abolmaali (1999) a curve fitting approach is presented to define the cyclic diagram from experimental results.

Standard design methods

Having considerable research work and results on connection behaviour the semi-rigidity and partial strength nature is identified, characterized and built into the design methods. As a beginning, in the 1980's summary of the developed design methods can be found in Kulak et al. (1987) and Murray (1988) with a focus on the US approaches and significant studies are reported on the monotonic moment-rotation relationship by Akiyama (2000), Nethercot (1985) and Jaspart (1991). These researches resulted new information mainly on the monotonic behaviour of various kind of joint types and the developed method is based on the component model. This knowledge is reflected in the Eurocode standards. The results of the Eurocode 3 design method are compared with the experimental moment-rotation relationship, as can be found in Guisse et al. (1996), Vandegans (1997) and Bernuzzi (1998). The design method of the Eurocode 3 has general nature, which attempts to provide a unified method for large range of joint types, which can cause contradictions between experimental and design values on the field of moment resistance and initial stiffness, as presented in Wald and Steenhuis (1992), Shi et al. (1996), Broderick and Thomson (2000) and Thomson and Broderick (2002) or in the post-elastic branch of the joint response, as shown by Kato et al. (1990) and De Stefano and Astaneh (1991).

Although, the occurred local damage of the steel structures due to earthquake events highlighted the incomplete nature of the design methods. For this reason international research projects have oriented to examine the structural components and connections of steel frames to establish the cyclic response of the dissipative zones with the purpose to improve the structural arrangements and design methods from seismic point of view. The international research projects are referred by Wald (1993), Bernuzzi et al. (1997) and Mazzolani (2002). The design requirements of steel structural joints in seismic zones are collected in manuals – as an example can be found in a paper of Mazzolani and Piluso (1993) – but the appropriate determination of the cyclic behaviour requires reliable design methods, as also concluded by Akiyama (2000).

Conclusions on the previous studies

From the pervious studies it can be concluded, that the bolted end-plate type joints of steel and composite building structural elements:
  - have significant constructional advantages (simplicity, erection, economical);
  - have been widely investigated to utilize the semi-rigid and partial strength nature;
  - for the monotonic behaviour design models have been derived;
  - the cyclic behaviour provides with the opportunity to apply them in seismic resistant moment resisting frames.

In the investigated literature we did not find:
- cyclic test results on bolted end-plate joints of steel-concrete composite members;
- numerical models for the cyclic analysis of bolted connection components and joints of steel, composite and mixed – steel and concrete – joints;
- cyclic design model for end-plate type steel-concrete composite joints;
- proposals for constructional detailing to achieve improved seismic behaviour.

3.1.3 Purpose and research strategy

As it is discussed in the previous section the potential applicability of the typical bolted end-plate joints for moment resisting frames under seismic effects is proved by previous research. The <u>main aim</u> of the current research was to create the background knowledge and tools for the design recommendations of this type of joints under cyclic loading conditions.

The <u>particular purposes</u> were defined as follows:
- determination the cyclic behaviour modes of joints of steel and steel-to-concrete composite members by experimental testing;
- developing advanced numerical model to simulate the cyclic behaviour of the joint components on the basis of the geometry and material behaviour;
- qualitative and quantitative characterization of the cyclic behaviour modes and related joint details;
- cyclic design method development for the studied joint;
- practical constructional detailing proposal derivation on the basis of research experiences.

In the research activities experimental, numerical and analytical approaches are used. The applied <u>strategy</u> is illustrated in Fig. 3.1. The solid arrows indicate the completed work, while the dashed arrows show the possible application of the results and the further extension of the research.
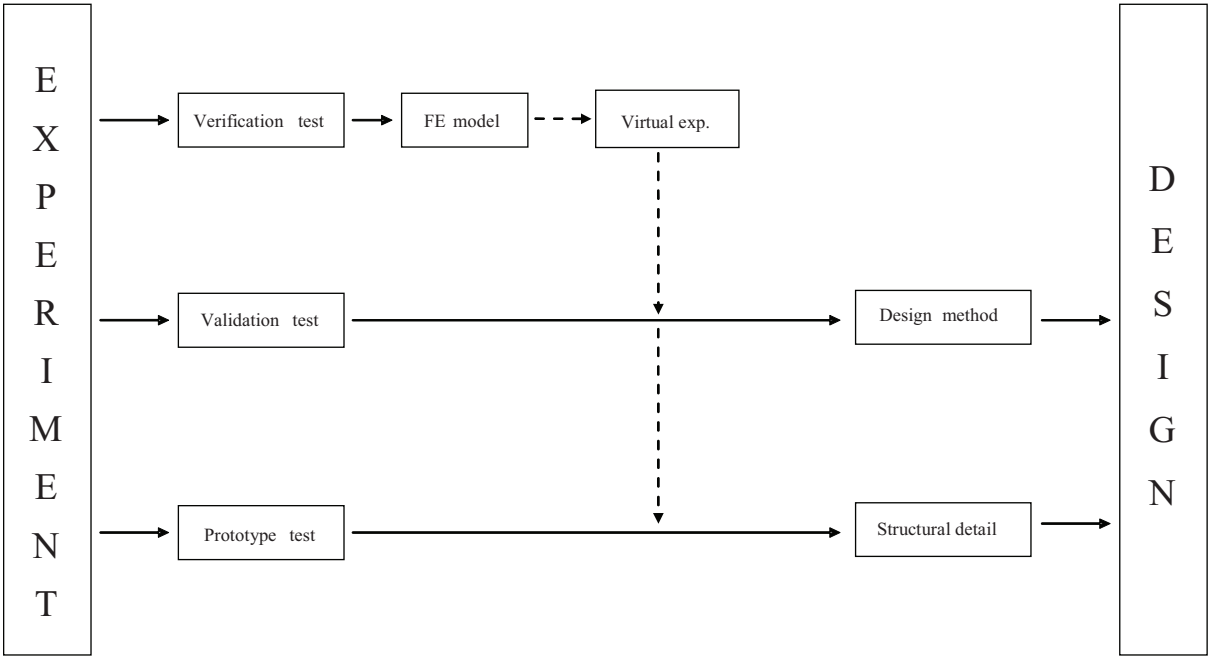

Figure 3.1: Applied research strategy – steel and composite joints of buildings.

The completed tests are performance tests in order to define the prototype behaviour ("prototype test") and to validate existing and develop new design methods ("validation test"). The results of the executed tests can be used for model verification, too. In the current research, however, the elements of the advanced numerical model are verified by existing own or available experiments. In the current phase of the research the developed FE model is completed and verified, the extension for practical design application is a possible further step in the research.

3.2 Experimental program

3.2.1 Studied joints

In the completed experimental programs, end-plate type joints of (a) steel, (b) steel-concrete composite joints are investigated, as illustrated in Fig. 3.2. In all the joints the structural element is welded to the end-plate by double sided fillet welds, and the plate is connected by bolts to the adjacent element. The tested joints and the test details are provided in Table 3.1 and are as follows:

Steel joints: 5 specimens (SS1 – SS5) with end-plate joints of steel members (Fig. 3.2). The test parameters are the type of sections (hot-rolled "plastic," and welded thin-walled "slender" H-sections), and end-plate connection arrangement (thickness, bolt grade) (Ádány, 2000). The joints are tested under cyclic bending.

Steel-concrete composite joints: 12 specimens (SC1 – SC12) with end-plate joints of composite members (Fig. 3.2). The test parameters are the type of sections (hot-rolled "plastic," and welded thin-walled "slender" H-sections), composite action (with reinforcement or stud), and end-plate connection arrangement (thickness, bolt grade) (Kovács, 2005). The joints are tested under cyclic bending.
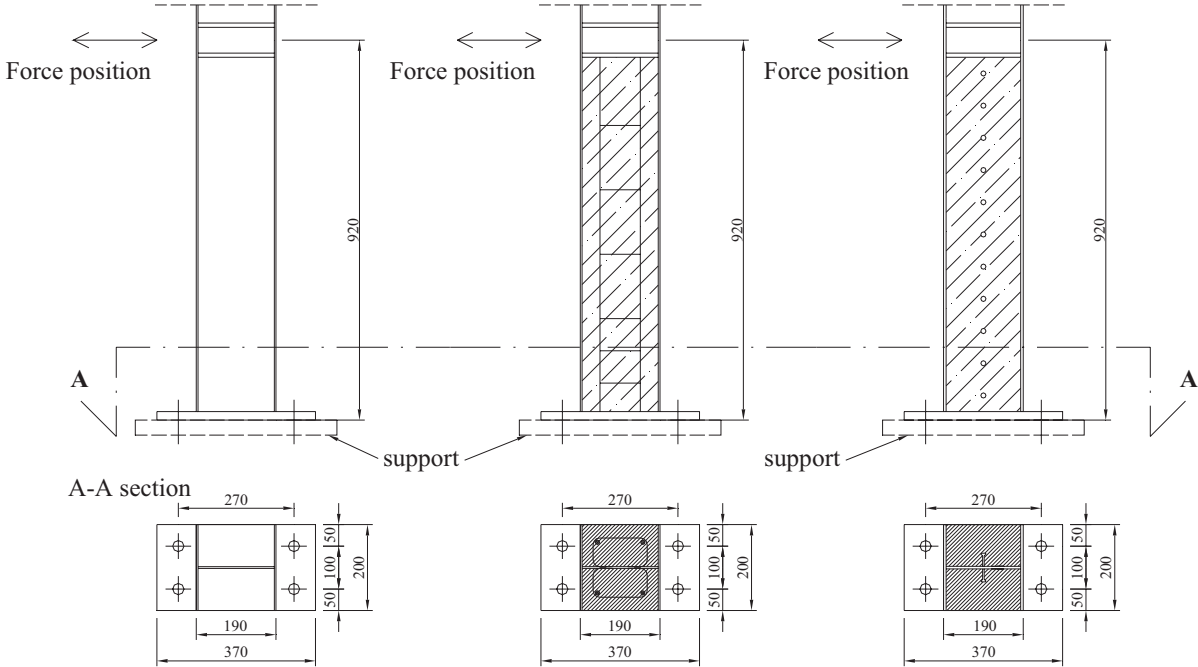

Figure 3.2: Steel and steel-concrete composite specimens.

3.2.2 Test specimens and set-ups

The experimental programs are summarized in Table 3.1, detailing the most important characteristics of the test specimens.

The specimens are tested in the arrangements as shown in Fig. 3.3. The set-ups for steel and composite joints are the cantilever type arrangement the specimens are connected to a rigid foundation, and the displacement controlled actuator applied the cyclic horizontal load.

In the experiments, the recommendations of ECCS (1986) for the loading history and evaluation of the test results are adopted. Due to the purpose of the performance tests, very detailed measurement of the joints is applied for both integrated (global displacements) and local (relative and local displacements and strains) test parameters.

| Specimen | Member section/ end-plate | Bolt | | End-plate thickness [mm] | b/t | | Behav. mode |
		no. / size	grade		flange	web	
SS experimental program – steel joints							
SS1	HEA-200 / extend.	4 / M16	8.8	25	10,0	20,6	3
SS2	HEA-200 / extend.	4 / M16	8.8	16	10,0	20,6	2
SS3	welded I / extend.	4 / M16	8.8	25	15,5	28,3	4
SS4	HEA-200 / extend.	4 / M16	8.8	25	10,0	20,6	3
SS5	HEA-200 / extend.	4 / M16	8.8	12	10,0	20,6	1
SC experimental program – composite joints							
SC1	HEA-200 / extend.	4 / M16	8.8	25	10,0	20,6	3
SC2	HEA-200 / extend.	4 / M16	10.9	25	10,0	20,6	3
SC3	HEA-200 / extend.	4 / M16	12.9	25	10,0	20,6	3
SC4	HEA-200 / extend.	4 / M16	10.9	16	10,0	20,6	1
SC5	welded I / extend.	4 / M16	8.8	25	15,5	28,3	3
SC6	welded I / extend.	4 / M16	10.9	25	15,5	28,3	3
SC7	HEA-200 / extend.	4 / M16	8.8	19	10,0	20,6	2
SC8	welded I / extend.	4 / M24	10.9	30	15,5	28,3	5
SC9	welded I / extend.	4 / M24	10.9	20	15,5	28,3	5
SC10	welded I / extend.	4 / M24	10.9	20	23,3	43,5	5
SC11	welded I / extend.	4 / M24	4.8	20	23,3	43,5	5
SC12	welded I / extend.	4 / M24	10.9	20	15,5	28,3	5

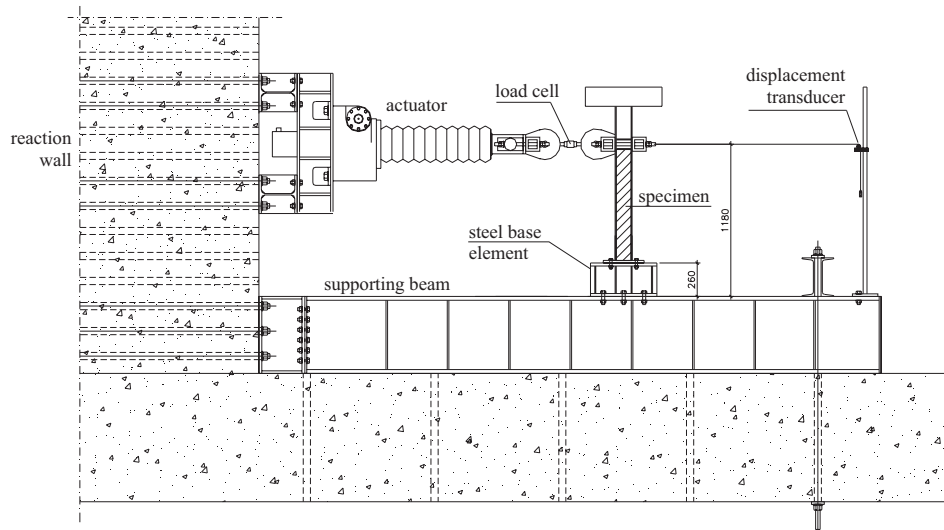Table 3.1: Test specimens and results.

Figure 3.3: Test arrangement.

3.2.3 Test results

From the measured data, the cyclic moment – rotation relationships are derived for all of the specimens.

On the basis of the experimental results, the cyclic behaviour modes of the joints are determined and characterized. These are the (1) end-plate failure, (2) combined end-plate and bolt failure, (3) bolt failure, (4) local plate buckling - type 1: symmetric and (5) local plate buckling - type 2: asymmetric. The observed pure and combined cyclic failure phenomena are summarized in Table 3.1 for each specimen by the above identification number of the failure mode.

3.3 Cyclic behaviour modes

In this section, the most typical cyclic behaviour modes are presented; more detailed description can be found in Ádány et al. (2001) and Kovács et al. (2002).

3.3.1 End-plate failure

This "pure" failure is experienced in both steel and composite specimens when a "strong" bolt is applied in "weak" end-plate (Mode 1 failure in Eurocode 3, EN 1993-1-8, 2004). The observed governing phenomenon is elastic/plastic deformation, the development of the yield line, and the cracking in the end-plate. The mode is illustrated by specimen SC4 in Fig. 3.4; it is shown in the cyclic moment-rotation diagram that the rotational capacity of the joint is large, with low resistance degradation and reasonable energy absorption.

3.3.2 Bolt failure

The bolt failure is experienced for both steel and composite specimens with a high end-plate thickness to bolt diameter ratio (Mode 3 failure in Eurocode 3). The main behaviour is the elastic/plastic elongation of the shank and the bolt fracture. This mode is shown by specimen SC5 in Fig. 3.5; due to the rigid-body type rotation, shown in the cyclic moment-rotation diagram near-zero level parts, a significant drop in the energy absorption with very limited ductility is found.

3.3.3 Combined end-plate and bolt failure

If the bolt and end-plate rigidities are not extreme, the elastic/plastic deformations can be developed in both components of the joint (Mode 2 failure in Eurocode 3). The behaviour is a combination of the previously discussed pure cases; the dominancy of one or other is dependent on the rigidity ratio of the plate and bolt. An example of this behaviour is illustrated by specimen SC7 in Fig. 3.6. In general, it is concluded that the most favourable cyclic behaviour can be obtained by this mode among the connecting element type failures. By properly adjusting the rigidity and strength of the elements, high resistance and stiffness, with low degradation and reasonable ductility and energy absorption, can be gained.
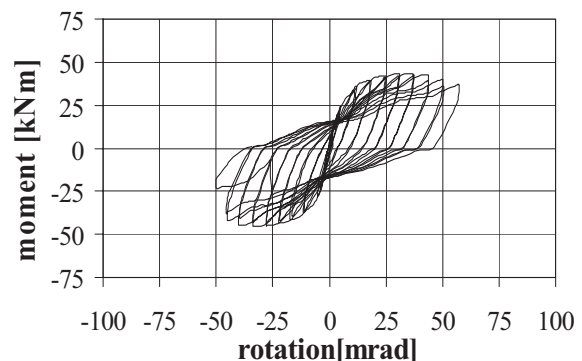

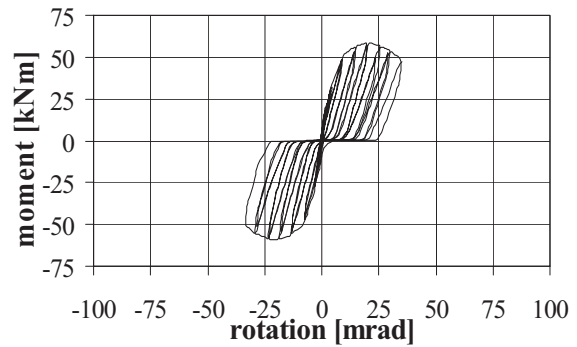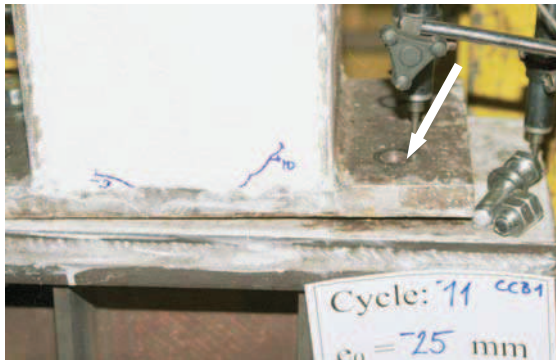
Figure 3.4: "Pure" plate-failure.
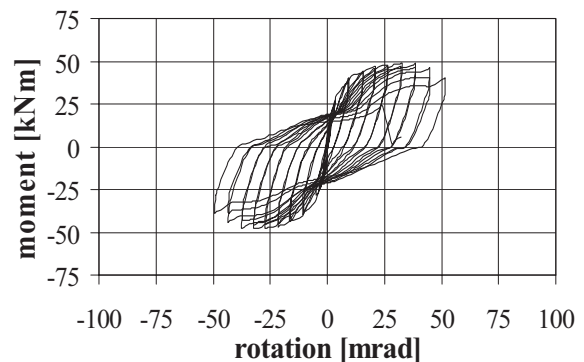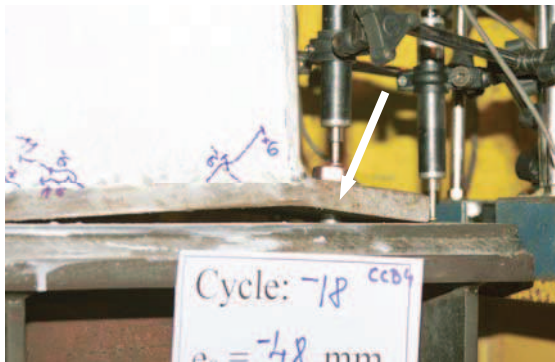
Figure 3.5: "Pure" bolt-failure.

Figure 3.6: Combined bolt and plate-failure.

3.3.4 Local plate buckling failure

The local instability phenomena are experienced in the element ends of both steel and steel-concrete composite specimens in the case of slender welded cross-sections (Class 4 section in Eurocode 3, EN 1993-1-5, 2005). The observed local buckling is symmetrical in steel and asymmetrical in composite specimens, as illustrated in Fig. 3.7 for specimens SS3 and SC9.
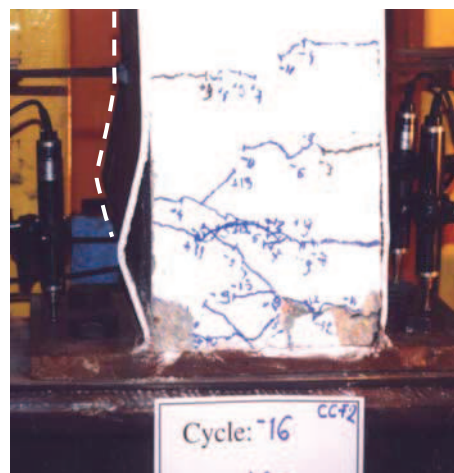

Figure 3.7: Plate buckling patterns; steel and composite specimens.

In the case of steel specimens, the flanges buckle first on the compressed side in a classical buckling pattern as marked on the moment-rotation curve in Fig. 3.8,a. The web buckling occurs after significant plastic deformation, causing fast degradation of resistance and stiffness. The final failure is caused by the cracking in the web-to-flange fillet weld, which is expanded toward the web.

In the case of steel-concrete composite specimens, the separation between steel flange and concrete filling is observed in the early cycles and is due to the different axial deformations. The elastic flange buckling happens on the various positions of the compressed flange in an asymmetrical buckling pattern, due to the supporting effect of the concrete (Fig. 3.8,b). In the increasing cycles, the phenomenon becomes plastic plate buckling and turns into a yield mechanism with three main yield lines. The final collapse is caused by the cracking and fracture of the tension flange due to low cycle fatigue, after the significant deterioration of the filling concrete. The nonlinear cyclic behaviour for this failure mode is significantly influenced by the applied composite action. In the case of specimens with reinforcement in the concrete several small cracks are developed, while when only headed studs are used one dominant crack is occurred. Although the two types of specimens had almost the same moment capacity, in the rotational capacity and degradation characteristics, however, the specimens with reinforcement showed better performance.

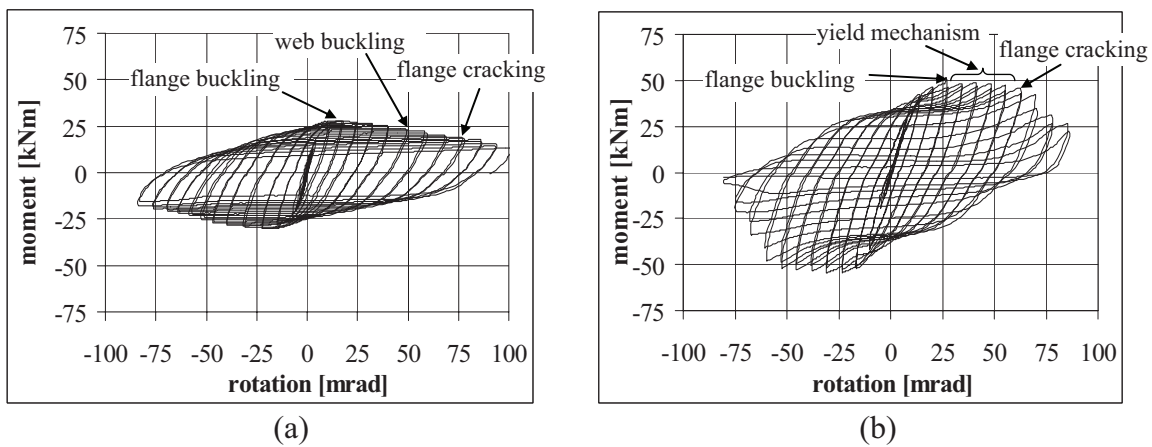(a)   (b)

Figure 3.8: Plate buckling moment-rotation curves; steel and composite specimens.

The two types of cyclic local buckling phenomena are evaluated in detail (Kovács et al. 2004). In Fig. 3.9, the cyclic parameters (absorbed energy and resistance ratios) show the quantitative difference in the cyclic buckling behaviour. In the stable cycles less than 10% degradation of the resistance ratio is observed in the case of composite specimens, while it is higher for steel specimens (about 20%), what shows the favourable effect of concrete filling.
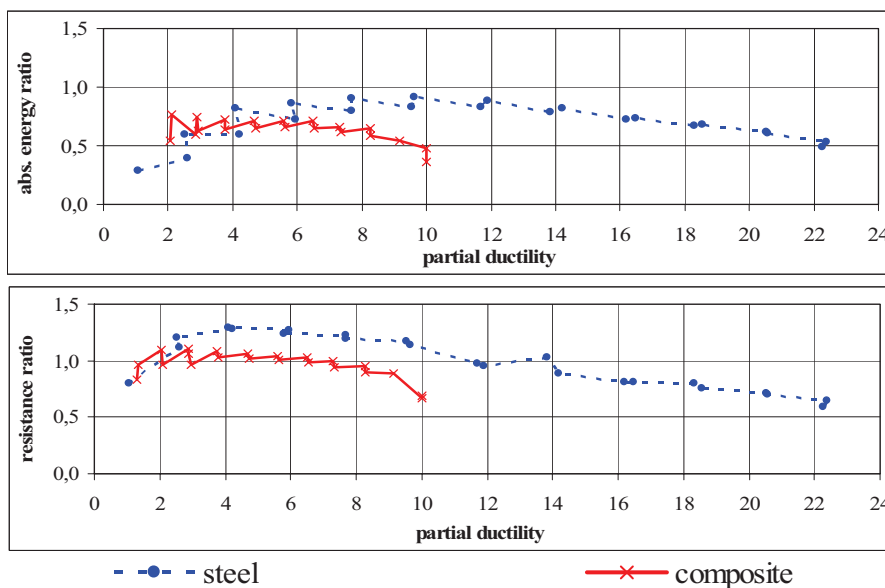

Figure 3.9: Cyclic parameters of plate buckling failure; steel and composite specimens.

3.4 Numerical modelling

3.4.1 General

The other direction of the research activities is the application of numerical models to study the cyclic behaviour of joints. The major problem in the development and application of these advanced models is that the cyclic behaviour is highly nonlinear which requires a complicated computational solution technique. In recent years, however, significant development in computer technology provides the opportunity to extend the application of the numerical models to perform parametric studies by virtual experiments.

The modelling process first concentrated on the bolted segments of the top-and-seat angle connection (Dunai et al. 1991b). The basic idea is extended in further research by more general 3D geometrical and material models of the joints and the development of an improved cyclic plasticity model for steel components.

Different levels of cyclic models of joints are studied, developed and applied, such as prediction model for hysteretic curve and degradation, component models and numerical simulation models. This section concentrates on the features of steel-to-steel and steel-to-concrete end-plate type joint cyclic simulation models and their verification process.

3.4.2 Requirements of the cyclic joint models

The basic requirement of the joint model is to simulate the cyclic performance on the bases of the joint geometry and material properties. To fulfil this requirement the model should have the following features:
- The model should consider the complex 2D or 3D geometry of the joint (surface or solid geometry model).
- The load model should follow the cyclic loading history.
- The material model should take into account the cyclic behaviour of the steel and concrete.
- The model should consider the local buckling of the slender plate elements under load reversal.
- The conditional connections between the joint components should be modelled under cyclic effects (contact – separation – re-contact).

The above-mentioned requirements result in a highly nonlinear mathematical model, including all basic type of non-linearity: geometric, material, as well as non-linearity coming from the conditional supports/connections. For the solution, a robust computational method should be used.

3.4.3 Features of the finite element models

<u>2D geometry models</u>

In these models the 3D geometry of the joint is transferred to the 2D space. The simplest 2D model concentrates on the plate bending phenomenon of a plate components of the joint. In this case the mid-surface of the plate component is modelled by plate finite elements. The model is used for the analysis of separated joint components (e.g. end-plate, angle). In cyclic analysis the pure plate models are rarely used since the behaviour is more complex in general and the bolts cannot be handled correctly.

The plane stress or plane strain 2D models can be used to model a plate – bolt sub-assembly, in which the 3D behaviour is reduced to 2D. Typical applications of these models are for bolted joint components, such as T-stubs or bolted angles. Although these models eliminate the transverse bending of the segments, the dominant behaviour can be simulated with appropriate accuracy in many cases. Such cyclic 2D T-stub and bolted angle models are introduced and presented by Dunai (1995) and Ádány (2000).

<u>3D geometry models</u>

The 3D finite element models have two major groups: shell models and solid models, depending on the type of the applied finite elements. In case of shell models, however, layered elements are preferred, in order to be able to smoothly follow the material behaviour through the thickness of the element.

The 3D joint geometry is modelled by the mid-surface in the shell models, by shell finite elements. The shell elements are connected to each other in different planes according to the joint's geometry. The bolts can be modelled as supporting springs or equivalent other finite elements (e.g. bars). The boundary nonlinearity can be considered on the contact surfaces by different methods (e.g. gap elements or uni-lateral material models). In the plates the spread of the plasticity should be followed through the thickness by the application of layered shell elements. The 3D shell models are used by several researchers to model joint components and complex joint, mainly for monotonic loading.

In the developed model the basic finite element is a degenerated layered shell element, with 8-node (Serendipity) isoparametric approximation and 5 DOFs per node. The element includes a self-developed, special foundation layer, which provides a Winkler-type foundation for modelling the supporting concrete and anchoring elements (Ádány, 2000).

The most correct geometry model of the joint is the 3D solid model. In this case solid finite elements are used to model all parts of the joints. Advanced models are developed and verified for monotonic loading analysis of joint components and complex joints (Gebbeken et al. 1994). These studies determined the main requirements of the solid element meshing to achieve the required accuracy.

<u>Cyclic plasticity material models</u>

The material nonlinearity is considered by applying cyclic plasticity material models. It is well-known from the experimental studies that the cyclic behaviour of steel material cannot be followed by the pure elastic-plastic, isotropic or kinematic hardening models. It is experienced from the tests, that such combined isotropic and kinematic hardening models should be used which can consider both the changes of the size of the yield surface and the translation in the stress space. Basically two types of models are developed which can fulfil this requirement:

- In case of two-surface models (Dafalias and Popov, 1975) an initial and a limiting surface is defined. The actual size of the yield surface and the actual value of the hardening parameter are calculated as a (non-linear) function of the stress history.
- The multi-surface models (Popov and Petersson, 1978) are the extension of Mroz multi-surface model. A set of yield surfaces are defined which correspond to certain states of the isotropic hardening. These surfaces move in the stress space, by which the kinematic hardening is considered. In the Petersson-Popov model the sizes of yield surfaces are not constant, but functions of the stress history.

Common feature of these models that not all the model properties can be derived from simple material tests. The properties are dependent on the applied model; they can be defined from combined testing and numerical calibrating. In the current research for the steel material of the structural elements and plates, the Petersson-Popov multi-surface material model is introduced. The original model is modified to obtain more accurate results in the range of moderate plastic strains (Ádány and Dunai, 1997a).

For concrete support, the unilateral Karsan-Jirsa cyclic model is used (Karsan and Jirsa, 1969). For the anchoring elements, the load-displacement relationship is established by the use of an analytical anchor-bar model.

Geometric nonlinearity

The geometric nonlinearity that follows the cyclic buckling of the thin plate components of the joint is taken into consideration by the Total Lagrangian approach, assuming large strains and small displacements.

Conditional supports

The nonlinearity coming from the conditional connections (contact – separation – re-contact phenomena between the end-plate and the supporting surface and/or between the bolt heads and the end-plate) is crucial; therefore, it has major importance in the model. It is handled by the application of uni-lateral material models in the special foundation layer of the shell element for the supporting concrete surface and the anchoring element (Ádány, 2000).

Computational solution technique

For the solution of the nonlinear system, the equilibrium path is followed by the Minimum Residual Displacement method (Chan, 1998), by carefully adjusting the control parameters to obtain accurate and efficient computations. The norm of the vector of unbalanced forces is used to measure the convergence. According to our experience, the convergence limit should be set between 0.01 and 0.001. In general: plastic behaviour may be followed well with larger tolerance (0.01 or above), buckling-like phenomena, however, require smaller tolerance (around 0.001 or smaller). The optimal number of iterations within one incremental step should be around 5, while for the maximal number of iterations 10 seems to be a reasonable value. The optimal size of the load increment is very much dependent on the problem and on the actual state of the model (percentage of plastic regions, contact-separation, near-buckling states, etc.). In general, the control parameters must be flexible enough to provide larger and smaller load increments. Extremely small load increments may also be necessary to follow separation and contact.

3.4.4 Model verification

The application of numerical models calls the attention of the key question of the numerical structural analysis. This is the balance between the accuracy and efficiency. The cyclic joint model should be accurate enough to be able to use the obtained results to derive the joint cyclic characteristics for practical purposes. It can be called as „engineering accuracy". The accuracy of the model should be verified by a systematic checking, using analytical and experimental references.

On the other hand the model should be applicable for virtual experiments on a realistic hardware/software background with realistic processing conditions. The efficiency of the model is very much dependent on the applied nonlinear solution techniques.

The verification of the cyclic joint models is a more complex problem compared to the monotonic FE models since this cannot be achieved in a single step. Instead, multi-level testing is necessary, which can assure that the model is able to describe all the important phenomena. In the case of the studied joints, the cyclic behaviour of steel and concrete materials, components (plate element, anchoring bolt), sub-assemblies (T-stub), and joints should be tested systematically. For the developed models, the above verification is completed on a set of benchmark examples as illustrated in the following section.

3.5 Cyclic tests by FE simulation

3.5.1 Material tests

Steel material

The Petersson-Popov multi-surface model is applied and tested on the basis of material tests (Popov and Petersson, 1978). It is found that the model, in general, describes the behaviour well; however, it is unable to handle correctly the Bauschinger effect, which is one of the characterizing phenomena of mild steel behaviour in the case of first yielding. A modification is proposed in order to follow the mild steel behaviour in the range of small plastic strains (Ádány and Dunai, 1997a).

The modified Petersson-Popov model applies three characteristic stress-strain curves and two weighting functions, as shown in Fig. 3.10. The three stress-strain curves correspond to three characteristic states of the steel material subjected to cyclic loading, and can be determined from the experimental curves. The weighting functions are used for the interpolation between the three characteristic states, so that the material behaviour could be described for any state.
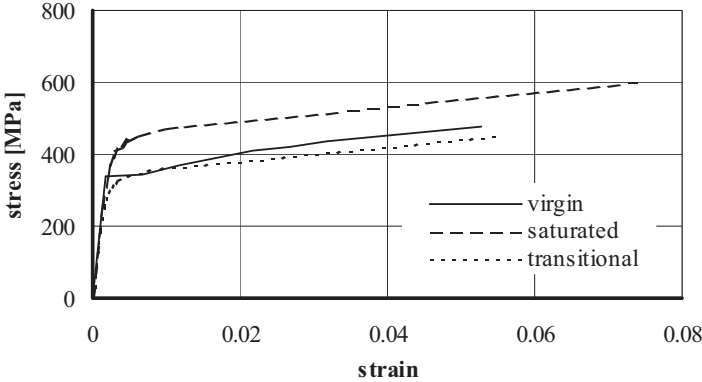
(a) stress-strain curves
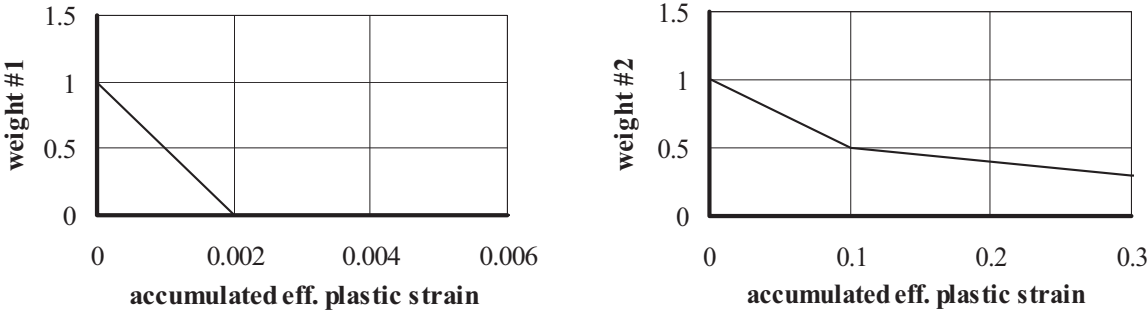
(b) weighting functions

Figure 3.10: The modified Petersson-Popov multi-surface model.

The material model is tested with various cyclic loading histories, both for normal and shear stresses; one example is presented in Fig. 3.11, where both the numerical and experimental stress-strain curves are plotted.

Concrete material

In the behaviour of the studied joints, the concrete did not have a dominant effect, and it is considered in a simplified way as a foundation layer for the end-plate. In this layer, the uni-axial cyclic concrete model is used, as proposed in Karsan and Jirsa (1969) and presented in Fig. 3.12. Since tension cannot develop between the end-plate and the supporting concrete, the concrete behaviour is unilateral, working for compression only. The numerical and experimental results are compared in Fig. 3.13.
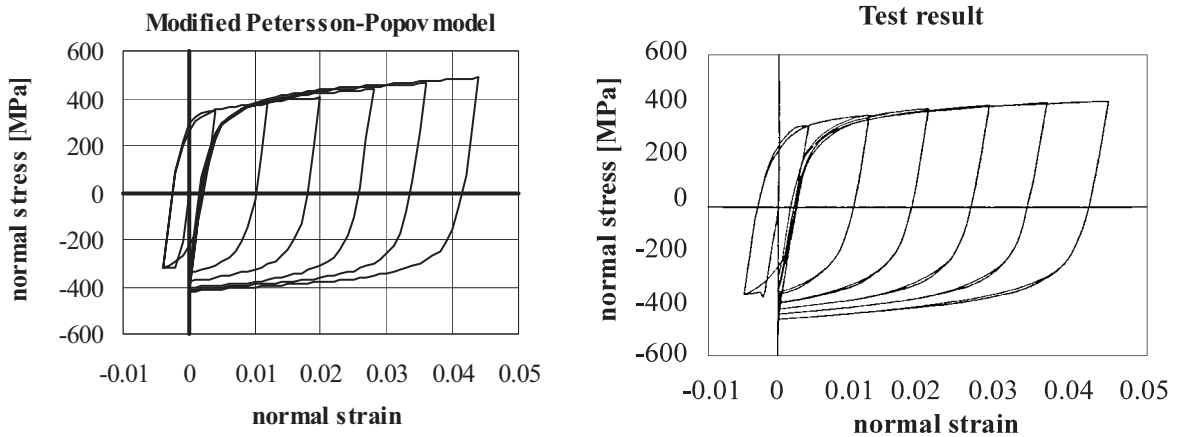
Modified Petersson-Popov model

Test result

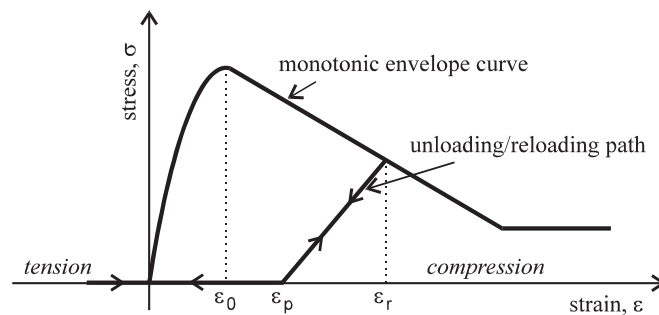Figure 3.11: Experimental and numerical stress-strain curves for steel.

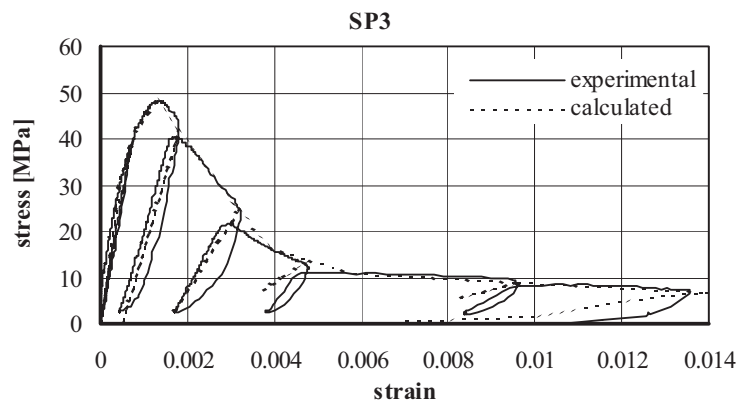Figure 3.12: Uni-axial cyclic material model for concrete.

SP3

Figure 3.13: Experimental and numerical stress-strain curves for concrete

3.5.2 Component tests

Plate element

A simply supported plate element is analyzed, subjected to alternate compression/tension, as shown in Fig. 3.14. The plate is thin enough to show excessive out-of-plane deformations due to buckling, and the applied load intensity is high enough to cause significant material yielding both for tension and compression. The problem is solved in parallel with the solution presented in Yao and Nikolov (1992). The main characteristics of the problem, the applied loading histories, and the complete results from further studies on the application of various material models can be found in Ádány (2000).
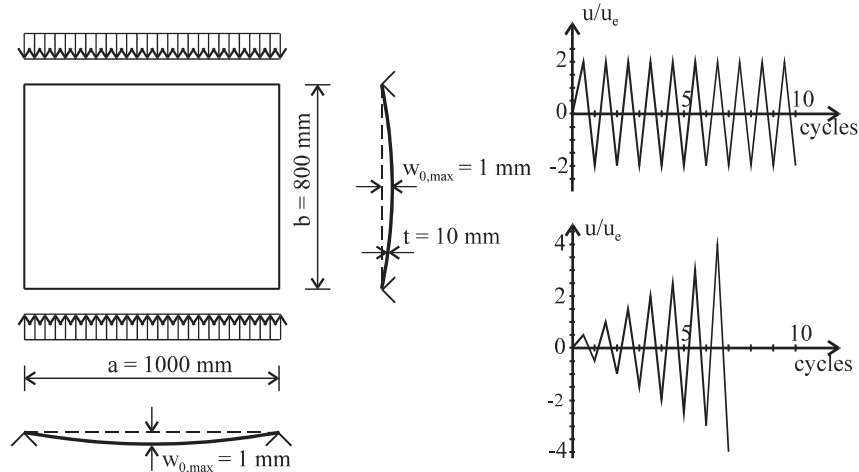
59

Figure 3.14: Cyclic plate buckling example.

The results of the analyses are presented in Fig. 3.15 for the second loading history. It can be observed from the results that the numerical model is able to describe all the important phenomena: plate buckling due to compression, increased out-of-plane deformations due to the compression of the curved plate (second-order effects), and the yielding of the material; all these results are in accordance with Yao and Nikolov (1992), both qualitatively and quantitatively.
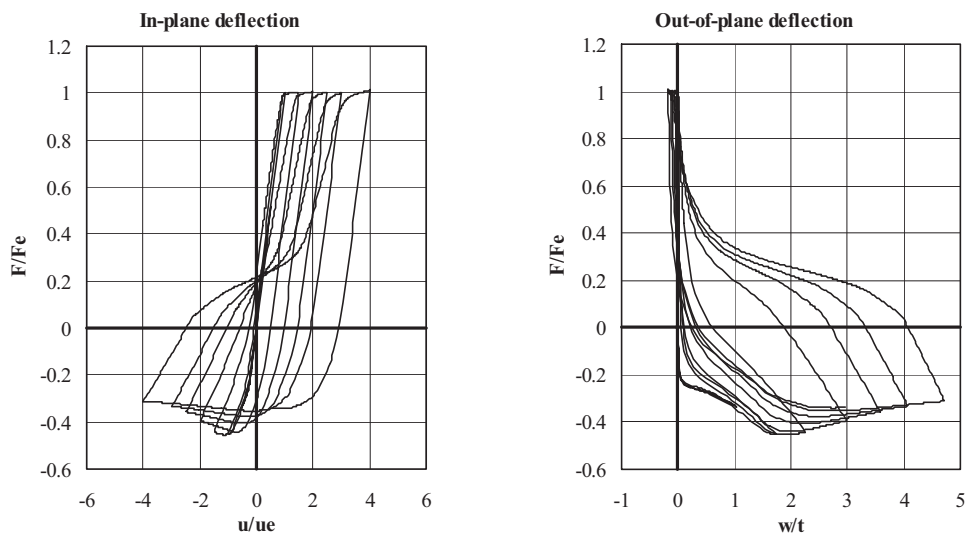

Figure 3.15: Cyclic plate buckling load-deflection curve – loading history 2

Anchoring element

The cyclic behaviour of the anchoring element is followed by a special, independent model; the results are built as input data into the foundation layer of the pertinent shell element. The details of the models and the application in parallel with experiments can be found in Ádány (2000) and Ádány and Dunai (2004).

3.5.3 T-stub tests

The T-stubs are the primary behavioural components of the studied joints, which is why they are intensively investigated – mainly under monotonic loading – both numerically and experimentally in the last two decades. Here, a cyclic numerical study is summarized, which is performed on T-stubs by applying the finite element model developed herein. The main geometrical dimensions are shown in Fig. 3.16, together with the applied loading history.
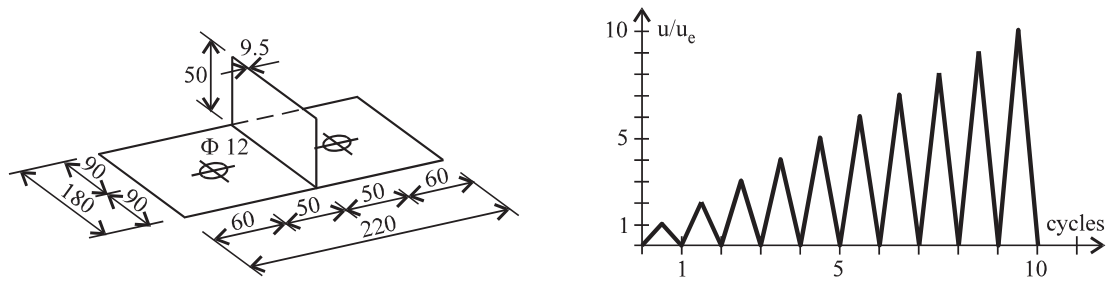
Figure 3.16: T-stub example.

The yield stress of the plate is equal to 320 MPa; the diameter of the bolt is constant (12 mm), while the yield stress of the bolt material is varied between 360 and 900 MPa, to cover all practical cases in the behaviour modes. The T-stub is assumed to be placed on a practically rigid surface, where it is connected by two bolts.

In the context of this study, various materials are assumed for the steel plates and anchoring bolts in order to obtain various behaviour modes. In Fig. 3.17 the deformation of two extreme conditions are shown, namely the relatively strong and weak bolts, comparing to the end-plate. In Fig. 3.18, four characteristic cases are presented by the cyclic force-displacement curves. The diagrams are non-dimensionalized, F_e and u_e being the force and displacement belonging to the limit of elasticity, respectively.

Figure 3.18,a shows the case (TS1) when the bolt is strong enough to remain elastic during the entire loading history; thus the force-displacement curve is basically determined by the elastic/plastic deformations of the end-plate. The other extreme case (TS4) is presented in Fig. 3.18,d, where the end-plate remains elastic. The behaviour is governed by the elastic/plastic elongation of the bolt, and the separation/re-contact, which can take place not only between the end-plate and the foundation, but also between the bolt head and the end-plate. Between the two extreme cases, a successive transformation is observed (see Figs. 3.18,b and 3.18,c). The behaviour is a combination of the two extreme cases, depending on the parameters of the T-stub, including plastic deformations of both end-plate and bolts, as well as separation – re-contact between the model components.

From the results, it can be seen that the applied model is capable to follow the extremely nonlinear equilibrium paths. More details about the behaviour, including explanations for the various parts of the force-displacement curves in several different cases can be found in Ádány (2000) and Ádány and Dunai (2004).
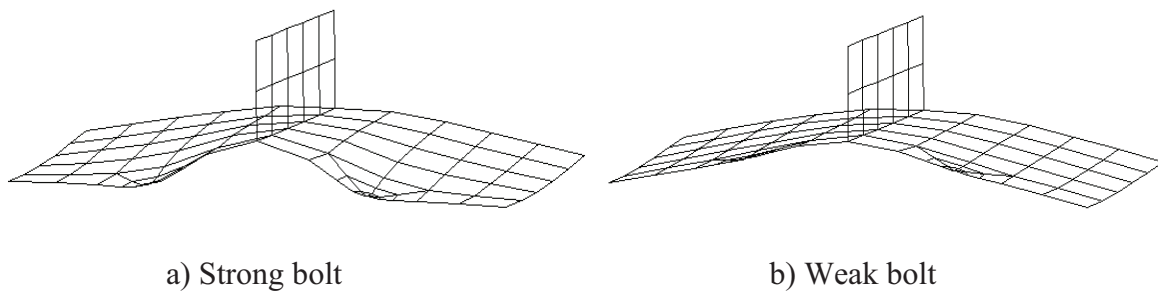

a) Strong bolt   b) Weak bolt

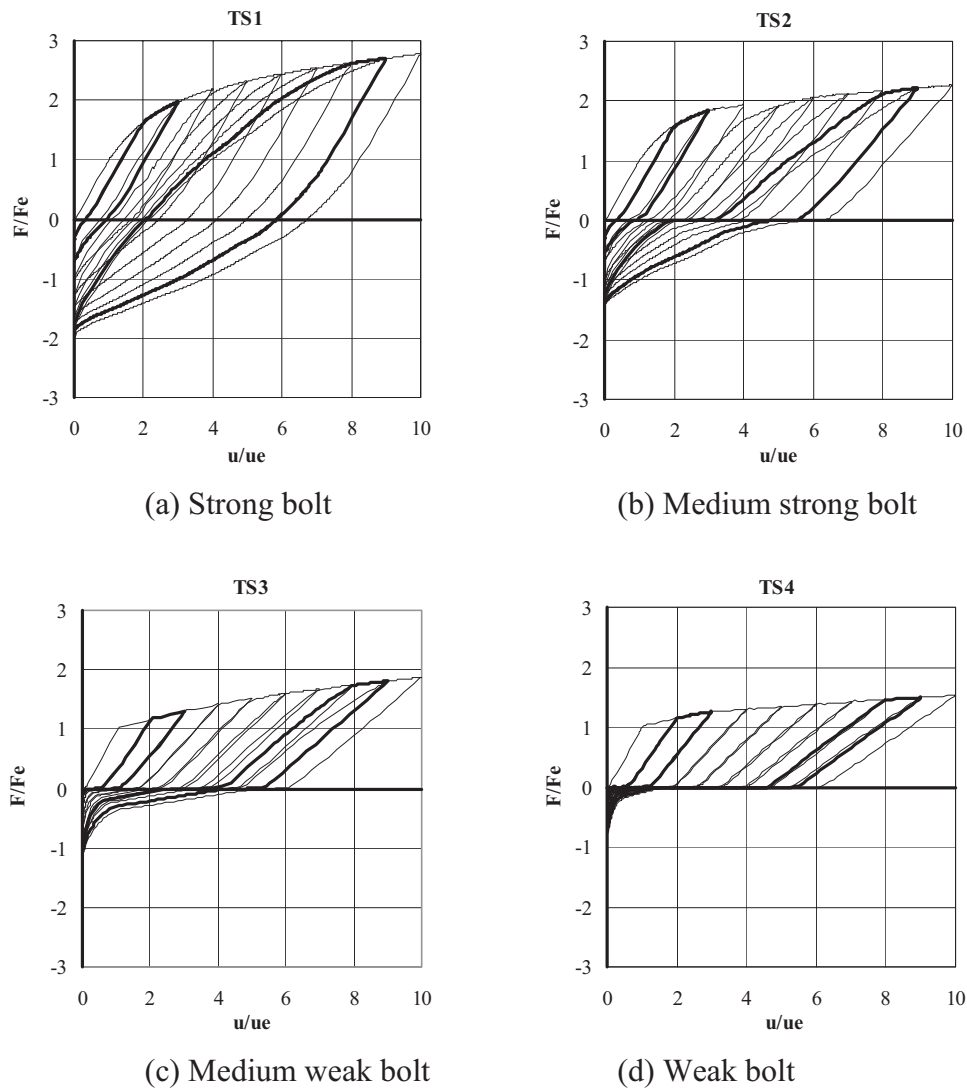Figure 3.17: Deformed geometry of T-stubs.

61

Figure 3.18: Cyclic load-displacement curves of T-stubs.

3.5.4 End-plate joint test

In the earlier phase of the research we studied steel and steel-to-concrete bolted end-plate type joints under monotonic loading by 2D models (Ádány and Dunai 1997b, Dunai et al. 1996a). The results can be extended for cyclic behaviour (Dunai and Lu, 1991b), however, the uncertainties in 2D models showed that in the further steps 3D models are required.

In the current phase of the research an illustrative example is performed on an end-plate joint using a 3D model. The geometrical and material properties of the analyzed joint are in accordance with the steel specimen SS2 of the experimental program reported in the previous sections and in Ádány (2000) and Ádány et al. (2001).

Figure 3.19 shows the monotonic moment-rotation curves, while Fig. 3.20 presents the original and deformed geometry in a typical state of the joint. It can be seen from Fig. 3.19 that the agreement between the calculated and experimental curves is excellent at the initial part of the curves, with good prediction for the initial rigidity. At the non-elastic region of the curves, however, differences can be observed due to the applied assumed material characteristics, and because the experimental moment-rotation curves are established as envelope curves (positive and negative) of a cyclic test curve.
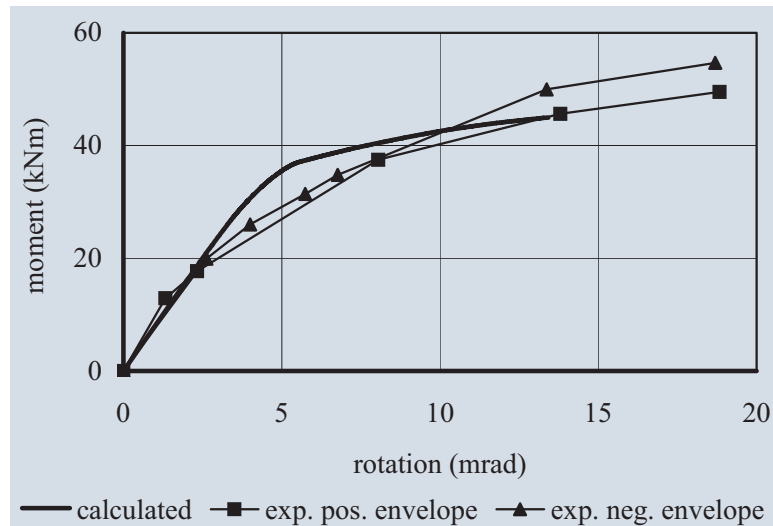
Figure 3.19: Moment-rotation curves of the studied end-plate joint.
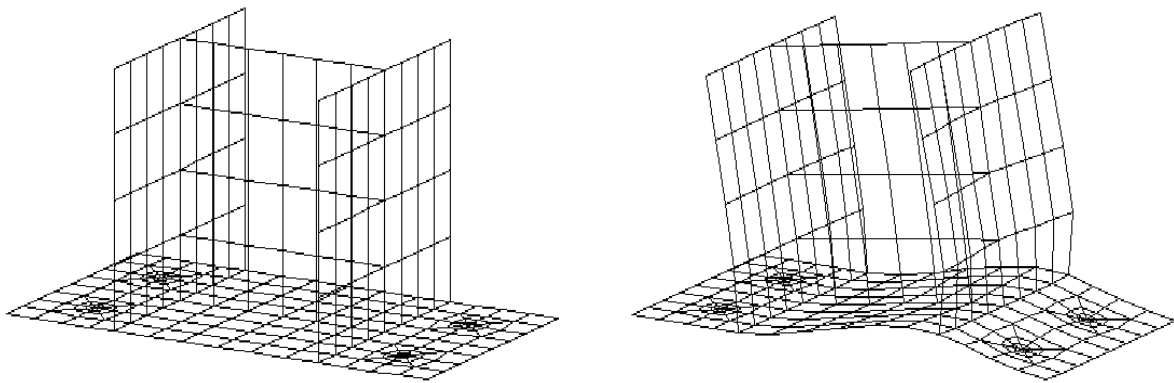
Figure 3.20: Deformed geometry of the studied end-plate joint.

3.5.5 *Application of the developed numerical model*

During the numerical investigation we developed a finite element model for the cyclic analysis of the steel, steel-concrete composite and steel-to-concrete mixed joints. The model accuracy is proved by a newly introduced set of cyclic benchmark tests. For the practical applicability the computational details are proposed.

The developed numerical model have not been applied for practical problems due to the lack of powerful hardware background in the last five years. Having the fast development in the computers, however, this requirement of the application is going to be fulfilled. The model is capable to complete virtual experiments. The results can be used for design purposes as it is described in Fig. 3.1.

3.6 Cyclic design modelling of composite joints

The results of the cyclic tests of composite joints showed the constructional arrangements which exhibit advantageous behaviour. The extension of the experimental experiences for design application is done by cyclic design modelling. It consists of two parts, as follows:

First a Eurocode 3 and Eurocode 4 – hereinafter EC3 and EC4 – standard based study is performed with the intention to develop a procedure to evaluate the monotonic moment-rotation curves which follows the test behaviour of the studied joints. The applied design standards: EN 1993-1-1 (2004), EN 1993-1-5 (2005), EN 1993-1-8 (2004) and EN 1994-1-1 (2004) – notes that previous, draft versions of the standards are used.

In the second part, starting from the monotonic design curve, using the experimentally determined performance parameters the cyclic moment-rotation curve is predicted.

3.6.1 Design model for monotonic behaviour

Review of the Eurocode design method

The EC3 defines the moment-rotation relationship of the joint with the design moment resistance ($M_{j,Rd}$), the rotational capacity (ϕ_{cd}) and initial rotational stiffness ($S_{j,ini}$), as shown in Fig. 3.21,a. During the tests the specimens are imposed by cyclic loading, the joints are described by the envelope curves that belong to the cyclic moment-rotation diagrams (Fig. 3.21,b).

The EC3 applies the component method to establish the resistance and the stiffness of the joints. In case of the presented experimental tests the moment resistance ($M_{j,Rd}$) of the connection type behaviour specimens (Figs. 3.4 – 3.6) is determined by the component „end-plate in bending", which includes the effect of „bolts in tension". In case of the member end type behaviour of the composite section (Fig. 3.7) the recommendation the EC4 (EN 1994-1.1) is followed to evaluate the moment resistance ($M_{pl,Rd}$).

(a) standard M(Θ) diagram   (b) cyclic and envelope curves
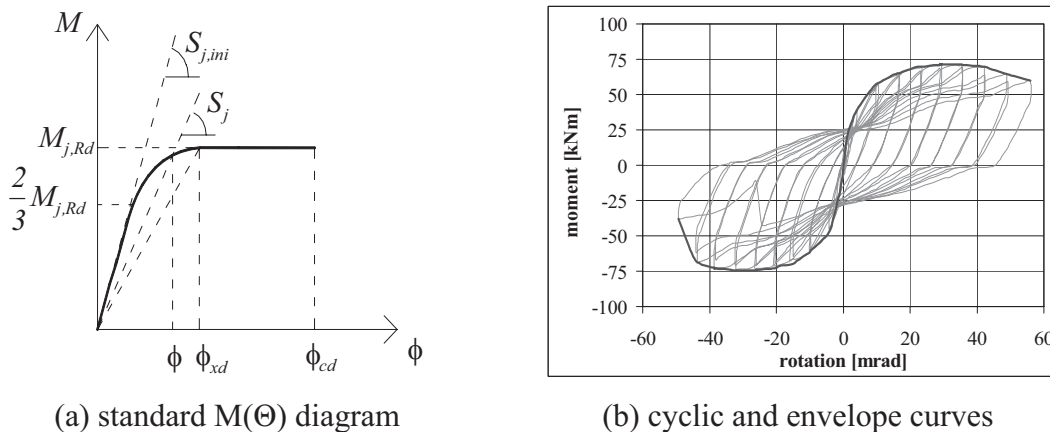
Figure 3.21: Moment-rotation diagram.

In the EC3 and EC4 procedures the evaluation of the resistances contain partial factor to ensure the safety level EN 1990 (2001). This γ_M partial factor includes the uncertainty in the material property γ_m - eliminated by material test results – and the model uncertainty γ_{Rd} – determined from the comparison of the experimental and design resistances.

The rotational stiffness ($S_{j,ini}$) of the joint is calculated in accordance of the EC3 recommendations (EN 1993-1-8, 2004). In the calculation the stiffness coefficients k_5 (end-plate in bending) and k_{10} (bolts in tension) are taken into account in accordance of the above considerations.

Comparison of design and experimental results

From the comparison of design and experimental results it is found that in case of the connecting element type failure modes the model uncertainty ($\gamma_{Rd} = M_{Rd,\exp} / M_{j,Rd}$, the ratio of the test and design moment resistance) is significant $\gamma_{Rd} \approx 1{,}47 \div 1{,}51$, the moment resistance of the joint is underestimated and in certain cases the design and the experimental failure modes are different. In case of the presented experimental program the standard EC3 procedure overestimates the initial stiffness in all cases ($S_{j,ini} / S_{j,ini,\exp} \approx 110 \div 244\%$, the ratio of the test and design initial stiffness) and the results have large scattering (note that similar observations can be found in Thomson and Broderick 2002).

Modification of the resistance model

The aim is to improve the resistance model with the modification of the design model characteristics, but keeping the basic EC3 formulas, to have design values closer to the experimental results. It is found that the modification of the lever arm h_r, in accordance of the experimental observation a better coincidence can be achieved. The proposed modification is shown in Fig. 3.22.
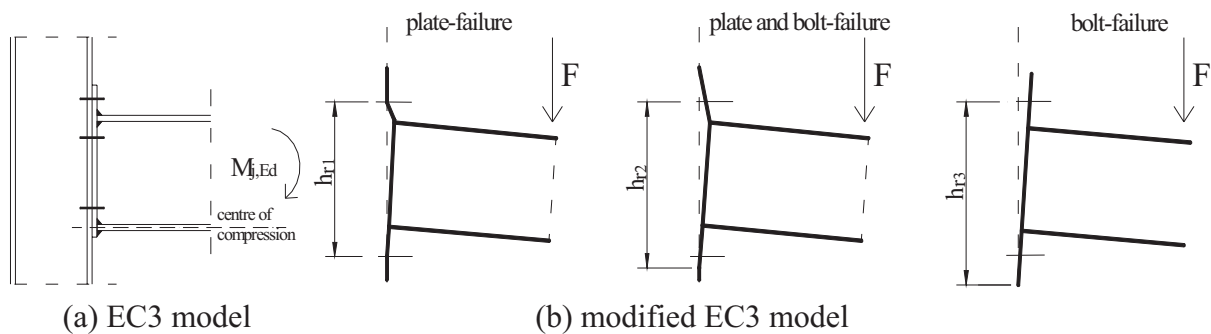

Figure 3.22: Moment resistance model.

Modification of the stiffness model

In the presented experimental program, the initial stiffness $S_{j,ini}$ depends on the k_5 (end-plate in bending) and k_{10} (bolts in tension) stiffness parameters, which modification is introduced. The details of the proposed modification can be found in Kovács (2005).

The original k_5 formula is coming from the stiffness of the both-end-fixed-bar model, however the experimentally observed deformed shape of the end-plate is between the extreme cases of fixed-fixed and fixed-simply-supported models. Introducing an α non-dimensional correction factor, which depends on the geometry and the thickness of the end-plate the k_5 stiffness coefficient is modified.

The k_{10} parameter means the normal stiffness of a tensioned bar, with the consideration of certain prying force. In EC3 it is assumed that the prying force is resulted in a 1,25 increment of the bolt force. From our previous research (Dunai, 1995) it is known, that the effect of the prying force is significantly increasing in non-symmetrical cases, for example in the case of flange angles or extended end-plate connections having bolts only in the out of flange region. From the comparison of experimental and EC results it is verified, if larger effect of the prying force is taken into consideration (decreasing the k_{10}) better coincidence is achieved.

Results of the modified design procedure

The design joint parameters are evaluated by the above detailed modification resulted in the modified joint moment resistance and rotational stiffness ($M_{jm,Rd}$, $S_{jm,ini}$). The plastic moment resistance $M_{pl,Rd}$ has not changed. The model uncertainty of the modified resistance model is expressed by $\gamma_{Rd,m} = M_{Rd,exp} / M_{jm,Rd}$.

From the results of the comparison it is concluded, that introducing the proposed modification the design resistance model is improved, the uncertainty of the resistance model is reduced ($\gamma_{Rd,m} = 1,05 \div 1,21$). The design initial stiffness is decreased in case of all specimens ($S_{jm,ini} / S_{jm,ini,exp} \approx 76 \div 152 \%$), but it is found that in certain cases it is still overestimated and the deviation of the results is still significant. Further studies are required to clear the problem (Dunai et al. 2004)

Extension the design monotonic moment-rotation curve to large rotation region

The model of EC3 procedure shows stable behaviour after reaching the moment resistance of the joint (as shown in Fig. 3.21,a), it does not reflect on the further behaviour. A simple experimental based procedure is introduced to control the behaviour of the joint in large deformation/rotation regions by a second order polynomial, as shown in Fig. 3.23.

For specimens having connecting element type failure second order polynomial curve is used over the moment level of $2/3\, M_{jm,Rd}$ until the specimen reaches the rotational capacity (Fig. 3.23,a). In case of local plate buckling type specimens quadratic curve follows the behaviour over the moment $4/5\, M_{pl,Rd}$ and before the crack propagation of the flange occurred (Fig. 3.23,b).

(a) connecting element type failure   (b) local plate buckling type failure
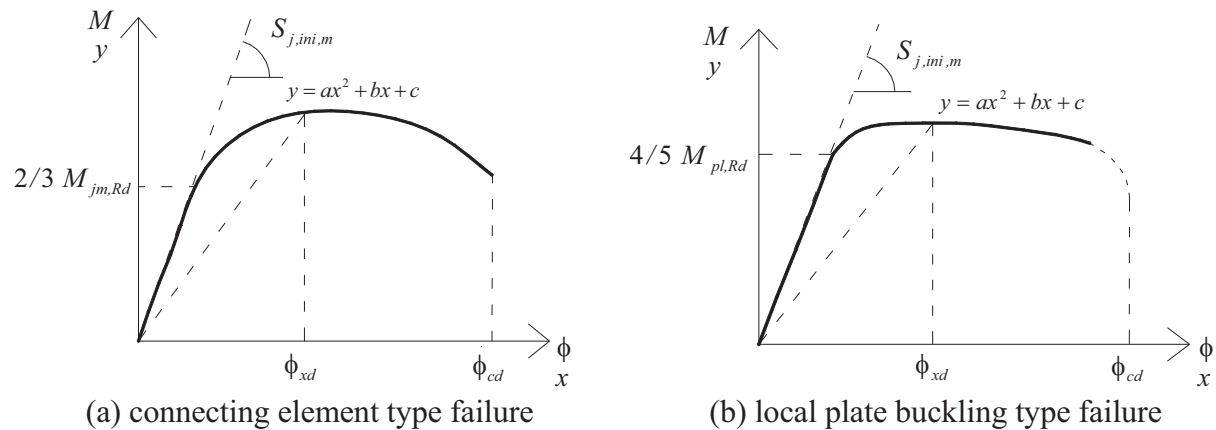
Figure 3.23: Extension of design moment-rotation curve.

The representing a , b and c parameters of the quadratic curve are established from experimental based considerations for each failure modes as the mean values of the corresponding specimens.

The comparison of the envelope curve and the EC3 and modified EC3 methods with the proposed polynomial function are presented in Fig. 3.24. It is noted that the design monotonic curve is assumed to be symmetrical about the origin.
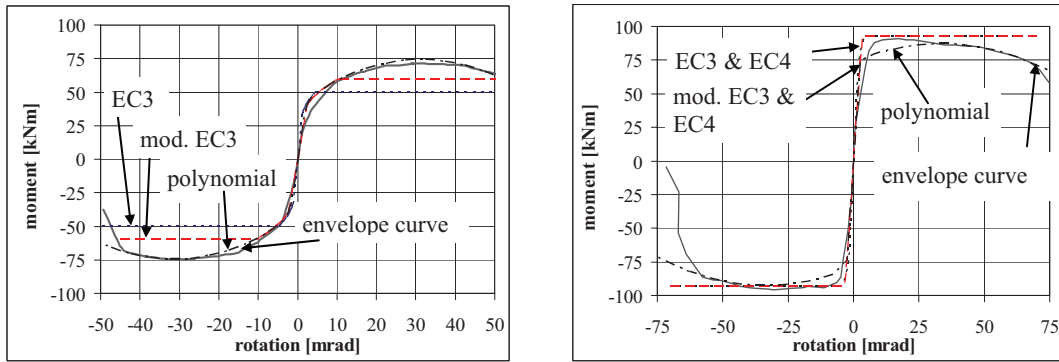
(a) connecting element type   (b) local buckling type

Figure 3.24: Results of the modified design method – M(Θ) curve.

3.6.2 Prediction model for cyclic behaviour

A semi-empirical method is developed to predict the cyclic moment-rotation relationship of the joints, including the member interacting zone. The method defines the typical hysteretic cycle belongs to the behaviour mode, and – by applying the standard cyclic loading history (ECCS, 1986) – the hysteretic diagram is built up by multi-linear hysteretic cycles. The degradation tendency during the consecutive cycles is expressed by a performance coefficient, which is experimentally determined by the linearized degradation of the rigidity. The proposed method is able to approximate the cyclic response and the absorbed energy of the studied joints for each observed failure mode types. It is based on the knowledge of the monotonic moment-rotation curve, which is established by the previously discussed EC3 modified design method. Note that it can be done by monotonic experimental tests or by finite element analyses, too.

Typical hysteretic cycle

An example of the typical cycle for end-plate type behaviour is presented in Fig. 3.26,a. The linear polygonal approximation of the cycles achieves good coincidence, as shown in Fig. 3.26,b). The tangents of the polygonal lines of the typical cycles are derived from experimental observations in the function of the initial rotational stiffness ($S_{j,ini,m}$) of the monotonic curve. The model uses performance coefficient to include the peculiarities of each behaviour mode type, which are defined as representing parameters for the failure mode types and calculated form experimental results. The proposed method follows the cyclic behaviour in stable plastic cycles, as shown in Fig. 3.25.
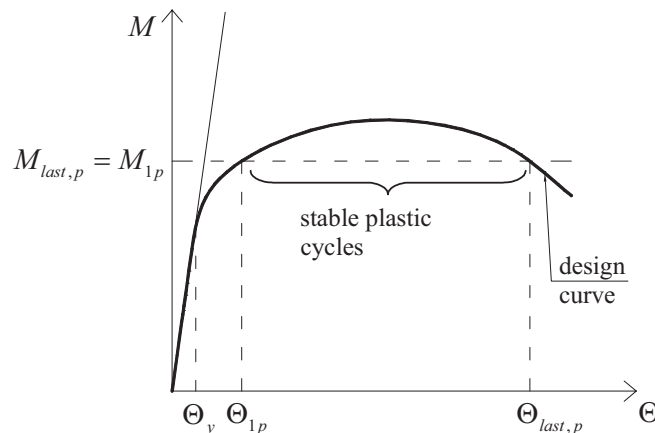

Figure 3.25: Notation for design curve.

The approximation of the cycle starts from the (M_{1p}, Θ_{1p}), point of the monotonic curve, with the determination of the unloading path (from M_{1p} to $M = 0$) and the loading path of the negative direction (from $M = 0$ to $-M_{1p}$) by experimentally based performance coefficients, reaching the negative part of the monotonic curve. The unloading path, coming from $-M_{1p}$ is also determined by the performance coefficients. The loading path of the positive direction reaches the monotonic curve at the rotation level Θ_2, which is determined according to the applied loading history. The hysteretic curve can be calculated cycle by cycle using the above detailed process.
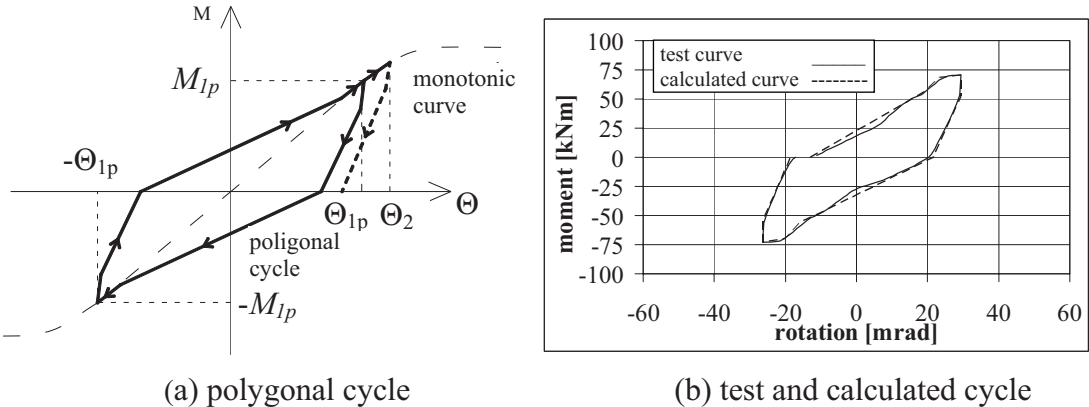

(a) polygonal cycle   (b) test and calculated cycle

Figure 3.26: Typical cycles.

The approximated curve of the most complex behaviour (local buckling of composite section) is considered as the "base curve", as shown in Fig. 3.27,d. The unloading path of each curve is defined by the same way of the two lines, as it is marked by dotted line in Fig. 3.27. From this "base curve" the diagrams, which belongs to the other above mentioned behaviour modes, can be reached by neglecting each part, as it is indicated in Fig. 3.27,a, b and c.

The approximated hysteretic curve is introduced in the further cycles including all the peculiarities of each behaviour mode types.

Degradation during the consecutive cycles

The degradation tendencies of performance coefficients related to the unloading path of the hysteretic curve are defined by the rigidity ratio and it is obtained from experimental results for each cycle. The rigidity ratio is defined by ECCS (1986) recommendation. It is found that the degradation tendency of this rigidity ratio can be assumed as a linear function vs. the partial ductility. On the basis of experimental observations it is assumed that the tangent of the rigidity degradation is a characterizing value for each behaviour modes, as shown in Fig. 3.28.

68

(a) bolt failure   (b) plate-failure

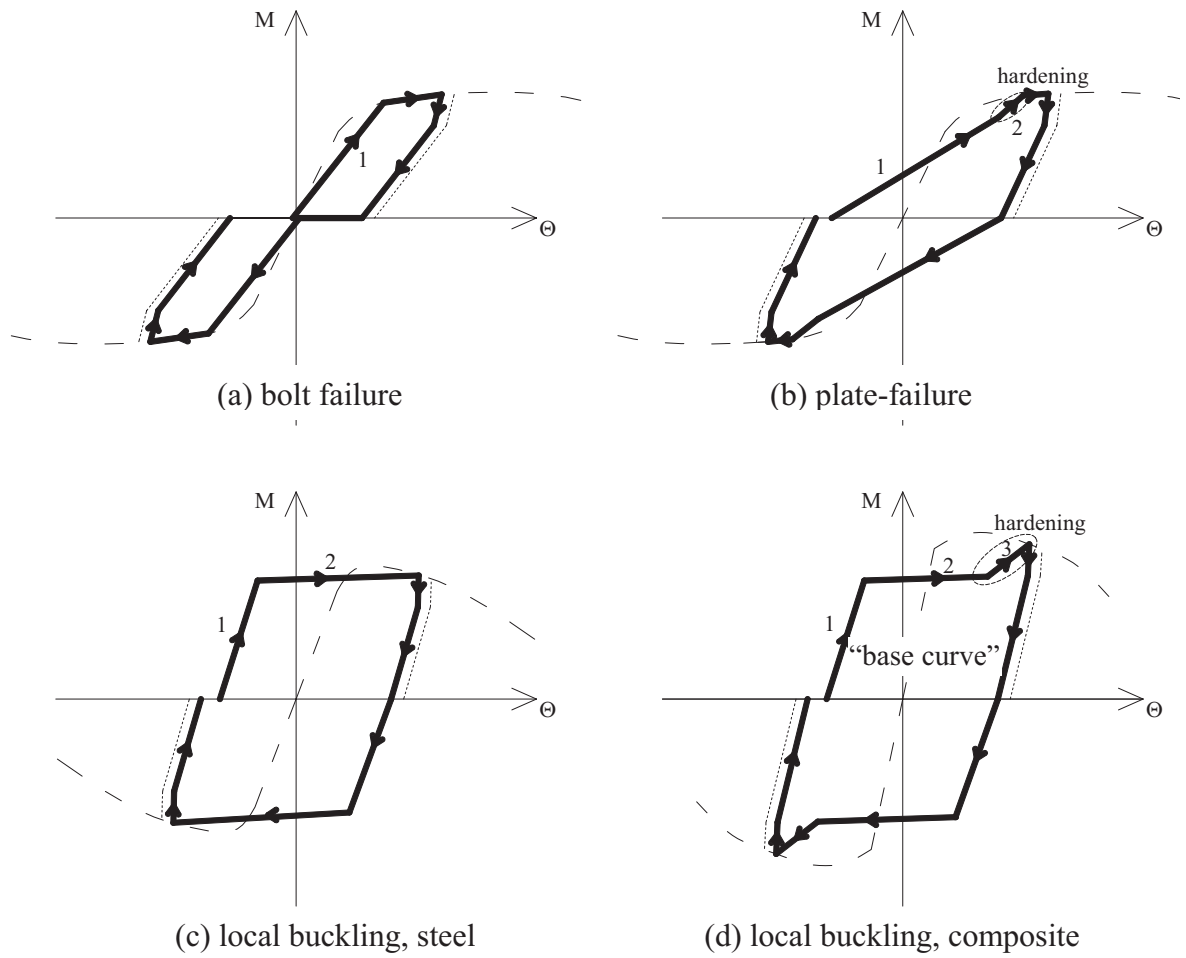(c) local buckling, steel   (d) local buckling, composite

Figure 3.27: Multi-linear hysteretic typical cycles.
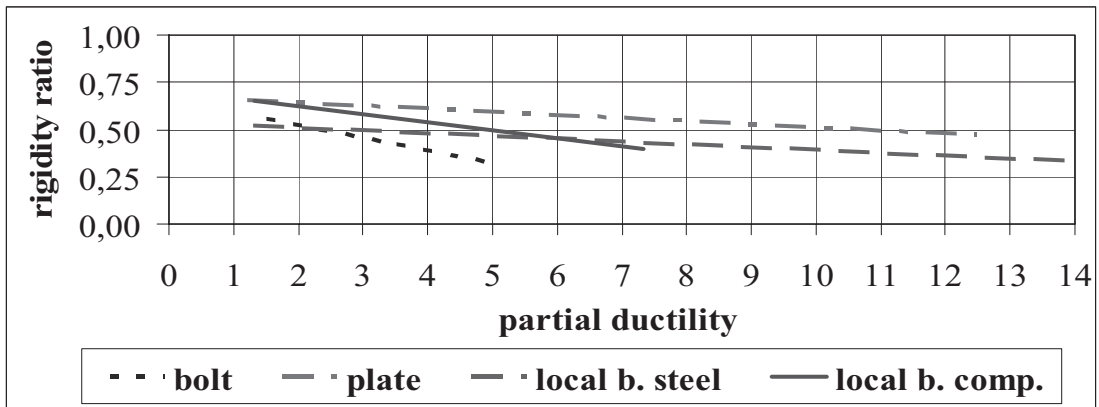

Figure 3.28: Rigidity degradation tendencies in each behaviour mode.

The approximated hysteretic moment-rotation relationship

The developed method is applied by using the modified EC3 design monotonic curve to approximate the cyclic response of the joints. From this monotonic curve the hysteretic diagram is calculated cycle by cycle applying the ECCS (1986) loading history. The results are presented in Fig. 3.29 and show good coincidences with the experimental curves of Figs. 3.4 – 3.6 and Fig. 3.8.

(a) bolt-failure

(b) plate-failure

(c) local buckling, steel

(d) local buckling, composite
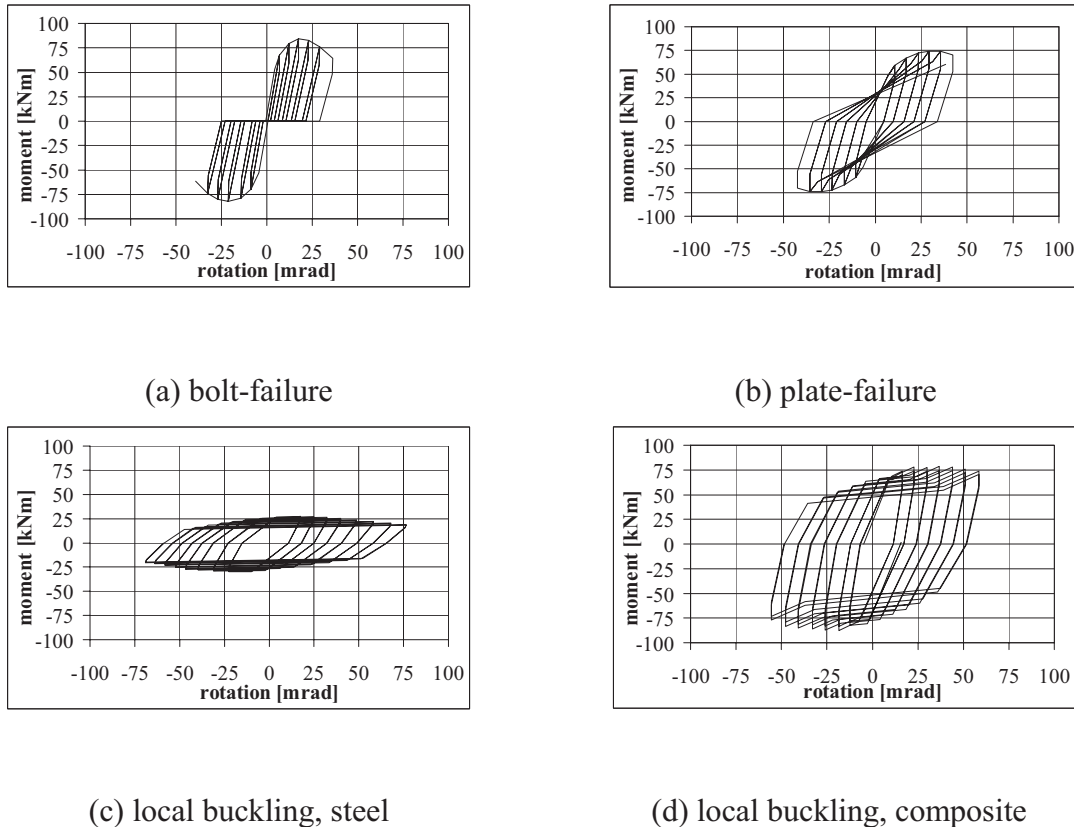
Figure 3.29: Predicted moment-rotation relationships.

The stable plastic cycles include the specialties of each behaviour mode type using experimentally detailed parameters (cyclic resistance degradation; increasing of the stiffness at the end of the cycles; specialties of the local buckling of steel and composite sections). The end of the stable plastic cycles is in accordance with the governing behaviour as follows: bolts elongation capacity, end-plate crack propagation and crack of the tension flange.

Comparison of the absorbed energy

The absorbed energy of the consecutive hysteretic cycles are established from the approximated curves and compared with the absorbed energy of the corresponding experimental results (Fig. 3.30), in case of three studied failure mode types of the composite specimens. The predicted absorbed energy shows good coincidence with the test result.
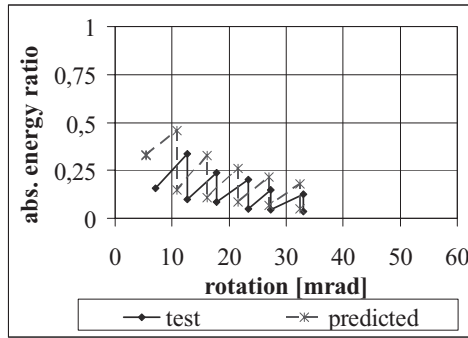
(a) bolt-failure
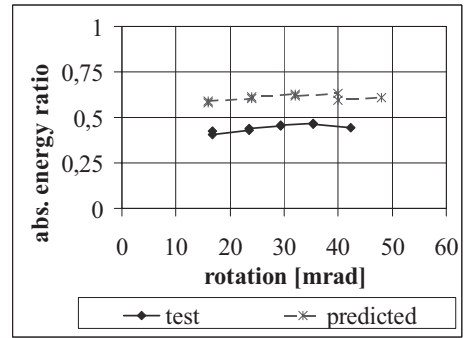
(b) plate-failure
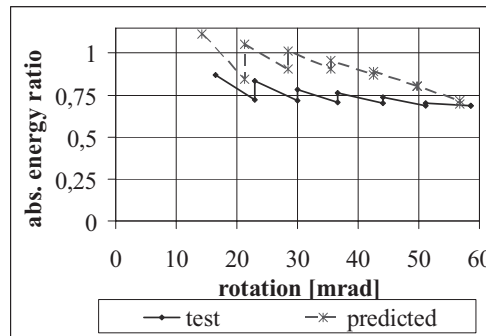
c) local buckling, composite

Figure 3.30: Absorbed energy ratios from experimental and analytical studies.

3.6.3 Application of the developed model

The developed model can predict the cyclic moment-rotation relationship of the studied type of composite joints with a good accuracy from practical point of view. Having the hysteretic curves, the cyclic parameters of the different joint arrangements can be calculated. These values can be used in the seismic judgement of the designed constructional details. On the other hand the hysteretic curves can be implemented in advanced structural models for time history frame analysis.

3.7 Conclusions

3.7.1 Experimental conclusions

Two sets of experiments on the cyclic testing of steel and steel-concrete composite joints are completed. The experimental program is planned to complete prototype and design tests. The cyclic behaviour of the 17 specimens is determined; four different behaviour modes are identified and characterized; the relationships of the detail parameters and their behaviour modes are established.

The experimental observations show that the combined bolt and plate-failure of the connecting element type behaviour and the local buckling-failure of the composite section are the most favourable behaviour from seismic design point of view. The hysteretic moment-rotation curve and the cyclic parameters express the seismic behaviour of the joints, which show that these specimens have significant plastic deformation capacity, high resistance and the hysteretic diagrams are stable; the specimens do not show significant moment resistance degradation until the crack start to propagate in the steel sections. The cyclic diagrams have a 'fat' shape, which reflects on the large energy absorption capacity. It is proposed to design the structural joints to follow the above mentioned behaviour modes.

3.7.2 Numerical approach conclusions

Two phases of the numerical investigation on joints under cyclic loading are completed: finite element modelling and model verification.

The cyclic finite element models are developed on the basis of essential requirements to cover the very complex phenomena. This is why the accuracy testing and efficiency evaluation of the models required a multi-step procedure. In the completed research a numerical model verification method is proposed, and a set of benchmark examples are introduced, which can be used to check the cyclic models and computational methods in a step-by-step manner.

The applicability of the numerical model is proved; it can be used to extend the cyclic test results by virtual experiments. This further step of the research combines the experimental and numerical approaches.

3.7.3 Design model conclusions

In the research an analytical study is completed in order to predict the hysteretic moment-rotation curve, and determine the cyclic parameters which can be used in the seismic design.

In the first step the design method of EC3 and EC4 is studied; it is found that in case of connection type behaviour the standard design model has significant uncertainty, which underestimates the moment resistance, overestimates the initial stiffness and in certain cases the design failure mode does not follow the experimental one. An improvement of the EC3 resistance and stiffness model is proposed. Since the EC3 design procedure does not reflect on the behaviour of the joints in large deformation regions, an extension of the model is proposed.

In the second step of the analytical studies a semi-empirical method is proposed to predict the cyclic hysteretic behaviour of the tested joints. The proposed method applies polygonal approximation of the hysteretic curve and coincides well with the experimental cyclic curve, and shows a good agreement for absorbed energy during the increasing cycles.

3.7.4 Proposal for joint detailing

During the extended – experimental, numerical and analytical – research activities of the last decade a lot of practical experiences are collected on the cyclic behaviour of the studied type of joints. On this basis, proposals are made for the advantageous constructional detailing which can be used directly in the design practice as a preliminary guidance. These proposals are detailed in Kovács (2005).

4. Non-conventional large scale steel structures

4.1 Introduction

4.1.1 Background

To design a large scale structure is always a challenge and great importance for the designer. It is especially true for a country, where the leading dimensions of the structures are not typical. Despite, in the last five years in Hungary two steel structural projects have been completed where the geometrical dimensions of the structures are "large" even in the international comparison, as follows:

- A research and development project is completed on a new generation of steel cooling tower system with a height of 100 to over 240 meters and diameter of 60 to 120 meters.
- A highway bridge project is completed on a new Danube bridge in Dunaújváros with a total length of 1676.8 meters, and a main span of 307.8-meter-tied arch bridge; this one is a world recorder in its category.

Beside the large geometrical sizes these structures are non-conventional in the sense of the application of new structural arrangements required by the structural behaviour, fabrication technology and erection method. These consequences cannot be handled automatically by the standardized design methods this is why research is required to support the realization. I have been involved in the design and research background development of both projects.

In the frame of the steel cooling tower structure project I supervised the sub-task on the joint of tubular members' development and research within a consortium of industrial and university partners. The three-dimensional joint of tubular members in the space structure is solved by 3D gusset plate and welded, bolted and pinned connections. We have been completed experimental model tests to characterize the governing behaviour phenomena and to check the different prototypes and design methods (Dunai et al. 2002). The experimental studies are extended by advanced numerical analysis for the verification of the sensitive constructional details (Vigh and Dunai, 2004). The final constructional details of the tubular joints and the pertinent design methods are determined together with the designers of the Pi-Hun Ltd (Cholnoky et al. 2006). The numerical part of the research is completed and presented by László Gergely Vigh in his PhD thesis under my supervision (Vigh, 2006).

Concerning to the Dunaújváros Danube bridge project I supervised a team on the expertise, research and design activities, as follows:
- preliminary studies on the main geometry and cable arrangement of the tied arch (Honfi et al. 2005);
- global stability of tied arch (Joó and Dunai, 2005);
- local stability of stiffened plate elements (Dunai, 2006);
- behaviour and resistance under wind loading (Hegedűs, 2005 and Goricsán et al. 2005);
- fatigue of orthotropic deck (Mihálffy et al. 2005);
- earthquake analysis and resistance checking (Vigh et al. 2006);
- constructional detailing (service and erection stages).

The above activities are completed in a close co-operation with the designers of Főmterv Co. (Horváth et al. 2006). In this Chapter I concentrate on the research on the global arch stability and on the design checking of the bridge during the erection process (advanced numerical modelling, analysis and design of joints and stiffened plates).

In the followings first I define the purpose and the strategy of the research and then I summarize the completed experimental and numerical studies of the two structures, in Sections 4.2 and 4.3, respectively. The design applications are referred by the published papers of the team.

4.1.2 Purpose and research strategy

The <u>main aim</u> of both research activities was to create the background for the design of the non-conventional structural details of the investigated structures.

The <u>particular purposes</u> were as follows:

3D tubular joint of steel cooling tower:
- identification and characterization of new behaviour modes of novel structural solutions;
- verification of existing design method for the new detailing;
- verification of joint prototypes in different developing phases;
- developing advanced design methods.

Tied arch bridge stability:
- verification of existing design methods for global arch buckling;
- developing and applying advanced design methods for global and local stability checking (independent checking).

Despite the different types of structures and physical phenomena in the two projects the overall research <u>strategy</u> was very similar, as illustrated in Fig. 4.1.

In both cases interacting experimental and numerical studies are completed in order to investigate the phenomena. The model tests are "verification tests", in order to develop advanced FE models. These models are used for design ("analysis" and "FE simulation") as well as for extending the test results ("virtual experiments"). On the bases of the laboratory and virtual test results the applicability of existing design methods are checked ("validation tests"). In the case of the joints the test are also applied as "prototype tests".
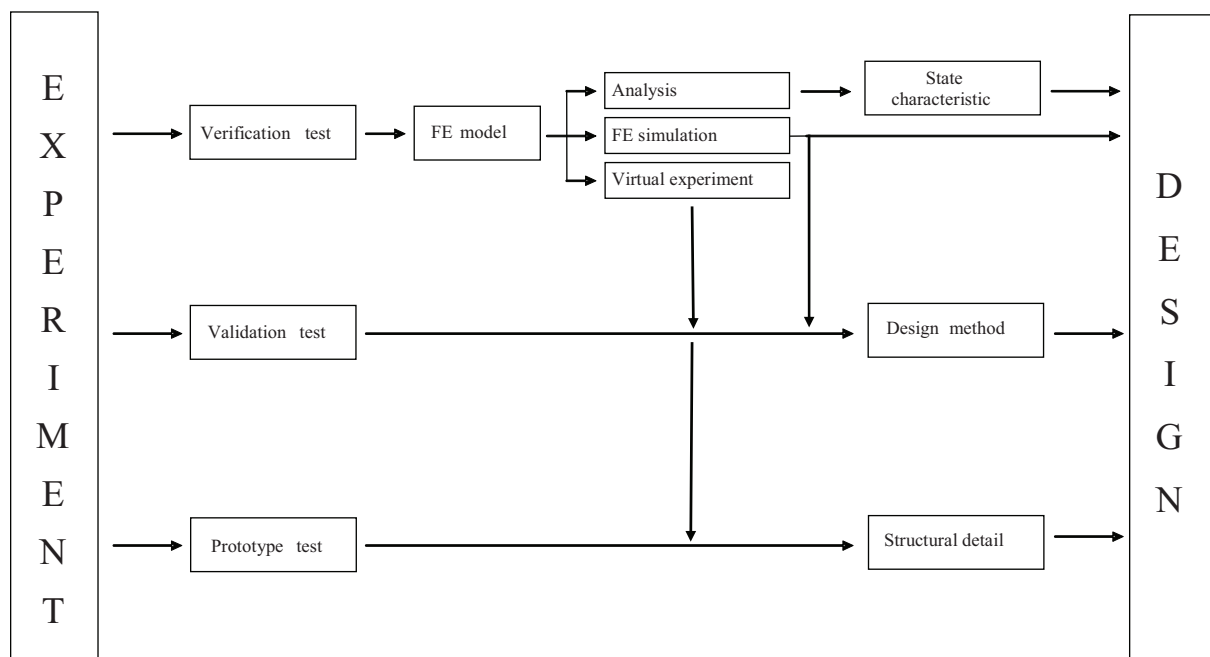

Figure 4.1: Applied research strategy – non-conventional large scale steel structures.

4.2 Steel cooling tower system

4.2.1 Structural arrangement and research program

Steel cooling towers are primarily implemented as a structure for large vents required for the operation of dry cooling systems for power plants (Cholnoky et al. 2006). On the basis of the result of previous developing phases of steel cooling towers an "optimal" structure of the cooling tower is decided, as shown in Fig. 4.2,a. The shape and the structural arrangement resulted in advantages in the construction properties: low ratio of applied steel material and minimal fabrication and erection time. The main steel structure consists of 2 bottom cones and 1 upper cylindrical 3D truss frameworks, with about 10 m node-to-node spacing. The main specialities of the structure can be described by three factors. Firstly, prefabricated tubular members with high radius-to-thickness ratio are applied (i.e. ~60). Secondly, a special joint has been developed to connect the structural elements, as shown in Fig. 4.2,b. Itself the joint is made of gusset plates welded to tubular elements. Then the thin-walled horizontal and vertical bars are connected to the joint by bolted end-plates. The diagonal bars are connected to the joint directly to the gusset plates by pinned connections. Although the presented joint configuration is highly advantageous with regard to easy and fast erection, the different connection types result in a complex interaction in the structural behaviour. The third special aspect is that the joint is non-planar due to the 3D shape of the structure, which even more complicates the structural behaviour.
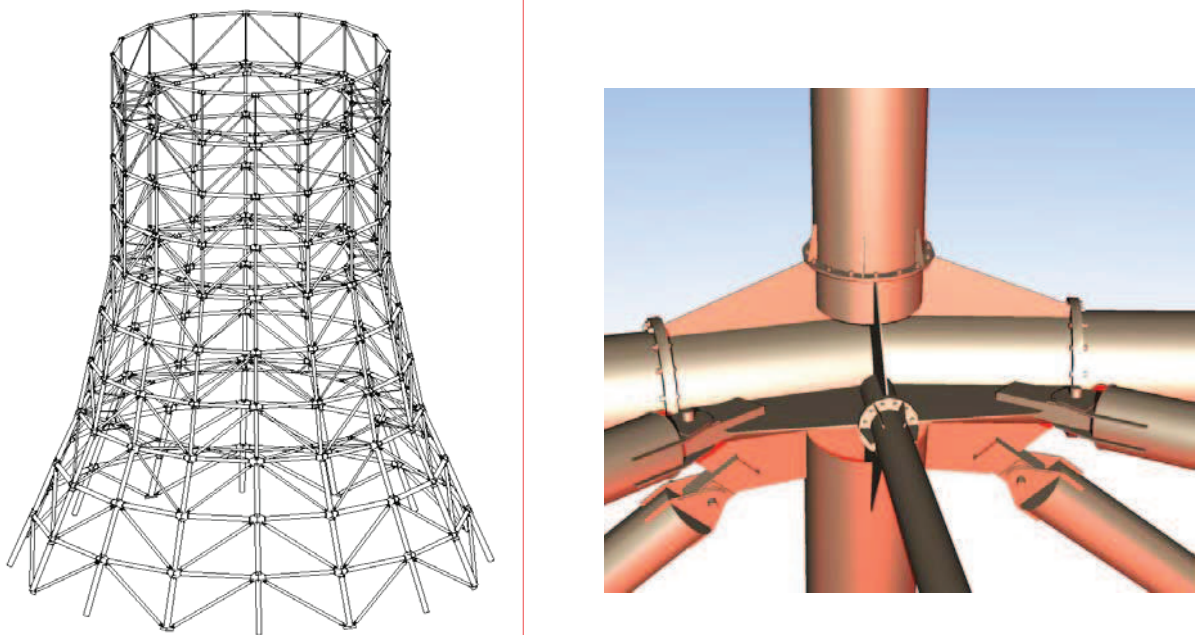
Figure 4.2: (a) Skeleton and (b) 3D joint of steel cooling tower.

The complex behaviour of the joint is studied by an interacting experimental and numerical research program. First the structural details are developed by preliminary design on the bases of standardised approximate design methods. The typical joint details are investigated by an experimental program; the test specimens are designed on the bases of the preliminary design method and by finite element simulation. In the tests the load transfer (elastic behaviour) and failure modes (ultimate behaviour) are determined. In parallel with the experiments finite element model is developed and verified and then virtual experimental program is completed on the parameters of the joints. The joint details are improved and design methods are developed and validated on the bases of the results of experimental and numerical studies.

4.2.2. Experimental model

The experimental study is designed under the following considerations:

- Full-scale model of tubes with a diameter of 500-900 mm cannot be tested in the available laboratory capacity that is why a model of scale 1:2.5 is developed.
- Due to the complex wind loading of the cooling tower the internal forces of the elements have a wide range in distribution and magnitude. In the experimental program the possible components are considered; the combinations are handled by the superposition of the load cases.
- The ultimate behaviour is studied in separated test with a focus on a certain targeted elements of the joint. By this strategy different failure modes of the same joint specimen can be analysed.

Test specimen

Figure 4.3,a shows the test model of the studied joint. It can be seen, that relatively long tubular elements with special ends for load introduction are connected to the joint. By this arrangement the forces and moments can be created in the joint and the local effect of concentrated forces can be eliminated.

The two studied structural details of the joint are shown in Figs. 4.4,a and 4.4,b. It can be seen, that the horizontal tubes are connected by bolted end-plate connections to the joint element, in which the load is transferred by the continued tubes. The upper vertical tube is connected to the joint element by similar bolted end-plate connection, but within the joint element the load transfer is solved by two gussets, which are built together by welding with the lower vertical tube. The diagonal bars are connected to the gussets by pinned connection. In case of the first prototype a simple pinned connections is used directly to the joint's gusset plate (specimen 1). In the second prototype this connection is reinforced, using rectangular hollow sections (specimen 2).

Test arrangement

The test setup can be seen in Fig. 4.3,b. The end of the lower vertical tube is supported by a pin and all the other ends of the tubular elements can be loaded by hydraulic jacks in different directions and arrangements, as it is shown in Fig. 4.5.
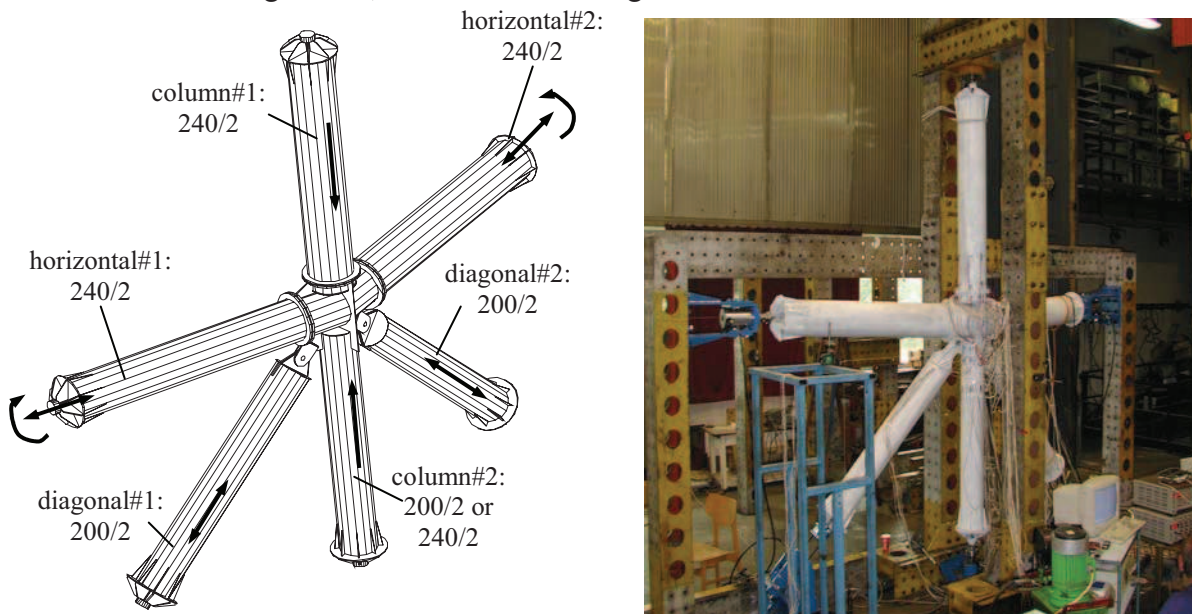

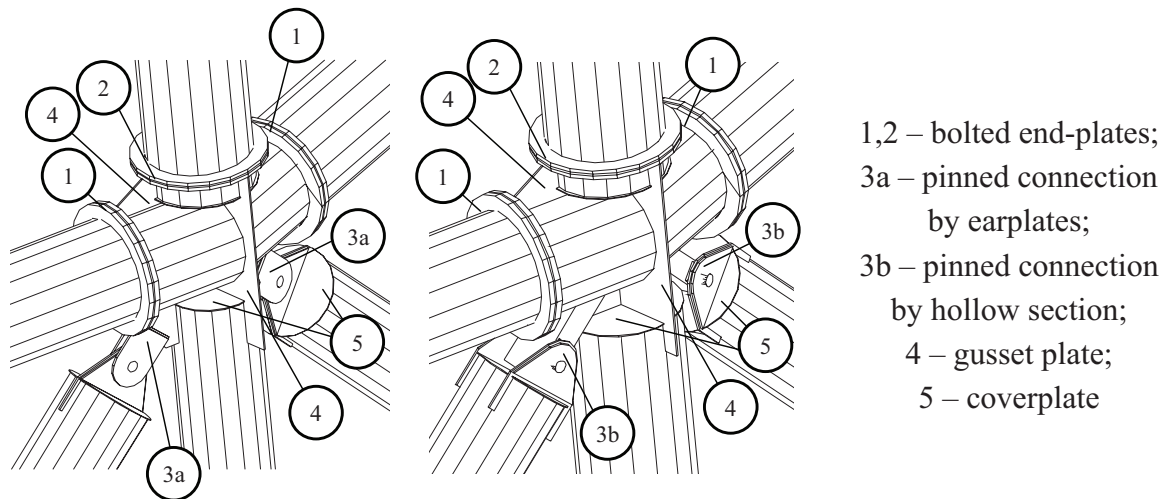Figure 4.3: Test arrangement: (a) specimen and (b) setup.

Figure 4.4: Joint details: (a) prototype 1 and (b) prototype 2.

1,2 – bolted end-plates;
3a – pinned connection by earplates;
3b – pinned connection by hollow section;
4 – gusset plate;
5 – coverplate
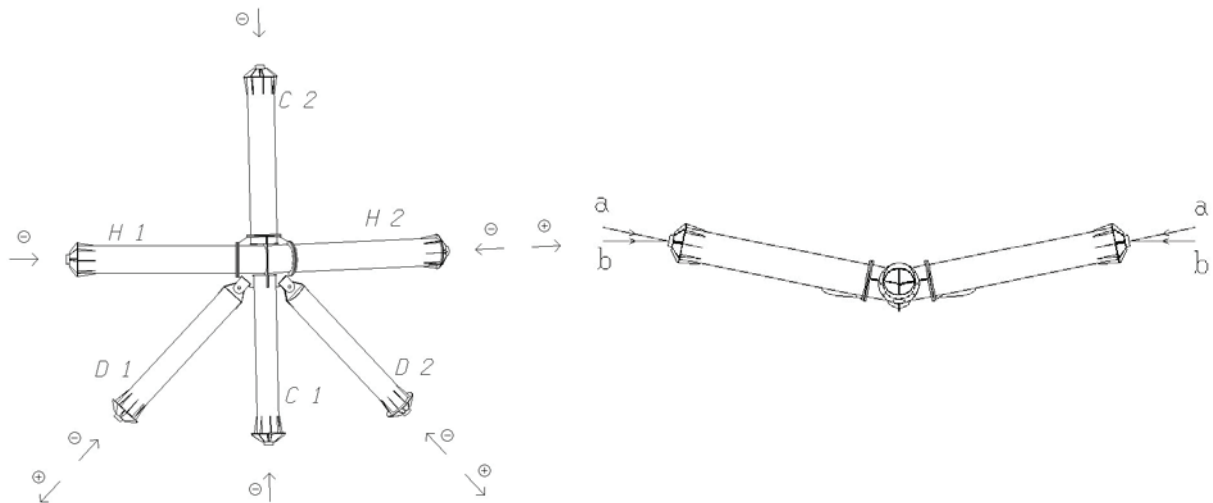
Figure 4.5: Loading system.

Measurement system

In the testing program the reaction force of the lower vertical tube is measured by a loading cell and the active forces are by the oil pressure. One or two hydraulic circles are used to model the different ratios of the load components at the ends of the members. The global deformation of the joint is measured by three displacement transducers in a selected reference point of the specimen. The stress transfer from the elements to the joint is measured by 92 strain gauges. These are placed on the outer surfaces of the tube ends in several sections, and on the connecting gusset plates.

Load combinations for elastic behaviour

There is a wide range of possible load combinations of internal forces in the connected elements of the studied joint. In the experimental program these cannot be followed by a simple loading system. Instead of that the stress distribution is followed by simple load cases and then the stresses from different internal forces can be obtained by the superposition of the pertinent load cases. Table 4.1 shows the applied load cases during the experimental study of the elastic behaviour. The table refers to the notation of Fig. 4.5. In the boxes of the table the '+' and '−' mean the directions of the applied force of the pertinent element while '0' indicates of the element is not loaded. The 'a' and 'b' codes after the '−' sign are related to the axial or bending effect of the applied forces in horizontal members, as it is shown in Fig. 4.5.

No.	C1	C2	H1	H2	D1	D2	No.	C1	C2	H1	H2	D1	D2	No.	C1	C2	H1	H2	D1	D2
1	-	-	-/a	+/a	+	-	9	-	-	0	+/a	+	-	17	-	-	0	-/a	0	+
2	-	-	0	0	0	0	10	-	-	0	+/a	+	0	18	-	-	0	0	+	0
3	-	-	0	0	+	-	11	-	-	0	+/a	0	-	19	-	-	0	0	+	+
4	-	-	-/a	0	+	0	12	-	-	0	0	0	0	20	-	-	0	0	0	0
5	-	-	-/a	0	+	-	13	-	-	-/a	-/a	+	+	21	-	-	-/b	-/b	0	0
6	-	-	-/a	0	0	-	14	-	-	-/a	-/a	0	+	22	-	-	-/b	-/b	0	+
7	-	-	-/a	+/a	+	-	15	-	-	-/a	-/a	0	0	23	-	-	-/b	-/b	+	+
8	-	-	-/a	+/a	+	0	16	-	-	0	-/a	+	+	24	-	-	-/b	-/b	+	+

Table 4.1: Load cases.

The load transfer in the 3D joint is studied by the application of the above load cases in the elastic range. The obtained stress distributions are evaluated by the superposition of the different load cases using the internal force obtained from the global structural analysis. From these results the typical tendencies are derived and the ultimate tests are designed.

4.2.3. Ultimate behaviour

After completing the elastic measurement program the ultimate behaviour of the joint is studied. The two specimens are tested in different load combinations focusing on the ultimate behaviour modes of the joint details called as „horizontals", „diagonals" and „columns" (these joint details' names mean the element end, bolts and end-plate connecting elements and gussets which take part dominantly in the given load transfer). The experimental findings are summarized for these joint details in the followings.

Behaviour of „horizontals": In these tests a constant compressive load is applied in the vertical members and tensile forces in the diagonals. After that the compressive load is increased in 'b' arrangement (see Fig. 4.5) in the horizontals, until the failure is occurred. In the increasing load steps, in the measurement points of H2 horizontal member, within the joint zone, in the compression part yielding is observed. When the plastic zone is extended the limit point is reached and the final failure is occurred by plastic buckling of the tube, as it is shown in Fig. 4.6 (failure mode #1). This load combination is applied to investigate the bolted end-plate connections of the horizontal members. At the collapse load level no any damages are experienced in the connections. The same load combination is applied in the second specimen, as well, but reduced number of bolts is used in the end-plate connections (only the half of the bolts is used. At the increasing load level the opening of the connection is observed (relative elastic displacement between the end-plates), but it did not lead to damages in the bolts nor in the end-plate. The final failure is occurred in the same way as described above (failure mode #1) in the element end, as shown in Fig. 4.6,b. This observation showed that the connection can resist the full strength of the connecting elements.

Behaviour of „diagonals": First this investigation is applied in specimen 1 (prototype 1) where a constant compressive load is applied in the vertical members and in H1 horizontal member, and the joint is supported effectively in the out-of-plane direction. After that the compressive load is increased in D2 diagonal until the failure is occurred. In the increasing load steps, in the measurement points of the connecting gusset plate of D2 diagonal, increasing tension stresses are observed, indicating significant bending. Plastic strains are indicated by the strain gauges in the gusset plate surfaces, as a result of significant out-of-plane bending. When the plastic zone is extended the limit point is reached and the final failure is occurred by plastic failure of the gusset plates on both element end and joint, as it is shown in Fig. 4.7 (failure mode #2). Due to this observation the diagonal connection is reinforced by rectangular hollow sections welded to the gusset plate and to the horizontal, as shown in Fig. 4.3,b and in Fig. 4.8. The new detailing is applied in the second specimen (prototype 2). The repeated test proved the strength of the modified connection. Note, that in the pinned connection no damages are observed in the tests.
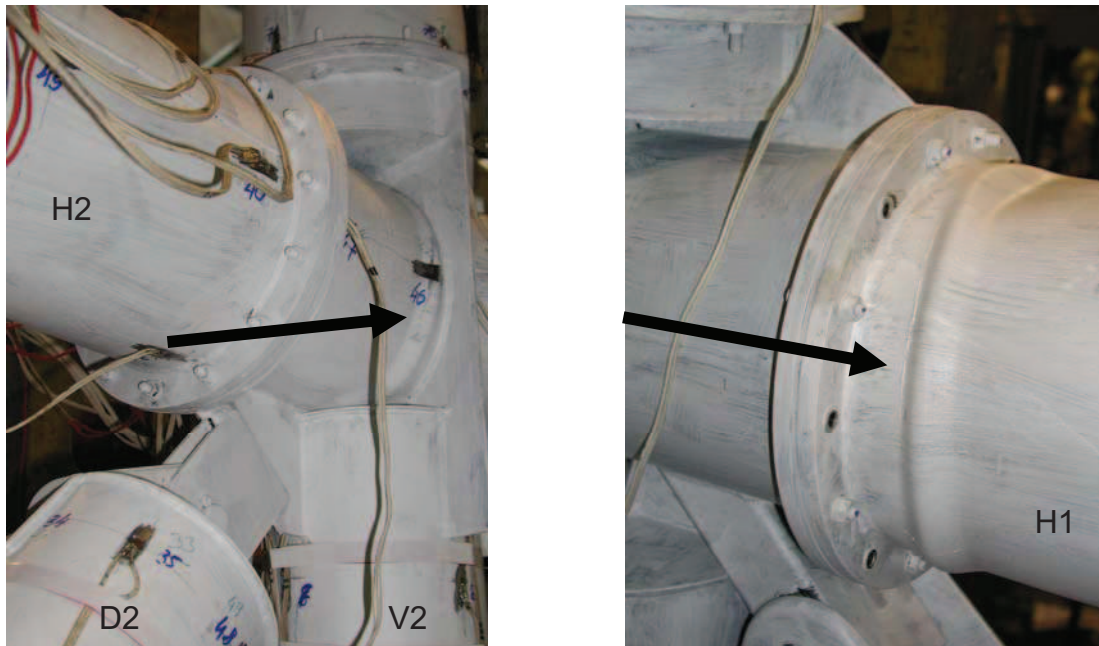
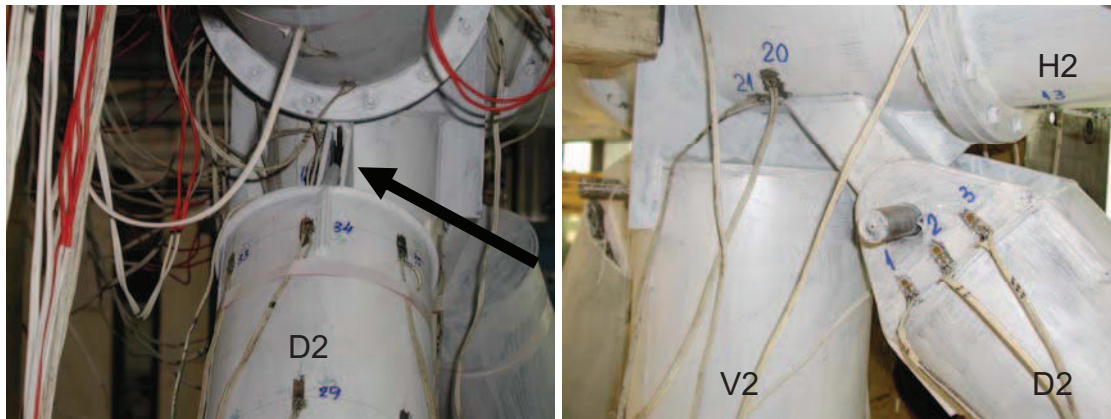Figure 4.6: Failure mode #1 in (a) prototype 1 and in (b) prototype 2.

Figure 4.7: Failure mode #2 in prototype 1.   Figure 4.8: Strengthened diagonal.

Behaviour of „columns": In these tests the joint is loaded by eccentric compression by the columns; the diagonals are inactive, and the horizontal members are applied as supports (with negligible compressive force). The compressive load is increased in the vertical member, and two different failure modes are observed.

In specimen 1 in the measurement points of the joint gusset plates yielding is observed mainly in the outer part (note, that the behaviour showed quite centric action). The plasticity is started in the upper part of the gusset (Fig. 4.9,a). The maximum load is reached and the signs of the plastic buckling are appeared in the gusset plate, the dominant out-of-plane deformation probably appeared in the covered part of the gusset plate (failure mode #3).

In specimen 2 the lower column section is modified, a column with bigger diameter-to-thickness ratio is used. The same load combination is applied and a sudden, shell buckling type failure, with diamond shape pattern is observed in the lower part of the column just under the welded gusset plate, as shown in Fig. 4.9,b (failure mode #4). This local phenomenon is occurred without any signs in the structure and resulted in a fast drop of the load level. The dangerous failure is studied in details by numerical analysis (virtual experimenting) in order to explain and to find the influencing parameters.

The above ultimate behaviour modes are characterized in parallel with the numerical studies in the following Sections.
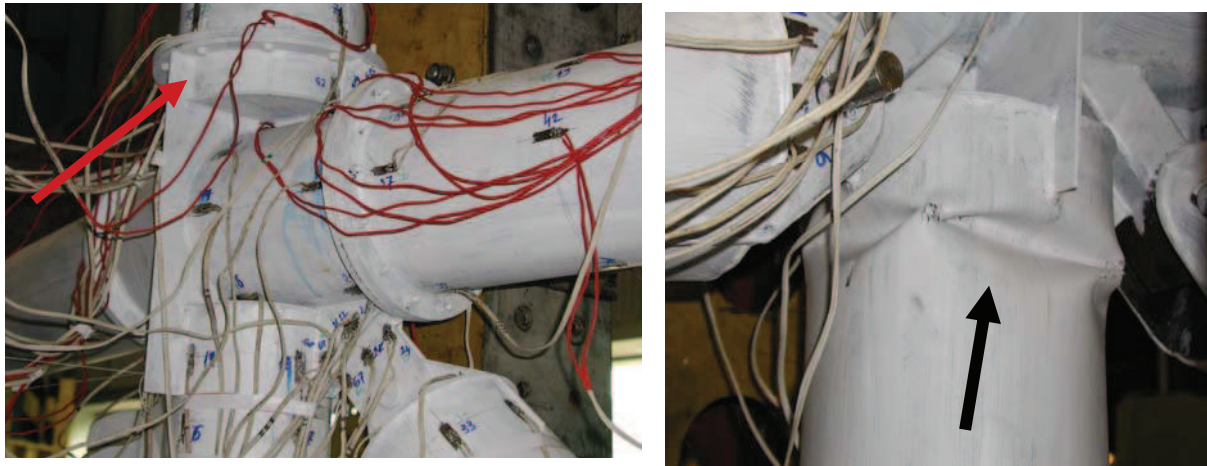
Figure 4.9: Behaviour of „columns": (a) failure mode #3 and (b) failure mode #4.

4.2.4. Numerical models

Modelling aspects

In advance and in parallel with the experimental tests different levels of numerical models are developed on the basis of the ANSYS finite element program system (ANSYS, 2001), with the aim to investigate the most dominant joint behaviour, as follows:
- yielding of the whole cross-section of the tubular member,
- local buckling of the tubular member,
- yielding of the gusset plate of the joints,
- buckling of the gusset plate of the joints,
- bolt failure: plastic deformation and fracture,
- bolt failure and plastic hinge at the intersection of the tubular wall and end-plate,
- plastic hinge at the tubular wall – end-plate intersection and in the end-plate.

Note, that the pinned connection of the diagonal is not part of the numerical study; the element end behaviour is covered by standardized design method.

Two numerical models are developed: a local model for the preliminary analysis of the bolted end-plate connection and a global model for the whole joint analysis.

Local model of the bolted end-plate connection

The local model is developed with the purposes (i) to verify the applied standardized connection design method and (ii) to determine the accurate and efficient model level what can be implemented into the global joint model. Different shell finite element models are developed and tested in a comparison and parametric study, as shown in Fig. 4.10. The models are described in details in Vigh and Dunai (2004). A local tubular member model is also developed to check the mesh accuracy for the application of buckling phenomena, as detailed in Vigh (2006).
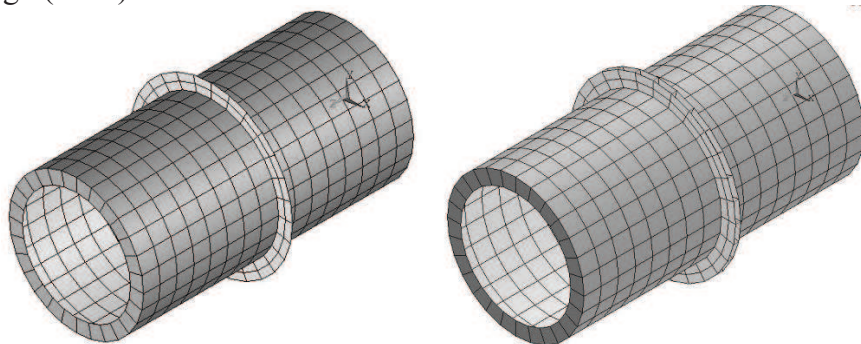

Figure 4.10: Finite element model of the bolted end-plate connection.

80

Global model of the joint

On the basis of the preliminary studies, the shell-element model of the whole joint, shown in Fig. 4.11, is developed. The model is developed for both actual structure and 1:2.5 scaled test specimen. To avoid the disturbance caused by direct loading, the length of the tubular members is determined as about five times of the diameter. The possible mesh densities are determined by the given bolt allocation. For most of the analyses, the shown mesh is eligible; however, for plastic analyses, the inner joint parts are refined to follow the local buckling phenomena.
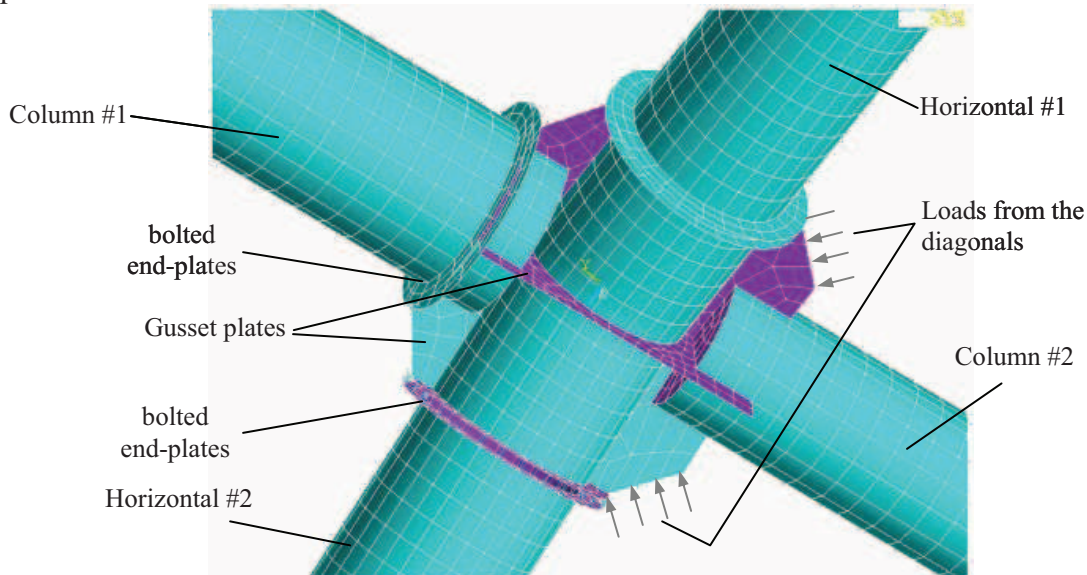

Figure 4.11: Finite element model of the joint.

The ends of the bars are loaded: the horizontals can be tensioned, compressed and/or bended; the verticals are always compressed. The compressed or tensioned diagonals are not modelled: the pinned connection gives the opportunity to substitute them by their load only. At the modelled bars, uniform load distribution is achieved by means of relatively rigid plates at the loaded end.

As the structural material, linear elastic or linear elastic – perfectly plastic material model is set, for the stability analysis and for the material and geometric nonlinear imperfect analyses (virtual experimenting), respectively. The bolt-representing springs are associated with bilinear spring characteristics derived from test results of bolts.

In the analysis, large strains and displacements are considered. During the virtual experimenting, force-controlled, arc length solution method is used. The iteration is completed on the bases of the Newton-Raphson method. The convergence of the iterations is checked by the Euclidian norm of the unbalanced forces and moments; the applied convergence tolerance factor is 0.1%.

A convergence study is done in case of the whole joint, subjected to a general load case (bended horizontals, compressed column and diagonals). Three meshes are tested: the total element number of 2844 (2712 nodes), 4920 (4774 nodes) and 9428 (9229 nodes). The difference in reaction forces (at the bottom column) and in maximal deflections is less than 0.5% and 1.7%, between first and third models. Finally, the second meshing – which uses twice number of elements as bolts are located around the circumference – is selected for the further elastic analyses (5364 elements and 5164 nodes at the final configuration).

The illustrated mesh is eligible for global analysis in general. In the case of local stress concentrations and local buckling phenomena, the model is refined locally.

4.2.5. Ultimate analysis of bolted end-plate connection

The different local models are first compared by the analysis of a typical connection configuration of the actual structure: with diameter D=600mm, thickness t=5mm, and with 14 pieces of M20 10.9 bolts. The numerical analyses are applied assuming different end-plate thicknesses (10-30mm) and the results proved that the separate modelling of bolts is required (Fig. 4.10,b), because of the experienced semi-rigid behaviour (Vigh and Dunai, 2004).

In the second phase the semi-rigid model is applied to complete a parametric study on the effect of end-plate thickness on the failure modes of the connection, with the purpose of standardized design method validation. The results of the parametric study are shown in the moment-rotation diagrams of Fig. 4.12. The different types of failure can be identified: rigid end-plate: cross-section plastic buckling (A); thick end-plate: bolt and plastic hinge in the intersection of tubular wall and end-plate (B); and moderate and thin end-plate (in the given case less than 15 mm): plastic hinge at the tubular wall-end-plate intersection and in the end-plate in the location of a bolt (C); this failure mode is illustrated in Fig. 4.13. Among the possible and still practical cases, pure bolt failure is not found. It can be also observed that increasing the end-plate thickness is not economical after reaching the B-type failure, since the differences in ultimate capacity are relatively small.

On the bases of the local analyses of the bolted end-plate connections it is concluded that (i) the bolts and contact of end-plates should be modelled in global model, and (ii) the practical standard based design model of the connection (Tóth, 2003) is validated.
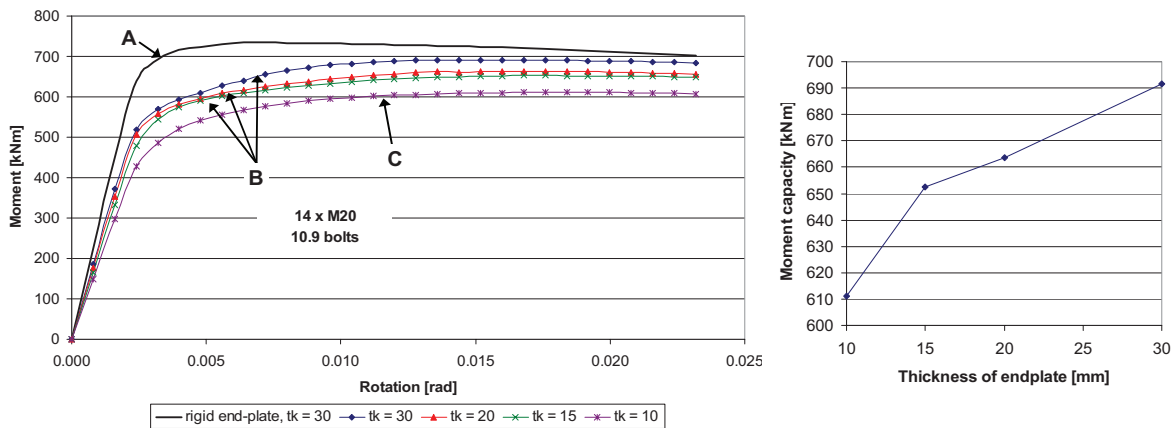

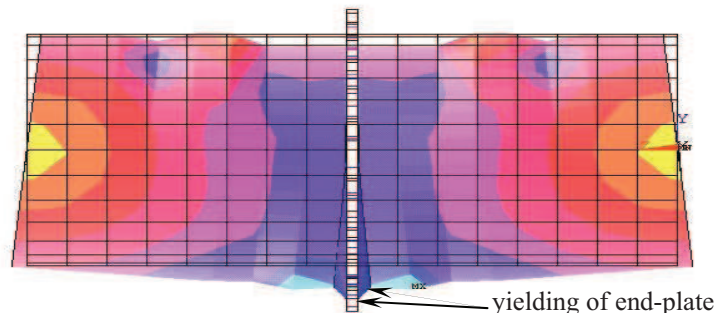Figure 4.12: Effect of end-plate thickness on ultimate behaviour.

Figure 4.13: End-plate failure (C-type).

82

4.2.6. Stability analysis of joint

In the first phase of the global joint numerical analysis, the elastic stability phenomena of the joint components are investigated. Based on the structural geometry and an actual load case including dominantly bended horizontal, compressed vertical and diagonal members, a parametric study is completed by changing the thickness of gusset plates and tubular bars, to investigate the buckling modes in each component.

The originally designed geometry results in dominant failure modes of the gusset plates, according to the expectations as the tubular bars are designed to avoid the local buckling. The first arising mode is related to the diagonals as Fig. 4.14,a shows. The figure also introduces the further buckling modes of the gusset plates: due to the bending of horizontals (Fig. 4.14,b) or due to the compression transferred from the columns (Fig. 4.14,c and d). Evaluating the results, it is concluded that the buckling of the gusset plate with the applied parameters is a possible failure mode that should be considered in the improvement of the joint.

(a)   (b)   (c)   (d)
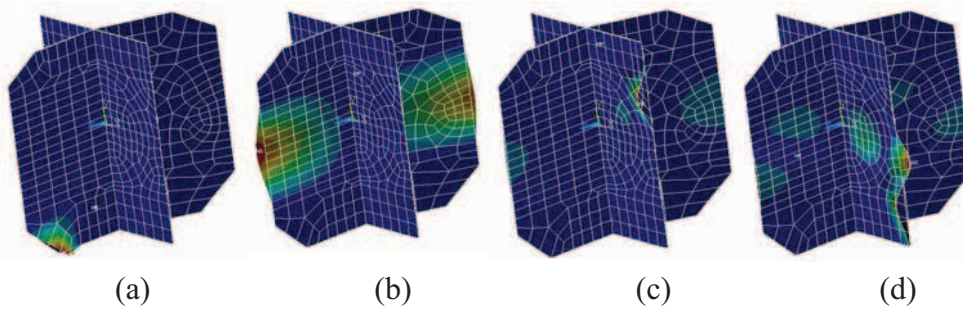
Figure 4.14: Buckling modes of the gusset plate.

Changing the plate thicknesses leads to local buckling of the tubular members (Figs. 4.15,a and b). However, the buckling shapes and locations are modified. In the columns the buckling appears on one side only (Fig. 4.15,c). Similarly, the buckling position is changing along the axis of the bar in the horizontals (Fig. 4.15,d). The reason is the interaction between the different members and their internal forces: the joint is forced to rotate around the longitudinal axis of the horizontal bars, causing additional bending in the columns and additional torsional moment in the horizontals.

The results of the stability analysis are used in the preliminary design during the prototype development and also in the test specimen design. The plate and shell components of the actual joints are designed to avoid local buckling phenomena.

(a)   (b)   (c)

(d)

Figure 4.15: Buckling modes of tubular joint components.

4.2.7. Elastic analysis of joint

The load transfer of the joint and the interaction of the members are investigated by linear elastic analyses of the experimental model. Different load cases are applied among the test program, detailed in Table 4.1. In this Section the results of the elastic analyses are illustrated for two load cases: load case no. 7: a general load case, representing the actual load ratios of the structure: compressed and tens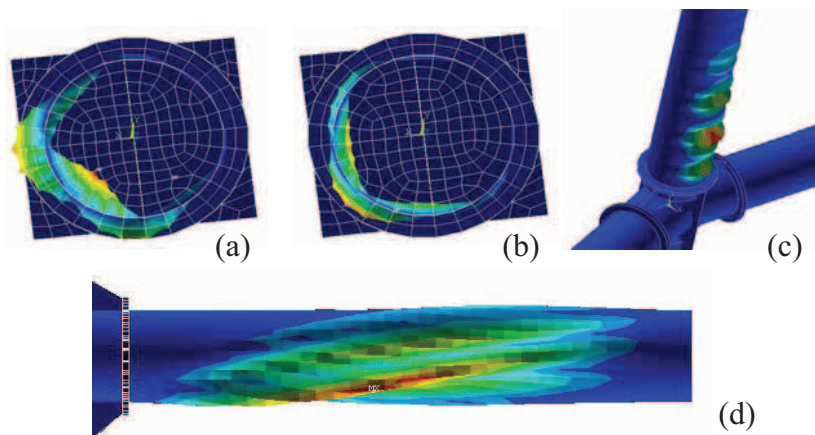ioned horizontals, compressed column, and tensioned and compressed diagonals; load case no.2: compressed column, without forces in the horizontals and diagonals.

Figure 4.16 shows the von Mises stress distribution in the joint under load case no. 7. In the intersection of the columns and the gusset plates stress concentration can be seen due to the axial force introduction and the additional extra bending of the column. Similar tendency can be observed in the case of compressed column (load case no. 2), as shown in Fig. 4.17.

Based on the analysed cases, good agreement is found between the numerical model and the tests, in the comparison level of reaction forces and displacements. At load case no. 7, at the load level of 40 kN in the column and 24 kN in the horizontals, the bottom reaction forces are exactly the same (37.96 kN), while the central displacements are 2.2 % bigger than in the test (5.03 and 4.92 mm, respectively). The model also follows the tendency of the complicated global stress distribution, as shown in the two figures. However, although the peak stresses are clearly observable, for their detailed analyses the mesh should be refined in the vicinity of geometrical intersections in order to get more accurate values.

On the basis of the elastic analyses (i) the global model is verified by test results ("verification test"), and (ii) the stress distribution of the structural joint is investigated for different load combinations.
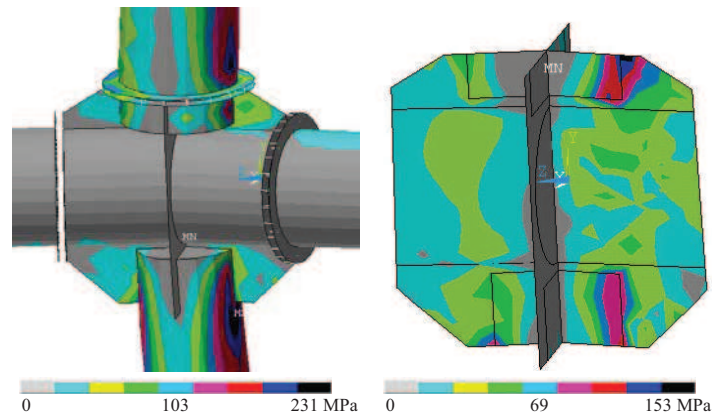

| 0 | 103 | 231 MPa | 0 | 69 | 153 MPa |

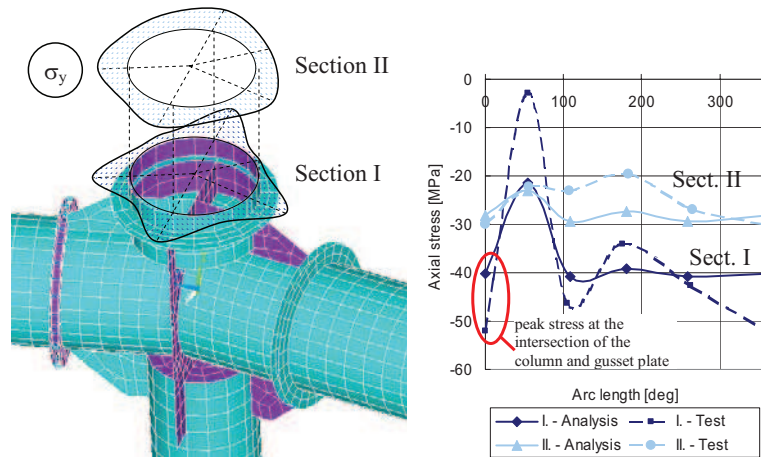Figure 4.16: Stress distribution in load case no. 7.

Figure 4.17: Comparison of test and analysis stress results in load case no. 2.

4.2.8. Ultimate analysis of joint – virtual experimenting

Geometrically and material nonlinear analysis on imperfect model are applied with the aim (i) to verify the finite element model in the nonlinear range, (ii) to explain the experimental observations by extended virtual experiments, (iii) to support the joint prototype development, and (iv) to create an advanced design tool for the virtual test based design of the joint. In the following the ultimate analyses for the simulation of different failure modes are illustrated.

Behaviour of „ horizontals"

In order to get the failure of the horizontals, the forces are applied eccentrically at their ends, creating bending and compression (load case no. 23 in Table 4.1). Considering the actual experimental conditions stabilizing the joint setup, the diagonals and the column are preloaded (tension and compression, respectively) by a relatively small force.

The collapse is occurred by local plastic buckling in the horizontal member, inside the joint, as it can be seen in Fig. 4.18,a. The figure shows that the same collapse phenomenon is observed in the virtual experiment as in the real test (compare Figs. 4.6,a and 4.18,a). The measured and calculated load – horizontal deflection relationships of the joint can be seen on Fig. 4.18,b. It is shown that the strength and ductility are close to the test results (ultimate load: compare 127.9 kN to 132.9 kN, difference 3.8 % and maximum displacement: compare 21.02 mm and 22.27 mm, difference 5.9 %, in the analysis and in the experiment, respectively). The difference is in the buckling location: in the test, it is close to the ending gusset plate. This difference may come from the geometrical imperfections of the test specimen.

Figure 4.18: Ultimate behaviour of "horizontals": (a) calculated failure mode, and (b) comparison of analysis and test results.

The phenomenon can be well investigated by the evaluated analysis results. Figures 4.19,a and 4.19,b show the representing moment-rotation and stress-strain relationships of horizontal details (the locations of the reference point can be seen in Fig. 4.18,a). Based on the evaluation of strains and stresses, the buckling load can be defined (Figs. 4.18,a and 4.19,b). It can be also concluded that (i) the plastic capacity of the tubular section is not reached and (ii) the end-plate connection does not fail before the instability phenomenon is appeared (the capacity of the end-plate connection as well as the capacity of the horizontals is not utilized). The load bearing capacity of the joint can be improved by increasing the plate thickness inside the joint to reach "uniform resistance design". In the actual joint design this observation is used in the joint prototype development. It is proved by both experimental observation and numerical separate analyses that the weakening of the bolted connections in the horizontals (even if applying the half bolt number of the designed one) does not influence significantly the described ultimate behaviour. Note, however, that the minimum number of bolts should be applied to avoid corrosion between the end-plates (standardized constructional rule).

a) moment vs. rotation curve
(at the end of horizontals)

b) stress vs. strain relationship
nodes at the buckling position
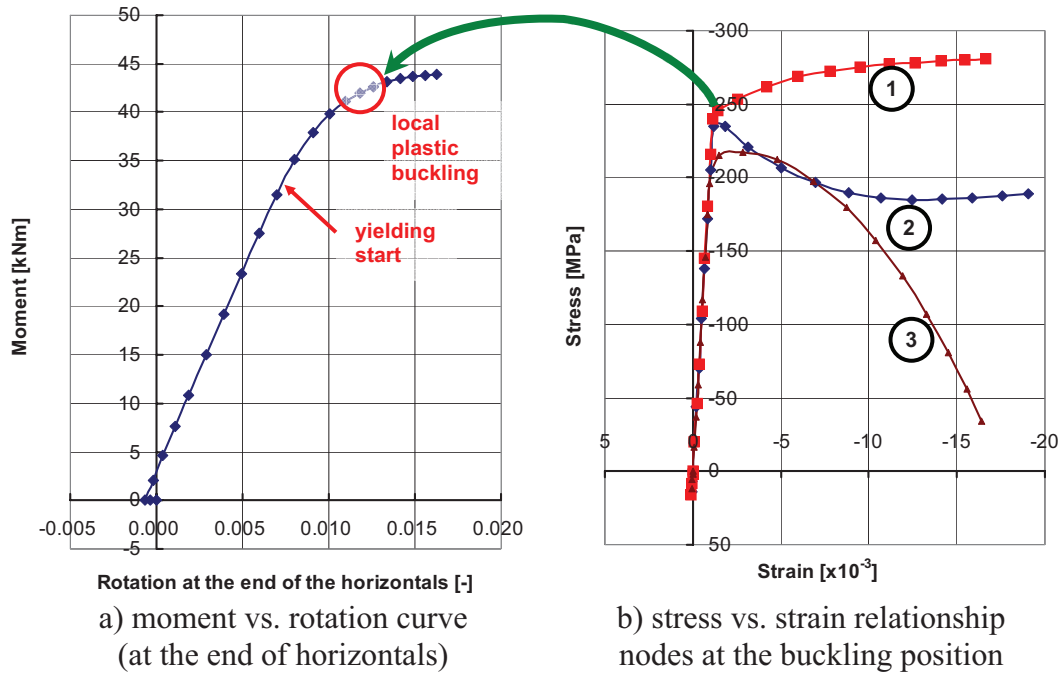
Figure 4.19: Details of ultimate analysis of "horizontals".

Behaviour of „columns"

The ultimate behaviour of the "columns" in specimen 2 is analysed in the same arrangement as it was in the experiments (Section 4.2.3). The analysis first completed on the perfect specimen; the observed failure mode can be seen in Fig. 4.20,a and the pertinent load-deflection diagram is shown in Fig. 4.20,b, together with ultimate load level obtained from the experiments. From the results it can be concluded that (i) the failure phenomenon is well simulated by the nonlinear analysis and (ii) the calculated ultimate load level of 242.5 kN is 22% higher than the test one (193.9 kN). Note that if the plate buckling is excluded, the load capacity of the perfect specimen is theoretically 358.9 kN; the difference from the above analytical result well represents the influence of the local plastic buckling.
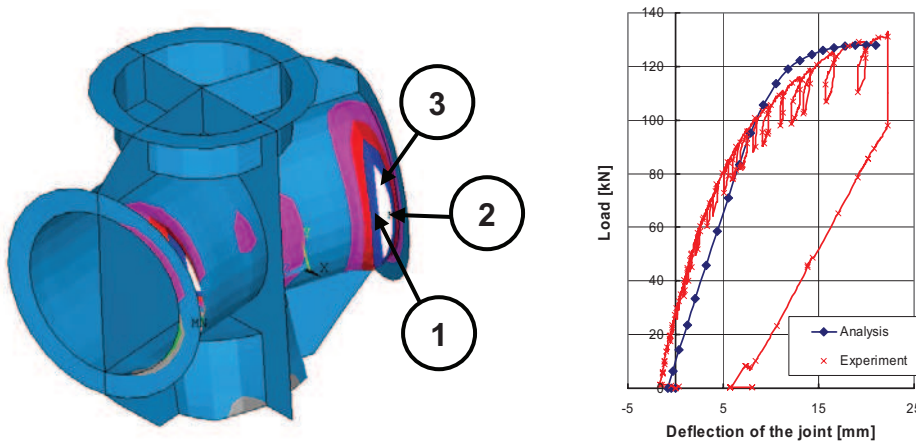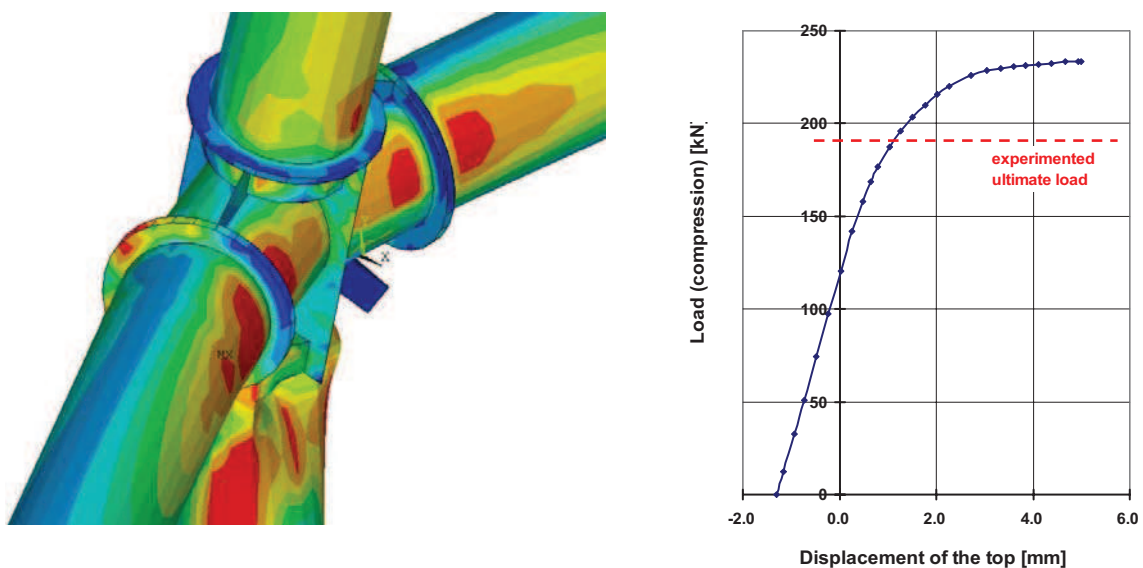

Figure 4.20: Ultimate behaviour of "verticals": (a) calculated failure mode, and
(b) comparison of analysis and test results.

86

Due to the observed unfavourable phenomenon and the differences in the calculated and measured ultimate loads an extended parametric study is completed by virtual experimenting in order (i) to find the explanation of the differences and (ii) to determine the effects of the influencing parameters.

The parametric study is completed to investigate the effect of different imperfections – in compatible with EN 1993-1-6 (2005) – and the radius-to-thickness ratio of the column.

Imperfections are summarized in Fig. 4.21, such as: curvature of the column as global imperfection (Fig. 4.21,a) and local distortion as local imperfection of the lower column (in specimen 2 it is caused by an accidental crash of the column and the diagonal, Fig. 4.21,b). The column ultimate test on specimen 2 is completed after the horizontals are failed, what is also considered as an "imperfection" from the column behaviour point-of-view (Fig. 4.21,c).
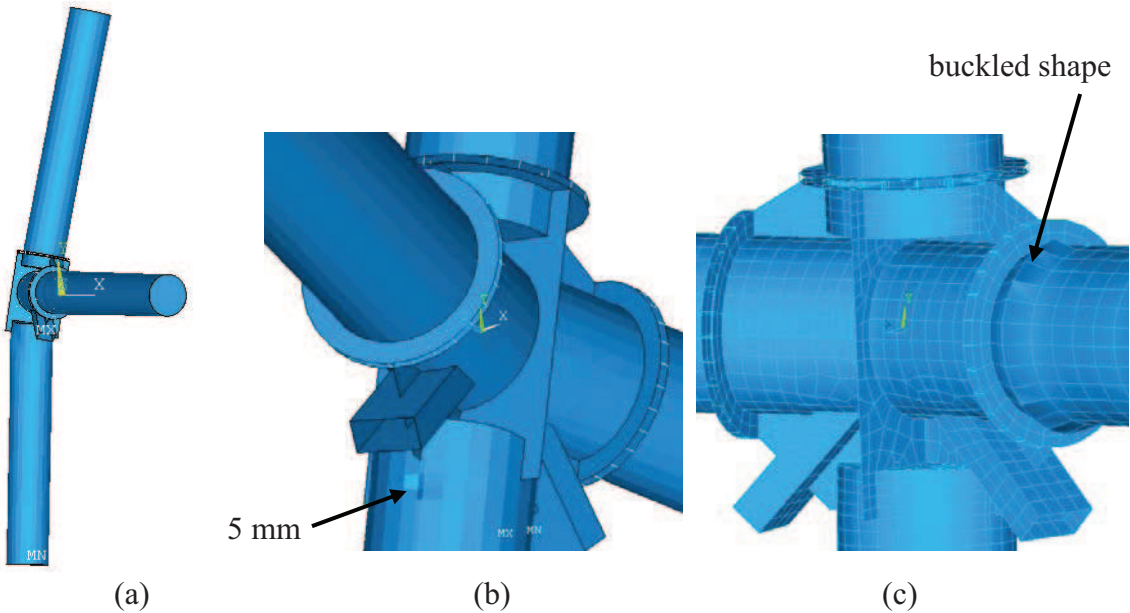

| (a) | (b) | (c) |

Figure 4.21: Applied imperfections.

The study is completed by different sizes and combinations of these imperfections on columns with five different radius-to-thickness ratios, as detailed in Vigh and Dunai (2004). Altogether 20 virtual tests are completed; here some of the findings are summarized.

Effect of global imperfections: Fig. 4.22,a shows the ultimate load vs. global imperfection relation, and Fig. 4.22,b illustrates the buckled shapes for 0, L/47 (30mm) and L/15 (95mm) imperfections. In case of the practical imperfections (L/70-L/35), the change in ultimate load is within 5% and can be neglected. Although an extremely big imperfection (i.e. 95 mm; L/15) would result in the experimental ultimate load, the comparison of the buckled shapes shows that it represent a different – rather bending type – buckling phenomenon and proves that not a large global imperfection reduced the load capacity. Note that, with regard to the test experiences, an imperfection of 40 mm can be considered as the most realistic.

Based on the results of studies on local accidental imperfection it is concluded that it has hardly any effect on the ultimate behaviour; e.g. the load capacity is reduced by 0.4% only.

Further investigations proved the important role of the horizontal failure as imperfection. It is observed that horizontals – even though they are not loaded – bear relatively high stresses due to the global curvature, as it is illustrated in Fig. 4.20,a. If the buckling of horizontal is assumed in the analysis as elastic imperfection it causes negligible changes in the ultimate behaviour, a theoretical case, however, eliminating the horizontals – as if they are not able to carry any load – results in a significantly reduced capacity of 166.5 kN, comparing to the previously obtained ultimate load level (242.5 kN), that is 14% smaller than the test value.

From this finding it can be concluded that the reduced rigidity of the horizontal due to the plastic deformation in it decreased the vertical ultimate load.

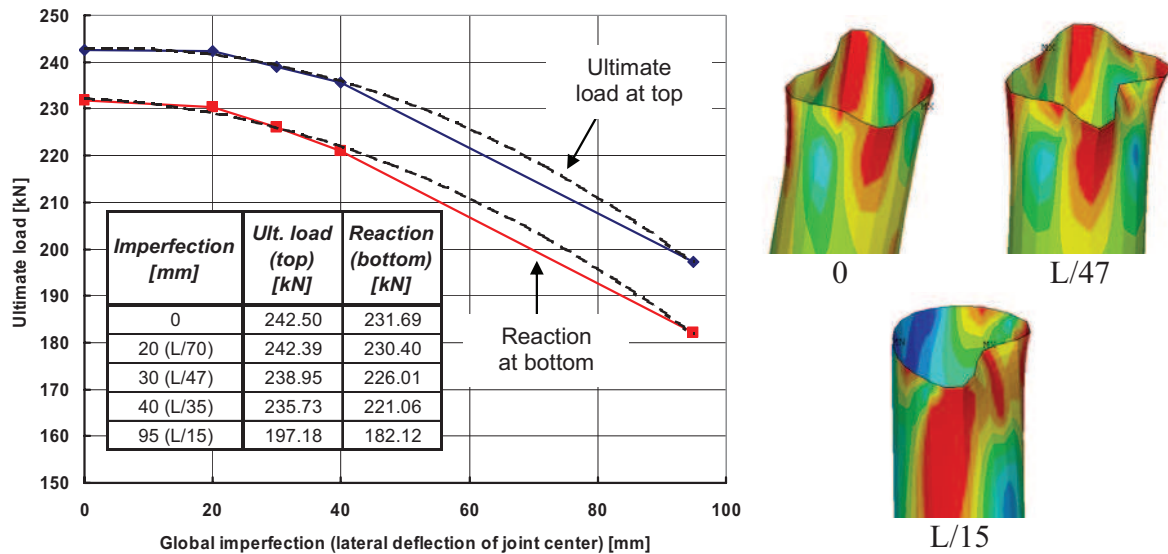| Imperfection [mm]	Ult. load (top) [kN]	Reaction (bottom) [kN]
0	242.50	231.69
20 (L/70)	242.39	230.40
30 (L/47)	238.95	226.01
40 (L/35)	235.73	221.06
95 (L/15)	197.18	182.12

Figure 4.22: Effect of global imperfections.

The parametric study is extended on the radius-to-thickness ratio of the column from 40 to 171.4. The ultimate loads and the load-deflection diagrams are shown in Fig. 4.23. The results show that the buckling mode does not change at higher value of R/t and the plastic instability becomes less dominant at increasing thickness, the stress distribution tends to the fully plastic one. In the practical range of the radius-to-thickness ratio – R/t~60 – the reduction in the ultimate load is significant. By increasing the wall thickness locally – in the joint region only – the load bearing capacity can be effectively increased.

R [mm]	t [mm]	R/t [-]	Ult. load (top) [kN]	Reaction (bottom) [kN]
120	3	40.0	359.7	345.9
120	2	60.0	241.0	229.6
120	1.5	80.0	170.6	163.1
120	1	120.0	104.9	100.8
120	0.7	171.4	68.7	65.8
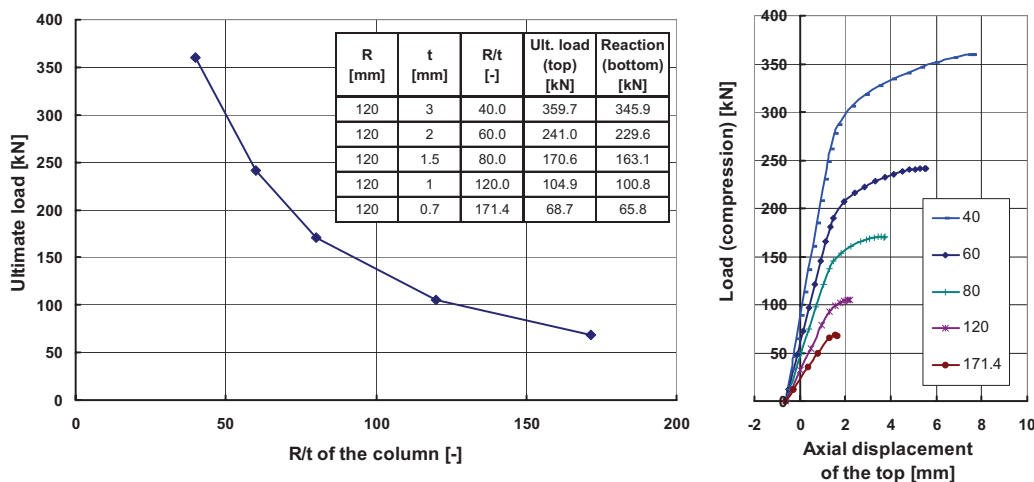
Figure 4.23: Effect of radius-to-thickness ratio.

Application of results in the design: the advanced finite element model is verified by the ultimate tests ("verification tests"). The FE model based virtual experiments are used to improve the experimentally investigated prototypes of the joints, what resulted the final constructional details of the steel cooling tower system. The developed and verified model and the computational method can be applied as advanced design tool for the virtual test based design of the joint, according to the general recommendations of the Eurocode: EN 1990 (2001), EN1993-1-5 (2005), EN 1993-1-6 (2005). The research results are directly applied in the design of an actual steel cooling tower under construction.

4.3 Dunaújváros Danube bridge

4.3.1 Structural arrangement and research program

The new Danube Bridge in Dunaújváros is designed by Főmterv Co., Budapest, with a total length of 1676.8 meters. In the main span a basket handle shaped tied arch bridge is designed with a length of 307.8 m. This is a world record span in its category; the largest similar structure is in Japan with its span of 254 meters (Yoshikawa et al. 1993). This type of structure is widely used in the last two decades in the leading bridge-building countries – mostly in Japan – as an alternative to the cable stayed bridges, typically in the range of 180-260 m spans. Currently the main structural system of the bridge is erected – as shown in Fig. 4.24 – and planned to open for the traffic in the summer of 2007.

The main bridge carries both tracks of the motorway on the same superstructure across the river. The cross arrangement of the road is: 2*3.75 m traffic lanes each direction, 3.50 m stop lane, 2*1.00 m safety zone in the 3.60 m wide middle zone between the two tracks and 1.60 m wide kerb. Bicycle road and sidewalk with spans of 2.40 m are designed on both sides of the bridge, and supported by cantilevers outside of the arches.

The arches and the webs of the stiffening girders are inclined by 16.5° to the vertical. The height of the circular shaped arches is 48 m; they are connected to each-other by eight beams with rectangular cross-sections, resulting in a Vierendeel-type solution. The arches are designed of S460 M steel grade, with a maximum of 50 mm thickness. The inside dimensions of the arch box cross-sections are 1960*3720 mm. The stiffening girders are parallelogram shaped box sections, with 2100 mm wide flanges and 3100 mm inner height. The walls of the arch and stiffening beam box sections are stiffened by open (plate and T-shape) longitudinal stiffeners.

The deck of the bridge is an orthotropic plate made of S355 J2G3 and K2G3 steel grade. The distances of the crossbeams are 3.80 m; the tied crossbeams are in a distance of 11.40 m from each other, connected by longitudinal beams.

The hanging elements are parallel cables with 11.40 m distances from each other. The cables are anchored to the beams and arches at diaphragms with the customary tubes.

The main bridge is assembled on a platform at the river bank and shipped to the final position.

Figure 4.24: The main span of the Dunaújváros Danube bridge in December 2006.

In this Section first I give an outline about the background research related to the global stability of the arch bridge. A bridge model of scale 1:34 is investigated by an experimental program; the test specimens are designed on the bases to reflect the global buckling phenomenon of the bridge. In the tests both elastic and ultimate behaviour are analysed experimentally. On the basis of test results different standardized design methods are evaluated and conclusions are drawn to be applied in the bridge design. In the second part of the Section I present the studies and checking of the bridge itself during the erection phases. The experimentally verified finite element models are used for the global and local stability checking of the bridge. In this Section the focus is on the stability and ultimate analysis of the stiffened plated components of the arch and stiffening beam in the region of load introduction during the erection phases.

4.3.2. Experimental program

Bridge model

The 1:34 scale bridge model is designed by a preliminary analysis, as it is shown in Fig. 4.25 and Fig. 4.26,a. The sections and scale are determined to have the same equivalent relative slenderness of the arches in the model and in the real bridge. The scale of the model is also determined to be compatible with the connection points of the reaction floor (1000 mm); these circumstances resulting in the distance between the cables 333 mm and the total length of the bridge model 8991 mm.

The local geometry – sections size – of the model is determined by instability analysis according to the main purpose of the experimental study. The welded box sections of the arches (100x40 mm), the cold-formed hollow section stiffening beams (80x40 mm) and horizontal connecting beams between the arches (40x40 mm) are designed with 3 mm plate thickness, to have the same equivalent relative slenderness of the arches in the model and in the real bridge. The secondary girder between the stiffening beams are designed from L 80x40x3 mm section. The deck plate is built from 3 mm thick plates. The applied steel grade in the bridge model is S235.

The high strength cables are installed in the model after preliminary tensioning ("ironing"), followed by tension tests to measure the elastic modulus. Their end joints in the model are constructed by built-in devices to adjust the pre-tensioning force.

Test arrangement

The bridge model is placed on four supports at each arch – stiffening beam connection point, simulating simply supported beam boundary conditions, as shown in Fig. 4.26,a. Two bearings are fixed and the others can move in longitudinal direction.

The load is applied on the bridge model by a hydraulic system, connected to every cable joints of the stiffening beam, as shown in Fig. 4.26,a. The loads are applied by four jacks through gravity load simulators. The jacks can be active or not during the loading process, so different partial/total load cases can be introduced in longitudinal direction. In the transverse direction the jacks can be connected to the model eccentrically, as it is shown in Fig. 4.26,b.

Measurement system

The behaviour of the bridge model is followed by measuring the force, displacements and strains. The displacements are measured in vertical directions by 6 displacement transducers and by geodetic tools (in selected load steps in 26-26 points, on both sides of the stiffening beam); the horizontal movement of the arches is measured in 5 points The strains are measured in altogether 95 points by strain gauges in 14 cross-sections: the strain gauges are placed on the flanges of the arches and the arch-connecting beam and on the lower flange of the stiffening beam.

More details of the model can be found in Joó et al. (2005) and Dunai et al. (2004).
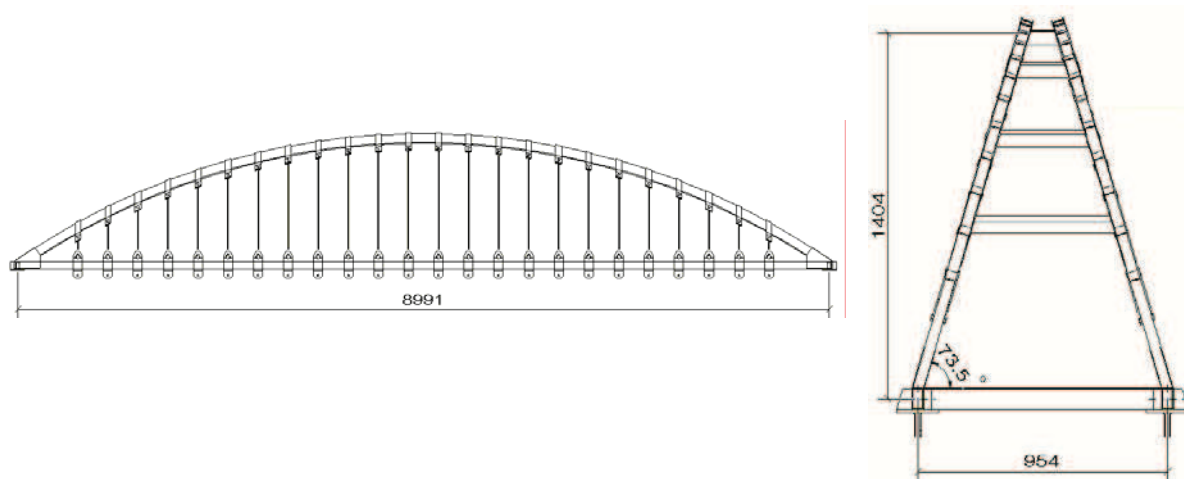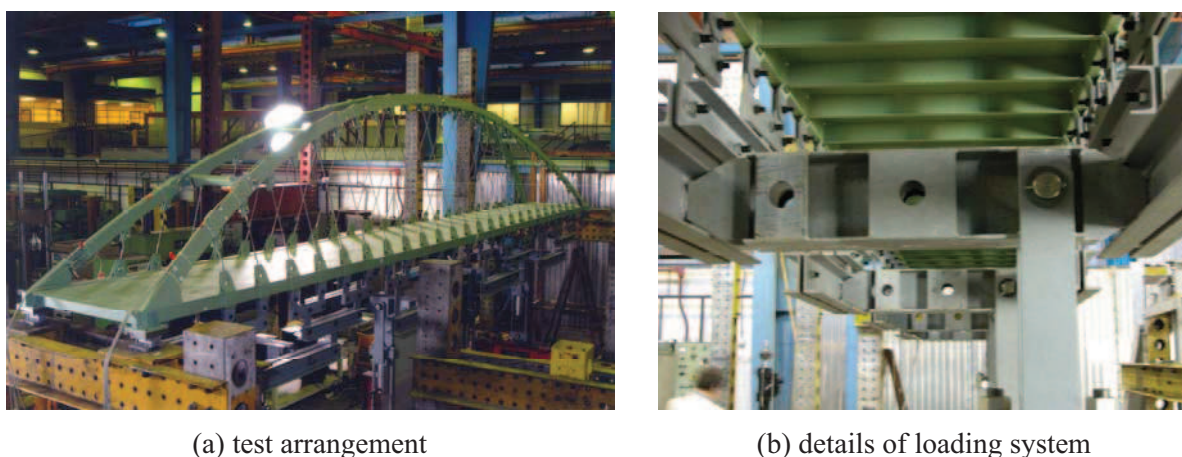
Figure 4.25: Bridge model geometry.

(a) test arrangement

(b) details of loading system

Figure 4.26: Bridge model test arrangement.

4.3.3. Experimental results

Elastic tests

In the first part of the experimental program elastic tests are carried out on the bridge model. The aim of the elastic test program is (i) to analyse the bridge model behaviour at various load cases, (ii) to test the measurement system and (iii) to use the measured data for verification of numerical models. Altogether 17 load cases are investigated.

Figure 4.27 shows the vertical deflections of the bridge model under total load (200 kN), half-sided partial load (30 kN) and partial torsional load (60 kN). The two different behaviour modes of the structure are clearly shown. For total load the structure is quite rigid due to the restraining effect of the compression force in the arch at the ends of the stiffening beams (horizontal tangent of the deflected shape). In the case of the partial load this behaviour is disappeared and the rotation of the beam end is experienced. For torsional load the two deflection modes are combined.

The arch horizontal deformation is also measured during the tests. The results for the three discussed load cases are presented in Fig. 4.28. It can be seen that the deformation amplitude for the torsional loading is almost the same as in the case of total loading ~2,5-3 mm, at the given load levels. For torsional load, however, the deformed shape corresponds to the torsional deformation and for total loading it corresponds to the first buckling eigenmode, as shown. In the case of half-sided partial loading there is no significant horizontal deformation due to the small axial force in the arches.
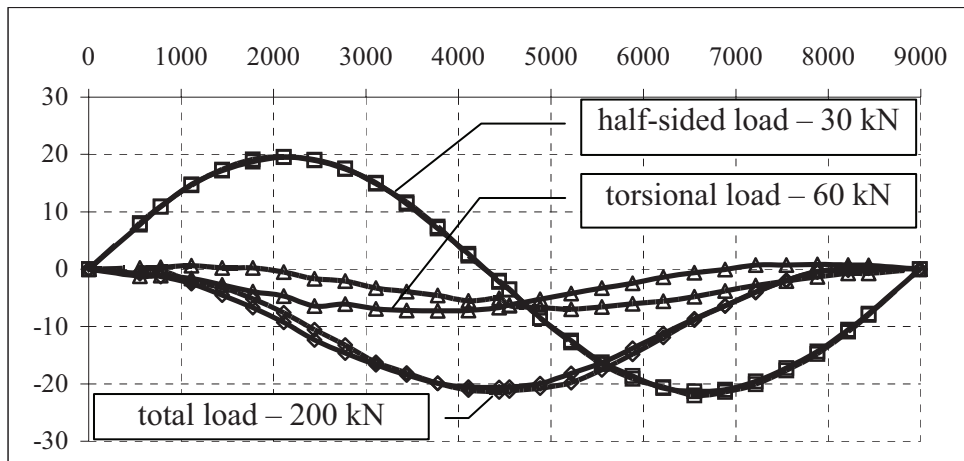
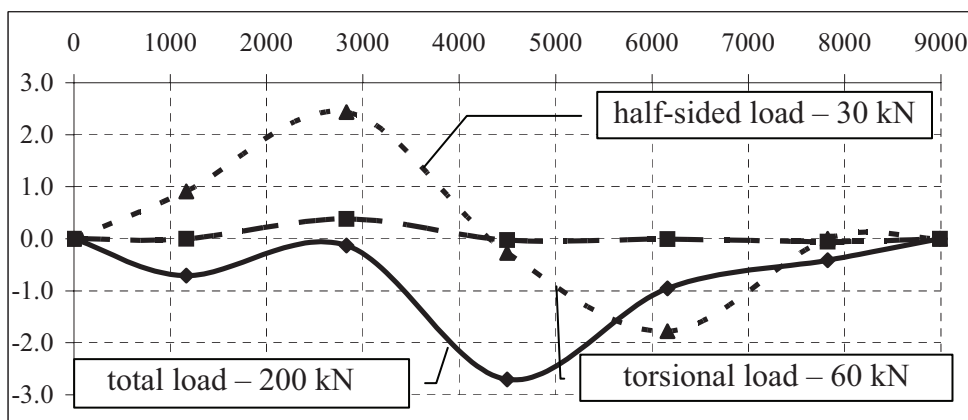Figure 4.27: Measured vertical deflections [mm].

Figure 4.28: Measured horizontal deflections [mm].

The measurements by the strain gauges in the elastic range of testing are evaluated to obtain stress distribution and from these the internal forces are derived in the cross-sections. These results are used in the planning of the ultimate testing program and also in the numerical model verification (Joó et al. 2005).

Ultimate tests

The aim of the ultimate tests is to determine the safety of the bridge model against global failure. By the proper design and testing process of the bridge model it was possible to study two failure modes on it: firstly for total loading (out-of-plane buckling), and secondly for half-sided partial loading (in-plane buckling). Plastic hinges are not allowed to be developed in the arches after the first test by release the load from the structure. By this way the slightly deteriorated model could be used to study the in-plane buckling mode as well.

In the first phase of the ultimate test the total load is applied in increasing steps with continuous monitoring the measuring devices. Due to the dominant axial force at the end of the arch out-of-plane buckling is happened, as it is shown in Fig. 4.29,a. The behaviour can be followed by the load-horizontal displacement diagram in Fig. 4.29,b. The nonlinearity of the curve starts at the load level of about 200 kN; the plateau like behaviour is experienced from 270 kN and the reached ultimate load is 300 kN (without the self-weight of the model and the loading system). At the limit point plastic local buckling of the more compressed web of the arch near the lowest connecting beam started; at this point the load is stopped to avoid the creation of the failure mechanism. The different behaviour of the ends of the arches – due to the different initial imperfections in the structures – can also be observed.
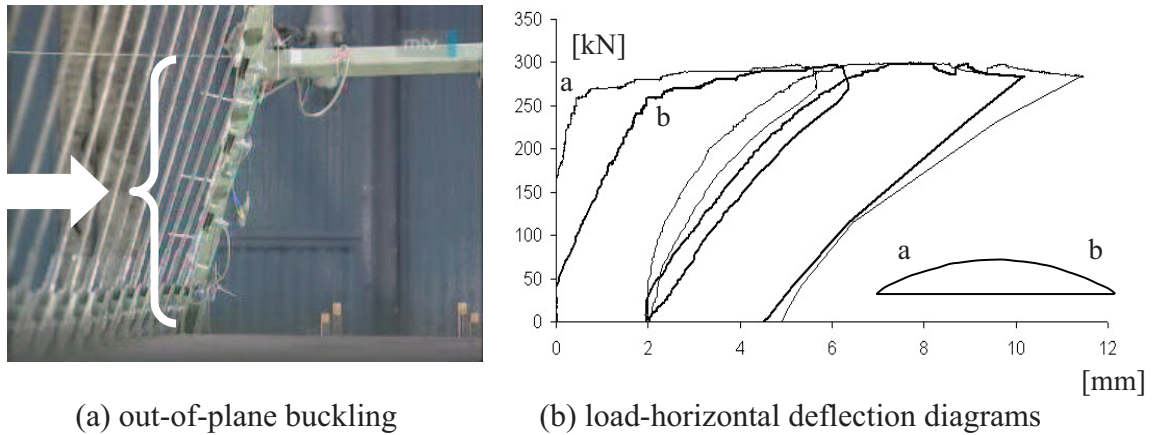
(a) out-of-plane buckling   (b) load-horizontal deflection diagrams

Figure 4.29: Ultimate behaviour under total loading.

The in-plane buckling type failure of the model is investigated under dominant bending moment, when half-sided partial load is applied. Due to this load the arch had significant vertical deformations, as it is already experienced in the elastic tests. By increasing the load plastic zones are appeared in the arches and the large deformations distorted the shape of the arch, as it is shown in Fig. 4.30,a. It explains the early nonlinear relationship of the load-vertical displacement curve in Fig. 4.30,b. The final failure is a plastic in-plane buckling at a load level of 110 kN (without the self-weight of the model and the loading system). The load is stopped at the limit point to avoid the total plastic mechanism. The model had significant residual deflections (max. 25 mm) after unloading.
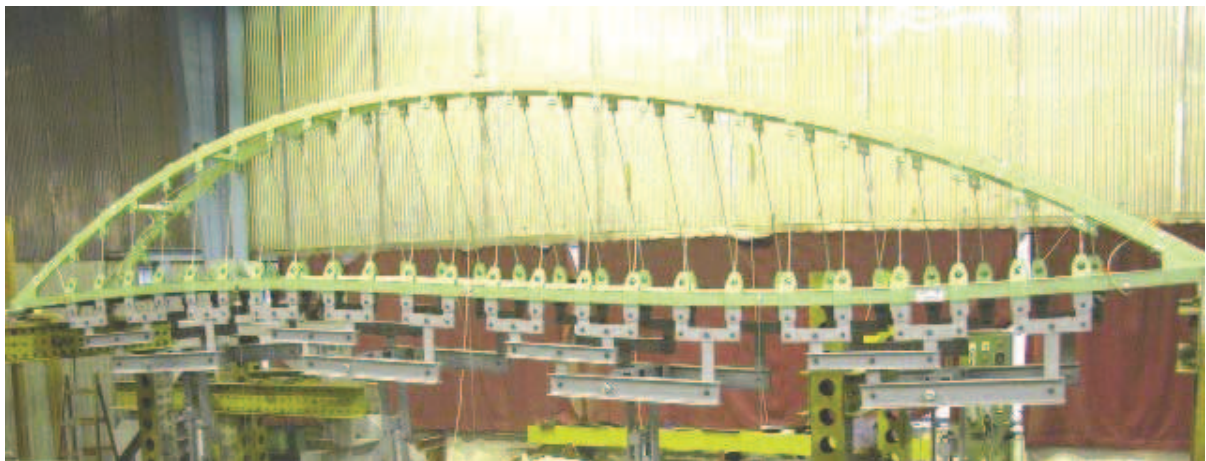
(a) in-plane buckling
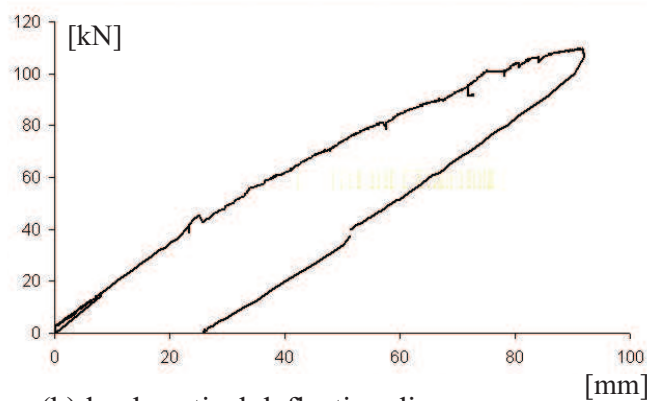
(b) load-vertical deflection diagram

Figure 4.30: Ultimate behaviour under half-sided partial loading.

4.3.4. Numerical analysis of bridge model

Models

In advance and parallel with the experimental tests beam and shell finite element models are developed to follow the linear and nonlinear behaviour of the bridge model. The finite element models are developed in ANSYS finite element program system (ANSYS, 2001). The beam is build by ~6000 elements and 72000 DOFs: 72000 (Fig. 4.31,a). In the shell model 17000 elements with 102000 DOFs are used (Fig. 4.31,b).

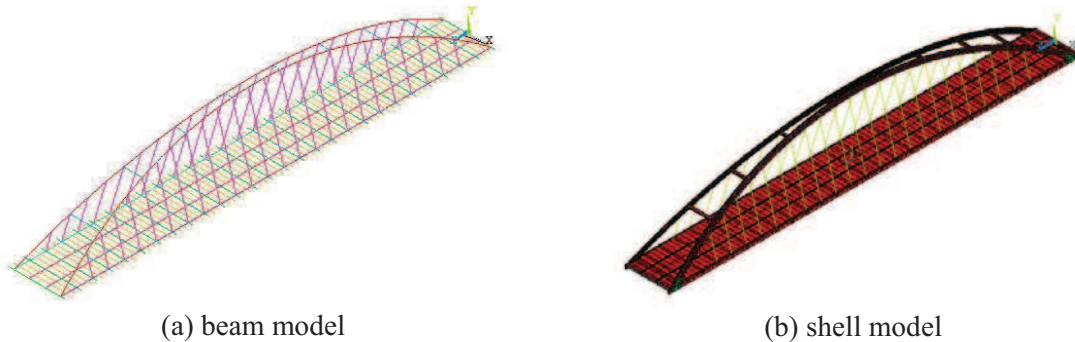| (a) beam model | (b) shell model |

Figure 4.31: Finite element models of bridge model.

Analysis

By both the beam and shell models linear, stability, geometrically nonlinear and geometrically and material nonlinear analyses are carried out.

By the linear analyses the elastic results of the testing program and the models are compared and verified.

The stability analysis is used to calculate the arch slenderness: preliminary design of bridge model and design method comparison.

Geometrically nonlinear analyses are carried out on imperfect models to calculate the second order effect on the internal forces: design method comparison. The relevant buckling shape is applied for the distribution of the imperfections with the amplitude calculated by the Eurocode 3 recommendations, as to be detailed in the next Section.

In the geometrically and material nonlinear analysis the observed material properties are used – determined by tension tests – and the distribution and sizes of geometric imperfections are adjusted by a calibration study: ultimate model verification by the experimental results through the comparison of displacements, stresses, internal forces and the features of the nonlinear behaviour.

The vertical deflections are in good correlation in the two cases, the stiffness of the model corresponds to the stiffness of the specimen, as shown in Fig. 4.32,a.

In case of total loading – where the failure is the out-of-plane buckling of the arch – the geometrically and material nonlinear analysis is applied to analyse the effect of various imperfection distributions and sizes. The test behaviour shows different horizontal deformation of the arches during the ultimate test, as it is shown in Fig. 4.32,b. The out-of-plane buckling mode is, however, symmetrical to the mid-span of the model, which results in similar horizontal deflections of the arches. To obtain the observed horizontal deflections in the two arches the first buckling mode as imperfection is applied only on the half of the bridge, with the amplitude of 2 mm. By this adjusted imperfection the experimental behaviour and the ultimate load is predicted with good accuracy.
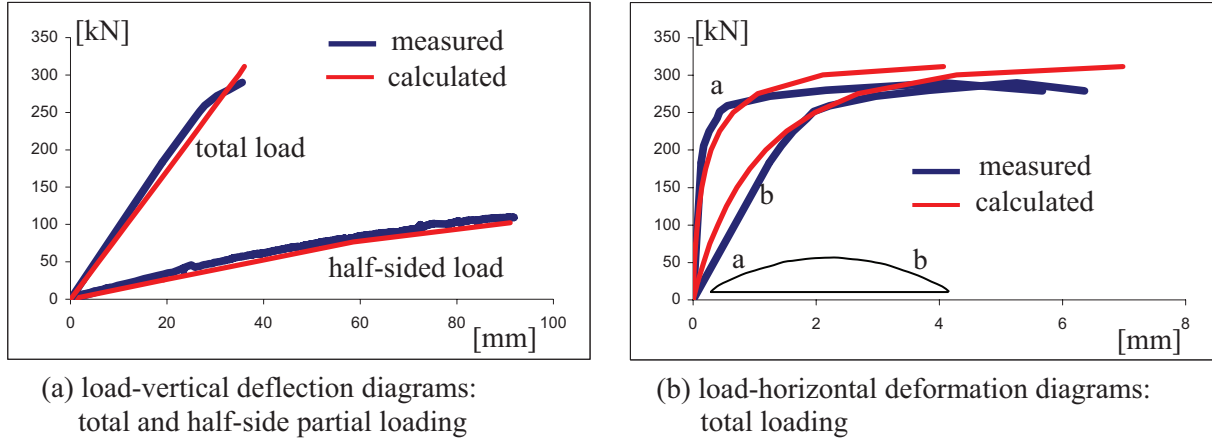
(a) load-vertical deflection diagrams:
total and half-side partial loading

(b) load-horizontal deformation diagrams:
total loading

Figure 4.32: Comparison of experimental and numerical ultimate results of bridge model.

4.3.5. Evaluation of design methods for arch bridge stability

Design methods

The arch strength of the bridge model is checked by three standards, as follows: the Hungarian Standards (HS 2002), Eq. (4.1), the Japanese Standard (JHSB 1994), Eq. (4.2), and the Eurocode 3 (EC3; EN 1993-1-1, 2004) standard Eq. (4.3), interaction formulae. The most conservative is the JSHB, where the linear interaction between the buckling resistance and bending strengths is used. The HS checking is divided into the buckling and the strengths checking, as shown by the two checking conditions in Eq. (4.1). The EC3 applies the combined interaction formulae of the internal actions. These methods are used in the bridge model checking and the safeties against the observed ultimate load are calculated (the notations can be find in the end of the Section).

$$\frac{N_{Ed}}{N_e} + \frac{\psi_y M_{y,Ed}}{M_{y,e}} + \frac{\psi_z M_{z,Ed}}{M_{z,e}} \le 1 \; ; \; \frac{N_{Ed}}{N_{ke}} \le 1 \tag{4.1}$$

$$\frac{N_{Ed}}{N_{ke}} + \frac{\psi_y M_{y,Ed}}{M_{y,e}} + \frac{\psi_z M_{z,Ed}}{M_{z,e}} \le 1 \tag{4.2}$$

$$\frac{N_{Ed}}{\chi_y \frac{N_{Rk}}{\gamma_{M1}}} + k_{yy} \frac{M_{y,Ed}}{\chi_{LT} \frac{M_{y,Rk}}{\gamma_{M1}}} + k_{yz} \frac{M_{z,Ed}}{\frac{M_{z,Rk}}{\gamma_{M1}}} \le 1 \; ; \; \frac{N_{Ed}}{\chi_z \frac{N_{Rk}}{\gamma_{M1}}} + k_{zy} \frac{M_{y,Ed}}{\chi_{LT} \frac{M_{y,Rk}}{\gamma_{M1}}} + k_{zz} \frac{M_{z,Ed}}{\frac{M_{z,Rk}}{\gamma_{M1}}} \le 1 \tag{4.3}$$

In the advanced strength checking geometrically nonlinear analysis is carried out on imperfect finite element model to calculate the internal forces. The shapes of two elastic critical buckling modes are applied to the structure as geometric imperfections, in accordance with EN 1993-1-1 (2004) Section 5.3.2 (11), Eq. (4) and EN 1993-2 (2005) Appendix D 3.5. (1), Eq. (5). The out-of-plane and in-plane buckling modes of the arches are presented in Figs. 4.33,a and 4.33,b. The amplitudes of the imperfection are calculated by Eqs. (4.4) and (4.5). The obtained internal forces are substituted into the EC3 formula for cross-section checking under combined axial force and bending moments.

$$\eta_{init} = \frac{e_{0,d}}{\overline{\lambda}^2} \frac{N_{Rk}}{EI \eta''_{cr,max}} \eta_{cr} \; ; \; e_{0,d} = \alpha(\overline{\lambda} - 0.2) \frac{M_{Rk}}{N_{Rk}} \frac{1 - \frac{\chi \overline{\lambda}^2}{\gamma_{M1}}}{1 - \chi \overline{\lambda}^2} \tag{4.4}$$

$$\eta_{0,z} = \frac{l}{500} \; ; \; \eta_{0,y} = \frac{l}{250} \tag{4.5}$$

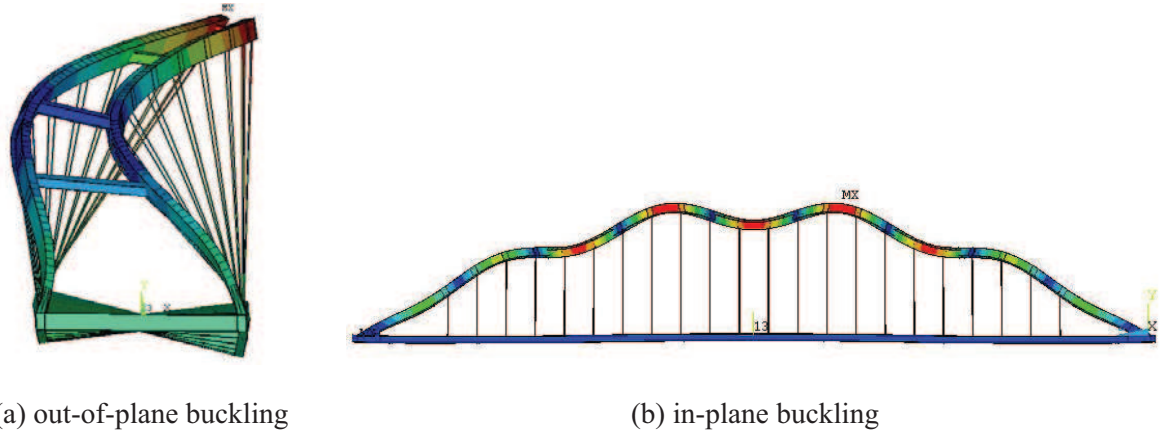| (a) out-of-plane buckling | (b) in-plane buckling |

Figure 4.33: Buckling modes of the bridge model.

In Eq. (4.4) the bending moment in the arch due to η_{cr} is determined by second order analysis on imperfect FE model, where the initial geometrical imperfection corresponds to the equivalent buckling mode. For total loading the critical cross section is at the first arch connecting beam and for half-sided partial loading it is at the quarter of the bridge model. The resulted imperfections are summarized in Table 4.2.

	in-plane imperfection [mm]	out-of-plane imperfection [mm]
EN 1993-1-1, Eq. (4.4)	3.44	17.30
EN 1993-2, Eq. (4.5)	17.98	35.96

Table 4.2: Applied imperfections.

Notations in Eqs. (4.1)-(4.5):

N_{Ed} ; $M_{y,Ed}$; $M_{z,Ed}$	design values of the internal forces,
N_{Rk} ; $M_{y,Rk}$; $M_{z,Rk}$	characteristic resistances,
	cross-section axial and bending resistances
χ_y ; χ_z ; χ_{LT}	reduction factors due to different buckling modes
k_{yy} ; k_{yz} ; k_{zy} ; k_{zz}	interaction factors
η_{init} ; η_{cr}	imperfection shape; buckling shape function
$\eta_{0,span}$; $\eta_{0,crit}$; $\eta_{0,exp}$	amplitude [mm] according to span; buckling shape; experimental test
α	imperfection factor
$\overline{\lambda}$	relative slenderness
$EI\eta^{''}_{cr,max}$	bending moment due to the buckling shape at the critical cross section
N_e ; N_{ke} ; $M_{y,e}$; $M_{z,e}$	design resistances according to HS, JSHB
	cross-section axial, element buckling, and bending resistances
ψ_y ; ψ_z	second order effect factors

Comparison of design and experimental resistances

The internal forces of the arches are determined according to the requirement of the different methods to be compared: in the case of experiment these are determined from the measured strains, from linear analysis of the FE models (HS, JSHB, EC3), and from geometrically nonlinear analysis applying the standard recommended imperfections (EC3 imperfect analysis based design).

The different standard design methods are applied to the bridge model at the load level of the ultimate load to calculate the safety against the two typical failures of the arches. The safety is

determined by the inverse of the utilization, and the results are enclosed in Table 4.3. The basic method is compared in the cases of the Hungarian, the Japanese and the EC3 standards. It can be concluded that the safety the highest in the Japanese standard, and the lowest in the EC3. Note that similar results are obtained about the safety of the Japanese standard by Kitada et al. (1989) and Nakai et al. (1995).

In the second step the alternative EC3 method is applied using geometrically nonlinear analyses of the imperfect model. The obtained safety is highly dependent on the size of imperfection. If the imperfections are used according to EN 1993-1-1 (2004) the safety against the failure is smaller compared to the safety by the application of imperfections according to the EC3 bridge standard, EN 1993-2 (2005). As it is expected, the method, which uses more conservative size of the imperfection, results in a similar safety as in the basic method of EC3.

	total loading	half-sided partial loading
HS	2.25	3.06
JSHB	3.07	3.28
EC3	2.20	1.87
EC3 Geom. nonlin. Eq. (4.4)	1.45	1.84
EC3 Geom. nonlin. Eq. (4.5)	2.29	2.15

Table 4.3: Safety against various standards and loading.

The results show the min. of 1.9 to a max. of 3.3 safety factors; the less conservative values are by the EC3. The alternative method of Eurocode – geometrically nonlinear analysis on imperfect geometry – results in different levels of safety, depending on the sizes of the imperfections. The results show, that the calculation of the imperfections by more accurate method results in closer value to the experimental load-bearing capacity.

As a conclusion the application of the Hungarian standard for out-of-plane buckling of the bridge results in the same safety level what is used in the classical method of the Eurocode 3. In the case of in-plane buckling the Hungarian design formula is significantly on the conservative side comparing to the Eurocode 3 recommendations, and results in the same safety level as the Japanese standard.

4.3.6. Bridge design – numerical models

Erection method

In the followings a summary is presented about the work what is completed by my team in the stability design of the tied arch bridge during erection (note that we investigated the bridge stability in both temporary and final stages as co-designers). The checking of the bridge during erection phase required advanced numerical modelling and analysis – detailed in Sections 4.3.6 and 4.3.7 – and supplementary ultimate analysis of stiffened panels, as shown in Section 4.3.8.

The arch bridge is constructed on a platform at the river side providing with scaffolding for both stiffening beam and arch. After the beam-arch skeleton is completed the arch scaffold is removed and the parallel cables are installed. After that the bridge is supported at the positions of the final bearings temporarily. At this stage temporary supporting bars are installed near to the supports, to strengthen the structure over the barges, which are used for shipping the bridge to the final place. Figures 4.34,a and 4.34,b show the bridge resting on the barges, and the details of the supporting bars, respectively. Two bars are installed by welding (fixed end bars) and one is with pins at both ends (hinged bar). On the two barge groups the 2x2 scaffolds support directly the stiffening beam through a hydraulic system providing with uniformly distributed 4x16 concentrated forces over the scaffolds.

The above method and arrangement required the solution of several engineering problems, such as the (i) load-bearing capacity of the barge-scaffold system, (ii) operation and control of the hydraulic system (iii) load-bearing capacity of the bridge and supporting bars, and (iv) navigation during the shipping process. Our task was the strength and stability checking of the arch bridge and the temporary supporting bars.

Figure 4.34: Erection of the arch bridge: (a) floating operation and (b) supporting bar details.

Beam and shell finite element global models are developed to follow the previously detailed erection phases of the arch bridge (model levels #1 and #2). In the governing phase of the erection, when the structure is supported by the barge-scaffold system, the relevant details of the bridge and the supporting bars are analysed by local models, using sub-structuring modelling technique (model level #3). In the followings the developed global and local shell finite element models are summarized.

Global shell finite element models

Two shell finite element models are developed on level #2 for the investigation of the erection process: model #2.1 concentrated only on one quarter of the structure, assuming double symmetry of the geometry, boundary conditions and loadings; model #2.2 is developed later on to consider the asymmetry of the equivalent geometrical imperfections during the independent checking of the structure by finite element simulation.

Figure 4.35 shows a general view about model #2.1, indicating the details which are analysed by local models. The characteristics of the two shell and the beam models are summarized in Table 4.4.
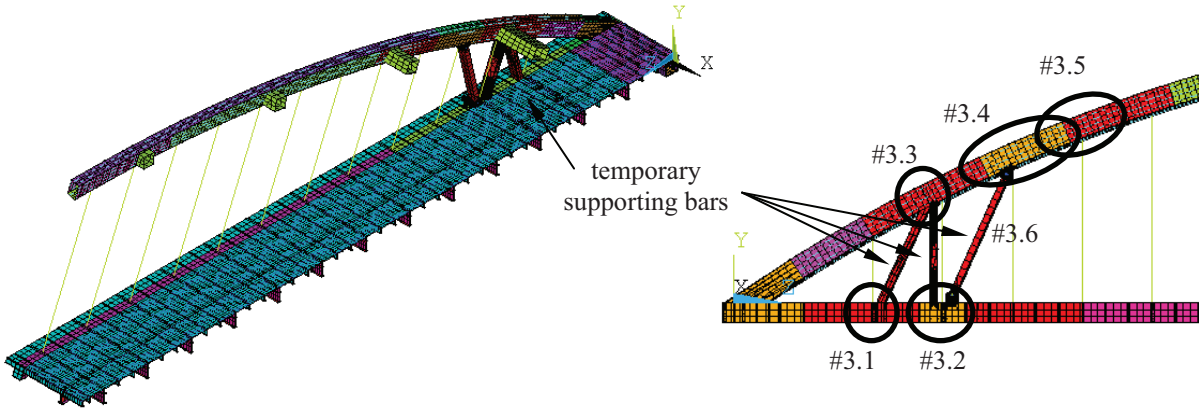

Figure 4.35: Global shell finite element model #2.1.

	Nodes	*DOFs*
model #1	56 773	340 638
model #2.1	42 170	253 020
model #2.2	63 444	380 664

Table 4.4: Characteristics of global finite element models.

Local shell finite element models

At the model level #3 six sub-models are developed for the marked details in Fig. 4.35:
- model #3.1: joint of stiffening beam and supporting bar 1,
- model #3.2: joint of stiffening beam and supporting bar 2&3,
- model #3.3: joint of arch and supporting bar 1&2,
- model #3.4: joint of arch and supporting bar 3,
- model #3.5: joint of arch and cable,
- model #3.6: supporting bar 3.

These models are separately developed owing refined mesh, however, their boundaries conform with the global model, from which the compatible displacements as the sub-model loads are derived. Figure 4.36 illustrates the mesh density of local models by model #3.4. The characteristics of the models are detailed in Table 4.5.
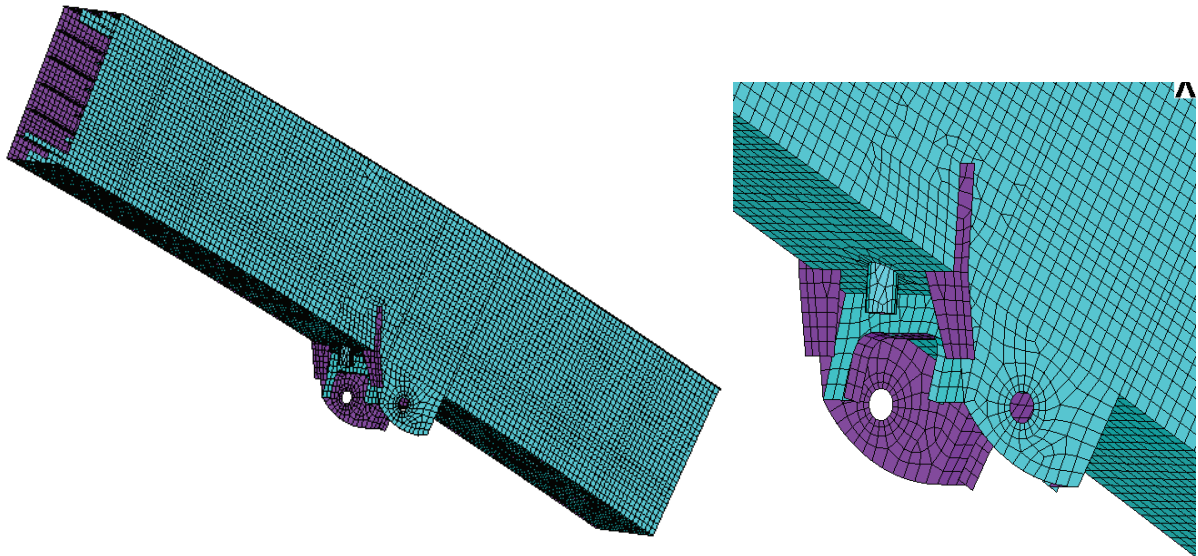
Figure 4.36: Local finite element model #3.4.

	Nodes	*DOFs*
model #3.1	16 654	99 924
model #3.2	21 019	126 114
model #3.3	26 262	157 572
model #3.4	22 719	136 314
model #3.5	14 357	86 142
model #3.6	25 688	154 128

Table 4.5: Characteristics of local finite element models.

4.3.7. Bridge design – numerical analyses

The erection phases of the bridge are checked on the basis of numerical analyses completed by the different levels and details of models. Note that we executed independent analyses and checking in order to verify the models and the applied design methods. The strategy of the analysis and checking is summarized in the followings and detailed in Dunai et al. (2006a).

Global stability of the arch

The standard based global stability checking of the arch is done first on the basis of the stability analysis by beam model #1. Figures 4.37,a and 4.37,b show the relevant in-plane and out-of-plane buckling modes, respectively; on the basis of the critical loads the slenderness of the arch are calculated and the standardized checking is executed. It is concluded that the in-plane behaviour is the governing during the erection, and in the final stage the out-of-plane buckling is critical, according to the dominancy of in-plane bending or axial compression.

The independent checking of the phenomenon is done by the finite element simulation – geometrically and material analysis with equivalent geometrical imperfections – using global shell model #2.2. The ultimate analysis proved the satisfactory resistance of the arch.

Supplementary analysis is completed to investigate the need of lateral bracing system installation between the hinged supplementary bars by stability analysis on model #1 (note that in similar bridge erection examples this type of bracings is used). The stability analysis proved the satisfactory resistance without lateral bracing during the erection of the bridge.

(a)

(b)
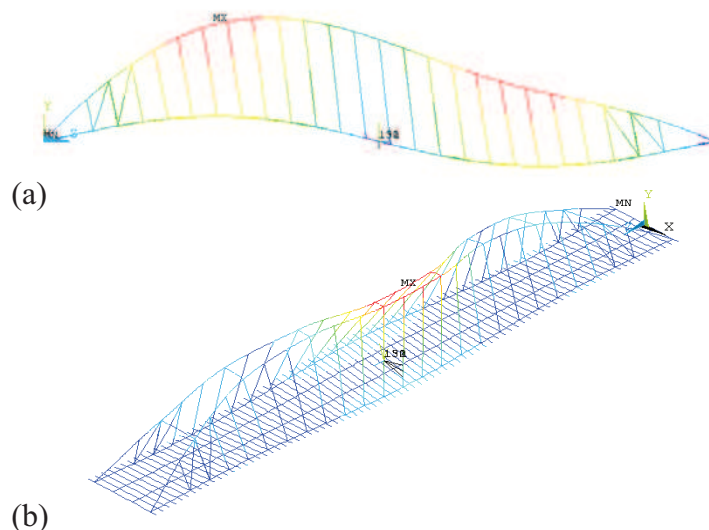
Figure 4.37: Global buckling modes of arch bridge during erection by model #1.

Strength of the details – stress concentration

The stress distribution in the relevant structural details is calculated by the sub-structuring technique using global model #2.1 and local models #3.1-3.6, and the stresses are applied for strength checking. Note that the nominal stresses are verified by the comparison of the results of global models #1 and #2.1 and of the local models.

The analysis and checking are completed in an iterative way: the constructional details are improved in the iterative steps of the design process according to the calculated capacities. The stress concentrations over the design strength are locally accepted; these regions are checked against the nominal yield strength to avoid plastic deformation in the structure. The pinned connection at the supplementary bar ends and beam/arch connecting gusset plates are checked on the basis of characteristic bearing strength and the pins are investigated by the recommendations of the Eurocode 3 (EN 1993-1-8, 2004). In these details the full resistances are utilized. Figure 4.38 illustrates the stress distribution by the analysis of model #3.3.

Figure 4.38: Stress distribution in arch and supporting bar 3 joint.

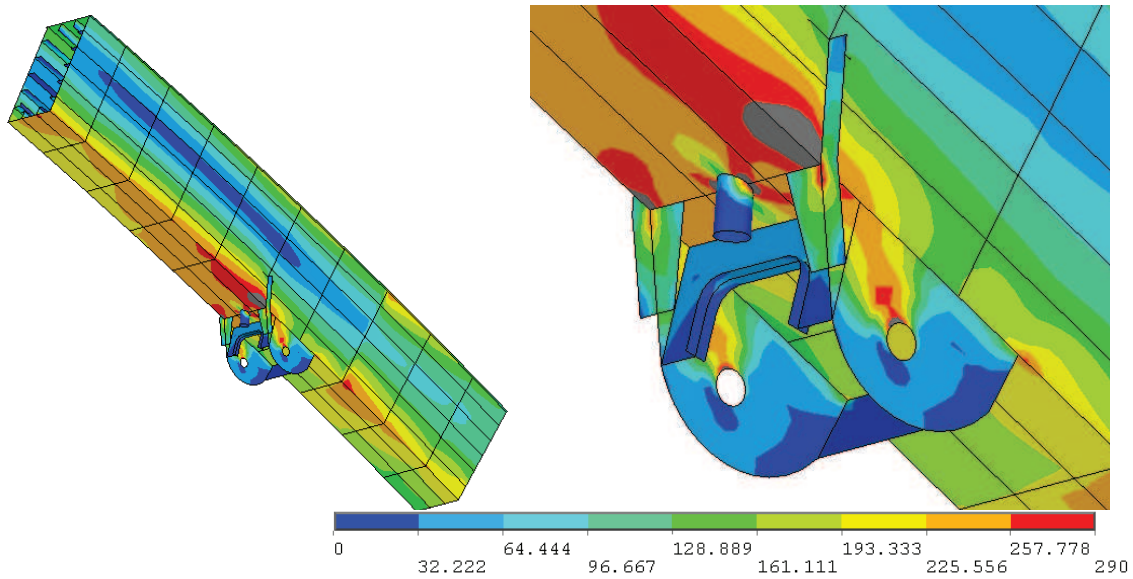Local stability of plate elements

The buckling resistances of the plate elements in the supporting zones are checked on the basis of the previously detailed analyses (Dunai et al. 2006a). These elements are classified according to the shapes and the stress field, as follows (Fig. 4.39):

1. dominantly compressed stiffened plates,
2. stiffened plate subject to complex stress field,
3. irregular configuration and stress field.

The resistance of the typical plate elements (no. 1 and 2) are calculated basically according to the application rules of the Hungarian and Eurocode 3 standards (HS and EC3). For no. 1 type of problem the buckling of fictive column (HS) and the interaction of plate-type and column-like (EC3) methods are used. In the case of no. 2 problem the orthotropic plate check is applied, where the plate slenderness is determined according to the critical load what is determined by energy method for typical plates (Vigh, 2006) and by the stability analysis of local model. For the irregular structural details (no. 3) the buckling phenomena are investigated by the local models and the generalized orthotropic plate design method is used (reduced stress method in EN 1993-1-5, 2005). Figure 4.40 illustrates the results of the stability analysis for arch and supporting bar 3 joint.
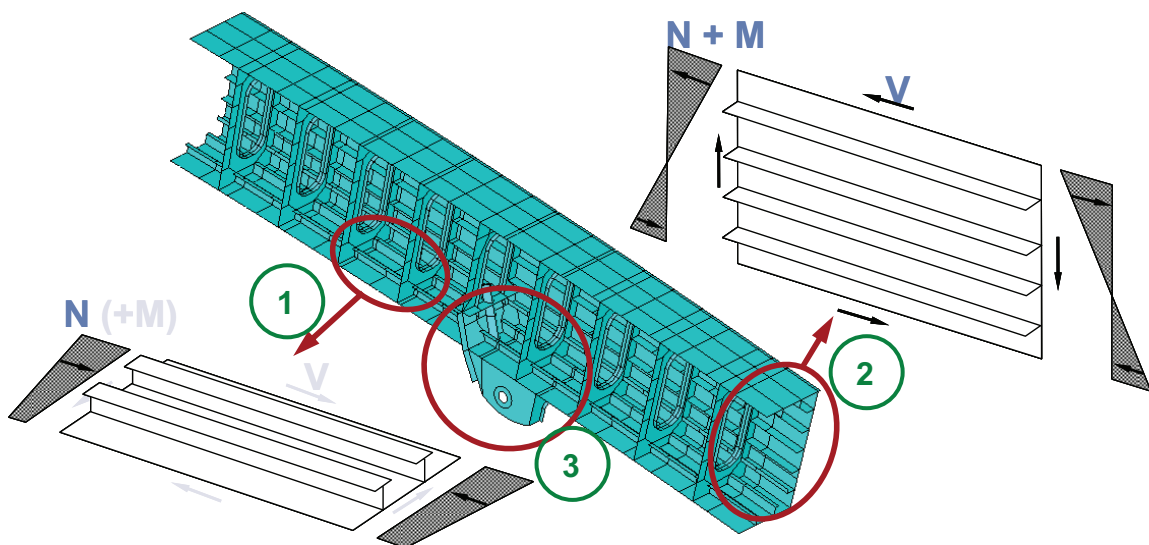

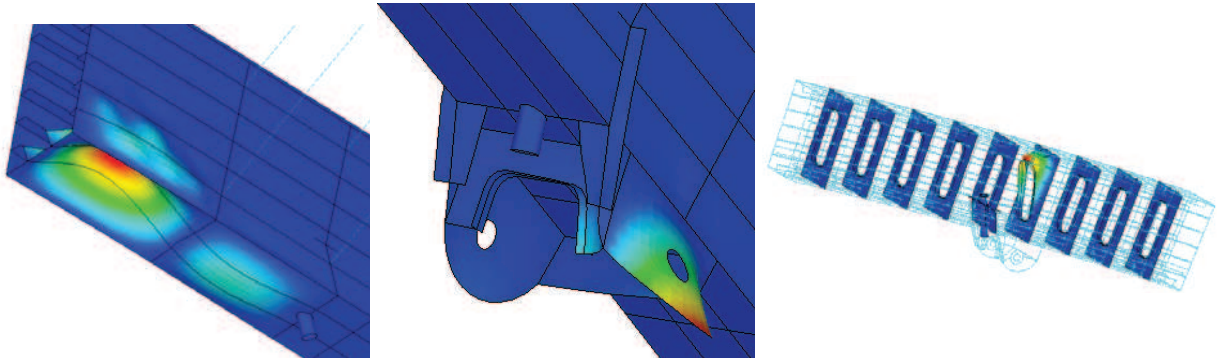Figure 4.39: Stiffened plates in arch and supporting bar 3 joint.

Figure 4.40: Buckling of plate elements in arch and supporting bar 3 joint.

The stability checking – similarly to the strength checking – is done in an iterative way. As a result, local strengthening are required and applied by additional diaphragms and stiffeners. Despite some components are overstressed up to 12% according to above detailed standard based calculations. The resistance of these elements is investigated by advanced method.

4.3.8. Ultimate analysis of stiffened plate elements

<u>Stiffened plate model</u>

Finite element simulation based stability checking is completed on six stiffened plates of the arch: 3-3 flanges and webs, with different thicknesses and stiffeners. The investigation follows the recommendations of EC3 (EN 1993-1-5, 2005). The applied finite element models are separated from the structure applying ideal boundary conditions and adopted stress distributions (model level #4). The finite element model is illustrated in Fig. 4.41. Note that this model level is verified by experiments on multi-stiffened plates in Vigh (2006).
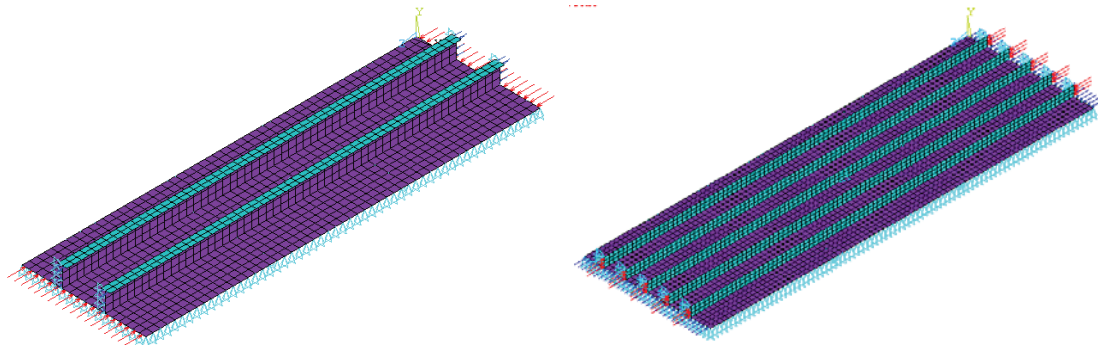
Figure 4.41: Stiffened plate shell finite element models #4.3 and 4.4.

| $e_{0w} = \min(a/400, b/400)$ | $e_{0w} = \min(a/400, b/400)$ | $\phi_0 = 1/50$ |

a) global imperfection of stiffener   b) imperfection of subpanel   c) local imperfection of stiffener
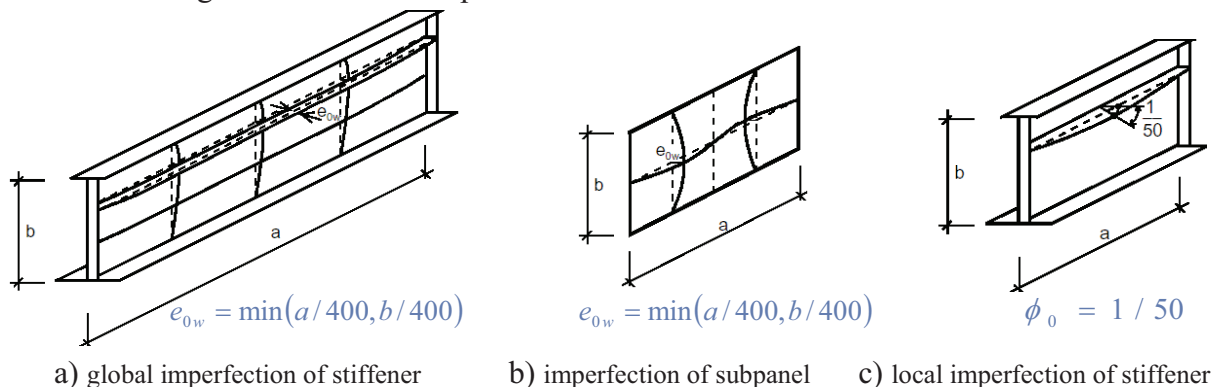
Figure 4.42: Equivalent imperfections for stiffened plate analysis of Eurocode 3.

In the material nonlinear analysis bilinear elastic-hardening plastic material model is used, with the characteristic yield strength. The equivalent geometrical imperfections are calculated on the basis of the buckling shapes, related to the overall buckling, local plate buckling and

torsion mode of the stiffener, as shown in Fig. 4.42. Due to the combined buckling modes of the stability analysis, the combination of the pure imperfections cannot be done in a unique way, by strictly following the standard recommendations. This is why in the analysis the scaling of the leading imperfection is done according to all the relevant modes, resulting in two extreme imperfection sizes, called "normal" and "large". "Normal" means the amplitude of the leading imperfection is calculated according to the global mode (typically the most dominant in the studied cases) and the "large" imperfection is on the basis of the biggest possible multiplier (typically the torsion of the stiffener). By this way the imperfection sensitivity of the stiffened plates is also studied.

Results

The results of the ultimate analyses of two typical stiffened plates are illustrated in Fig. 4.43 (flange, T-stiffener, – model #4.3), and Fig. 4.44 (web, plate-stiffener – model #4.4). The figures show the relevant buckling shapes and the load-deflection relationships for both "normal" and "large" imperfections. In the diagrams the applied load level, the resistances of the Hungarian and Eurocode 3 standards are also indicated (allowable resistances of HS, design resistances of EC3 and adjusted resistance of the HS due to different design methods).

The ultimate behaviour of the stiffened plates are evaluated and the conclusions are drawn on the (i) imperfection sensitivity of the plates with different geometrical arrangements and dimension; (ii) governing behaviour modes; (iii) safety checking against the applied load; and (iv) comparison of standard resistances (Dunai et al. 2006b). Concerning to the practical design problem the most important conclusion is that stiffened plates – failed by the classical stability checking methods – are proved (i) to have satisfactory resistances and (ii) the behaviour is linear at the practically applied load level.
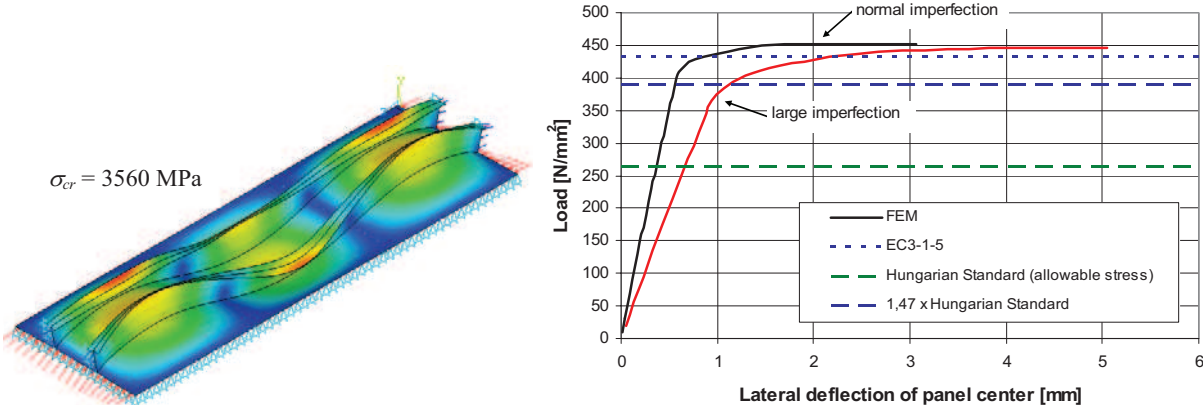

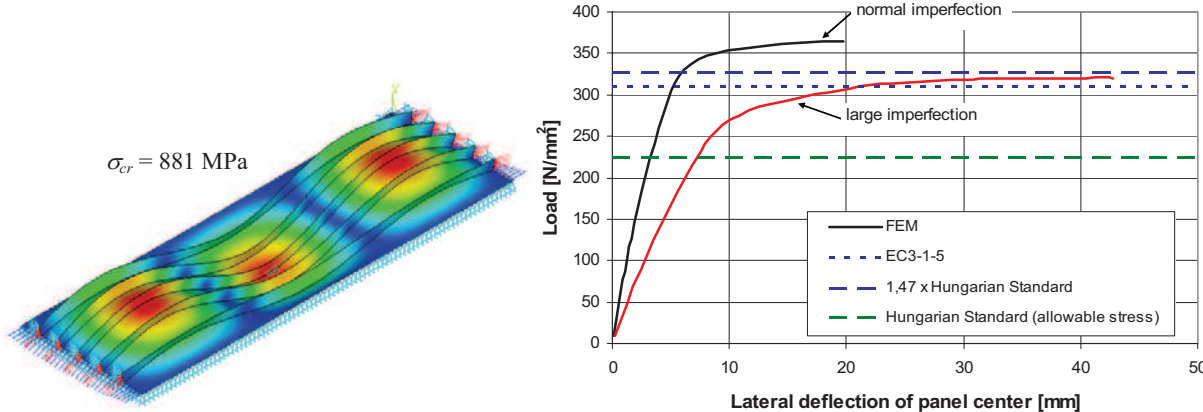Figure 4.43: Buckling shapes and ultimate analysis results – model #4.3.

Figure 4.44: Buckling shapes and ultimate analysis results – model #4.4.

5. Research results

5.1 Basis of theses

The new scientific results are achieved by a general research methodology what is developed for the investigation of complex steel structural problems. The strategy integrates the experimental and numerical research tools into a complex system and includes the human background which operates them.

The fundamental pillar is the experimental study: the different types of tests are defined according to the purpose what it is applied for. The evaluation method of experimentally observed behaviour modes is developed for the specific problems.

The numerical studies are based on advanced models which can consider the governing – in general complicated, highly nonlinear – phenomena. These are verified on test basis. The models are applied (i) directly in the design and/or (ii) for extending the tests (virtual experiments).

The developed strategy has been operated by a research team with international co-operation, and it has been applied for a wide range of structural problems; its applicability and efficiency has been proved. This research methodology provided with the basis of my own theses, as detailed in the followings.

5.2 New scientific results

Thesis #1

New steel cold-formed frame is developed, its behaviour is determined and the applicability is proved by experimental studies. Elements of the structure are: (i) portal frame composed of cold-formed C-profiles in web-to-web arrangement, (ii) self-drilling screwed connections, (iii) hollow-type section of column composed of double C-profiles.

1.1 The interacting stability behaviour modes of hollow-type double C-profile compression members are determined and a calculation method for the compressive resistance is derived.

1.2 The interacting element end and connection behaviour modes of frame corner joints are determined and the phenomena are characterized on the basis of local screwed connection tests.

Thesis #2

New composite floor beam is developed, its behaviour is determined and the applicability is proved by experimental studies. Elements of the structure are: (i) cold-formed C-profile beam, trapezoidal sheet and concrete slab with (ii) partially drilled self-drilling screw shear connector.

2.1 The classification of the self-drilling screw shear connector behaviour on the basis of push-out tests is done and the practically applicable configuration is determined.

2.2 The applicability of the partial shear connection and plastic stress distribution based design method for the composite beam is proved by beam tests.

Thesis #3

The cyclic behaviour of steel-to-steel and steel-to-concrete bolted end-plate type joints are determined by experimental and numerical studies.

3.1 The principles of the geometrically and material nonlinear shell finite element cyclic joint model are given. The degenerated layered shell finite element with a foundation layer is introduced and derived, to model the conditional supports and the concrete behaviour under the end-plate; the methodology for cyclic joint model verification is given.

3.2 The principles of a semi-empirical cyclic design model are determined on the basis of (i) monotonic moment-rotation curve; (ii) the behaviour mode dependent polygonal cyclic curve patterns and (iii) the experimentally determined degradation tendency.

Thesis #4

The background research on a steel cooling tower joint and on a basket handle type tied arch bridge with parallel cables are completed by experimental and numerical studies to support the design. The behaviour of the tubular structural joint and the stability phenomena of the tied arch are determined. On the bases of these results:

4.1 The applicability of the developed steel cooling tower joint prototypes and design methods are proved.

4.2 The safety of different design methods for the stability checking of tied arch bridge with parallel cables is determined; their applicability in the practical design is proved.

5.3 Application of results

Structural application

The research work produced applicable results in different structural problems, as follows:

The results of cold-formed structural research are directly applied in the development and design of the cold-formed steel framed building structure, resulting in patent and completed buildings. (Theses #1 and 2)

The results on the cyclic behaviour of bolted end-plate type joints can be used to determine the local ductility of the investigated details as a basis of the global ductility derivation of the seismic resistant steel and steel-concrete composite frames. The research also produced practically applicable constructional detailing rules. (Thesis #3)

The results on the steel cooling tower joint research are directly applied in the prototype development and design of the structural system; the first practical application of the structure is under progress. (Thesis #4)

The results on the global and local stability of tied arch bridge are used in the practical design of the Dunaújváros Danube bridge. (Thesis #4)

Research methodology application

The developed research strategy is proved to be efficient for the solution of this type of structural problems. The methodology has been applied in the ongoing and new research projects.

Education

The research results are applied in the education of finite element analysis based design methods for graduate and postgraduate students.

Knowledge extension

The research – beside the direct applications of the results – provided more general, applicable information by knowledge extension on the fundamental research fields of:

- interaction of stability phenomena in the behaviour of cold-formed structural elements,
- interaction of element and connection behaviour of cold-formed structures,
- composite beams with flexible connections;
- interaction of connection and tubular structural member behaviour,
- stability of arch bridges;
- nonlinear finite element modelling and application.

6. References

CHAPTER 2

AISI (1997). *Residential Steel Framing Manual*, American Iron and Steel Institute, Washington DC, USA.

Baigent, A.H., Hancock, G.J. (1982). "The behaviour of portal frames composed of cold-formed members", *Thin-Walled Structures – Recent technical advances and trends in design, research and construction*, Oxford, Elsevier Applied Science, 209.

Building Works Inc. (2003). *Prescriptive method for connecting cold-formed steel framing to insulating concrete form walls in residential construction*, Report, Cambridge, UK.

Chung, K.F., Shi, Y.J. (1999). "Lateral torsional buckling of gusset plates in bolted moment connections among cold-formed steel members", *Journal of Constructional Steel Research*, Vol. 46, No. 1-3, Paper No. 418.

ColdForm (2000). *Design of metallic cold-formed thin-walled members*, Rel. 3.0.

De Vos, G.P., Van Rensburg, B.W.J. (1997). "Lightweight cold-formed portal frames for developing countries", *Bldg Env.*, 32(5), 417.

Dubina, D., Stratan, A., Ciutina, A., Nagy, Zs. (2004). "Experimental research on monotonic and cyclic performance of joints of cold-formed pitched roof portal frames", *2nd International Conference on Steel and Composite Structures*, Eds. Choi, C.K., Lee, H.W., Kwak, H.G., Seoul, Korea, 176-190.

Dunai, L., Erdélyi, Sz. (2005). "Experimental investigation of composite light-gauge floor beams", *4th European Conference on Steel and Composite Structures*, Maastricht, The Netherlands, Eds. Hoffmeister, B., Hechler, O., Druck und Verlaghaus Mainz Publisher, Vol. B, 4.3-25 – 4.3-32.

Dunai, L., Erdélyi, Sz., Ádány, S. (2003a). "Design method of light-gauge composite beams", *International Conference on Advances in Structures: Steel, Concrete, Composite and Aluminium*, Sydney, Australia, Eds. Hancock, G.J., Bradford, M.A., Wilkinson, T.J., Uy, B., Rasmussen, K.J.R., A.A. Balkema Publishers, Vol. 2, 317-323.

Dunai, L., Erdélyi, Sz., Ádány, S. (2003b). *Design of light-gauge composite beams – method and design tables*, Design guide, Lindab Ltd.

Dunai, L., Fóti, P. (2005). "Experimental behaviour modes of cold-formed frame corners", *5th International Workshop on Connections in Steel Structures*, Amsterdam, The Netherlands, Eds. Bijlaard, F.S.K, Gresnigt, A.M, van der Vegte, G.J, AISC - ECCS, 243-252.

Dunai L., Fóti P., Fancsalli, A. (2000a). *Experimental study on sheared self-drilling screw connections*, Research report, Department of Structural Engineering, Budapest University of Technology and Economics, p. 80.

Dunai L., Fóti P., Kálló M., Kaltenbach L. (2000b). *Experimental study on frame corner joints of cold-formed C-profiles*, Research reports: 1-3, Department of Structural Engineering, Budapest University of Technology and Economics, p. 220.

Dunai, L., Jakab, G., Joó, A.L. (2004). "Experiments on C/Z-profile compression members", *4th International Conference on Coupled Instabilities in Metal Structures*, Rome, Italy, 429-438.

Dunai L., Joó, A.L., Kaltenbach L., Kálló, M., Futó, T., Tóth, A. (2007). *Experimental overlapped Z-purlins*, Research reports: 1-2, Department of Structural Engineering, Budapest University of Technology and Economics, p. 250.

Dunai, L., Kotormán, I. (2005). "Research and development of the Lindab light-gauge building system", *4th European Conference on Steel and Composite Structures*, Maastricht, The Netherlands, Eds. Hoffmeister, B., Hechler, O., Druck und Verlaghaus Mainz Publisher, Vol. A, 1.2-27 – 1.2-34.

Dundu, M., Kemp, A.R. (2006). "Strength requirements of single cold-formed channels connected back-to-back", *Journal of Constructional Steel Research*, 62, 250-261.

Earl Composite Systems (2001), *MetalStudCrete® (MSC) – shear transfer strip*, Report, Irwindale, California, USA.

EN 1990 (2001). *Eurocode: Basis of structural design.*

EN 1993-1-1 (2004). *Eurocode 3: Design of steel structures – Part 1-1: General rules and rules for buildings.*

EN 1993-1-3 (2005). *Eurocode 3: Design of steel structures – Part 1-3: General rules. Supplementary rules for cold-formed members and sheeting.*

EN 1993-1-5 (2005). *Eurocode 3: Design of steel structures – Part 1-5: Plated structural elements.*

EN 1993-1-8 (2004). *Eurocode 3: Design of steel structures – Part 1-8: Design of joints.*

EN 1994-1-1 (2004). *Eurocode 4: Design of composite steel and concrete structures – Part 1-1: General rules and rules for buildings.*

Erdélyi, Sz., Dunai, L. (2002). "Experimental study on connection of composite light-gauge floor system", *3rd European Conference on Steel Structures*, Coimbra, Portugal, Eds. Lamas, A., Silva, L.S., CMM Publisher, 441-450.

Erdélyi, Sz. (2005). "Numerical simulation of the behaviour of light-gauge composite floor beam", *15th Inter-Institute Seminar*, Budapest University of Technology and Economics, Budapest, Hungary, presentation.

Erdélyi, Sz., Dunai, L. (2004). "Behaviour of a new type of composite connection", *Periodica Polytechnica, Civil Engineering*, Budapest University of Technology and Economics, Vol. 48, Nos. 1-2, 89-100.

Erdélyi, Sz., Dunai, L. (2007). "Light-gauge composite floor beam with self-drilling screw shear connector; Experimental study", *Steel & Composite Structures*, submitted for publications; supported by the reviewers in January 2007.

Fóti, P. (2002). "Behaviour modes of self-drilling screw connections under shear loading – experimental study", *Scientific Publications of the Department of Structural Engineering of BME*, 29-38. (in Hungarian)

Fóti, P., Dunai, L. (2000). "Interaction phenomena in the cold-formed frame corner behaviour", *3rd International Conference on Coupled Instabilities in Metal Structures*, Lisbon, Portugal, Eds. Camotim, D., Dubina, D., Rondal, J., Imperial College Press, 459-466.

Fóti, P., Dunai, L. (2002). "Test based design method of moment resisting joints in cold-formed structures", *International Colloquium on Stability and Ductility of Steel Structures, Prof. O. Halász Memorial Session*, Budapest, Hungary, Ed. Iványi, M., Akadémia, 211-218.

Hanaor, A. (2000), "Tests of composite beams with cold-formed sections", *Journal of Constructional Steel Research*, Vol. 54, 254-264.

Iványi, M. (1983). *Interaction of strength and stability phenomena in the behaviour of steel structures; The role of plate buckling*, Doctor of Science Thesis, Hungarian Academy of Sciences.

Jakab, G. (2003). "Load-bearing behaviour and dimensioning of cold-formed C-sections under axial pressure load", Diploma work, Advisors: Saal, H., (Technical University of Karlsruhe) and Dunai, L. (Budapest University of Technology and Economics). (in German)

Jakab, G., Dunai, L. (2007). "Resistance of C-profile cold-formed compression members: test and standard", *Journal of Constructional Steel Research*, conference paper invited for journal publication in January 2007.

Joó, A.L., Dunai, L. (2002). "Numerical studies on the ultimate behaviour of steel cold-formed purlins", *6th International Conference on Computational Structures Technology*, Prague, Czech Republic, "Computational Steel Structures Technology", Eds. Topping, B.H.V., Bittnar, Z., Civil-Comp Press, 247-248 (on CD-ROM: ISBN 0-948749-81-4, 14 pages).

Joó, A.L., Dunai, L. (2004). "Geometric imperfections of Z-profiles for numerical models", *4th International Conference on Coupled Instabilities in Metal Structures*, Rome, Italy, 97-106.

Kachichian, M., Dunai, L. (2001). "Experimental study on the lateral stiffness of sliding connection of purlin-cladding system", *Scientific Publications of the Department of Structural Engineering, BME*, 77-82.

Kachichian, M., Dunai, L., Kaltenbach, L., Kálló, M. (1999). "Experimental study on the interaction of steel sheeting and Z-purlin", *6th International Colloquium on Stability and Ductility of Steel Structures*, Timisoara, Romania, Eds. Dubina, D., Iványi, M., Elsevier Publisher, 509-516.

Kirk, P. (1986). "Design of cold-formed section portal frame building system", *8th International Speciality Conference on Cold-Formed Steel Structures*, University of Missouri-Rolla, USA, 295.

Lakkavalli, B.S., Liu, Y. (2006). "Experimental study of composite cold-formed steel C-section floor joist", *Journal of Constructional Steel Research*, 62, 995-1006.

Lim, J.B.P., Nethercot, D.A. (2003a). "Serviceability design of a cold-formed steel portal frame having semi-rigid joints", *Steel and Composite Structures*, Vol. 3, No. 6, 451-474.

Lim, J.B.P., Nethercot, D.A. (2003b). "Ultimate strength of bolted moment-connections between cold-formed steel members", *Thin-Walled Structures*, Vol. 41, No. 11, 1019-1039.

Lindab patent (2002). *Light-gauge steel building system*, patent authors: Dunai L., Horváth L., Tóth E., patent announced by Lindab Ltd., Hungary, date of announcement: January 3, 2002, date of publishing: June 28, 2004. (in Szabadalmi Közlöny és Védjegyértesítő, 2004/6); patent number: P0200012.

Makelainen, P., Kankaanpaa, J. (1996). "Structural design study on a light-gauge steel portal frame with cold-formed sigma sections", *13th International Speciality Conference on Cold-Formed Steel Structures*, University of Missouri-Rolla, USA.

Mihálffy, A. (2004). *Studies on the behaviour of cold-formed frame corner joints*, Diploma work, Department of Structural Engineering, Budapest University of Technology and Economics, Advisors: Dunai, L., Fóti, P., Kotormán I.

Mujagic, J.R.U., Easterling, W.S., Murray, T.M (2001). "Standoff screws as shear connectors for composite trusses: push-out test results and analysis", *International Conference on Connection between Steel and Concrete*, Stuttgart, Germany, 1240-1249.

Nagy, Zs., Stratan, A., Dubina, D. (2006). "Application of component method for bolted cold-formed steel joints", *International Conference on Metal Structures*, Poiana Brasov, Romania, 2006, Eds. Dubina, D., Ungureanu, V., Balkema, 207-215.

Schafer, B.W. (1998). *CUFSM Users' Manual*, Cornell University, USA.

Tuza, G. (2005). *Experimental studies on bonded and mechanical steel connections*, Student scientific research work (TDK), Department of Structural Engineering, Budapest University of Technology and Economics, Advisors: Dunai, L., Fóti, P. (in Hungarian)

US Specification (2004). *Specification for the Design of Cold-Formed Steel Structural Members; Appendix 1: Design of Cold-Formed Members Using the Direct Strength Method.*

Yu, W.W. (2000). *Cold-formed steel design*, 3rd edition, John Willey & Sons.

CHAPTER 3

Ádány, S. (2000). *Numerical and experimental analysis of bolted end-plate joints under monotonic and cyclic loading,* PhD Thesis, Budapest University of Technology and Economics, Faculty of Civil Engineering, Budapest, Hungary; Supervisor: Dunai, L.

Ádány, S., Calado, L., Dunai, L. (2001). "Experimental study on the cyclic behaviour of bolted end-plate joints", *Steel & Composite Structures*, Vol. 1, No. 1, 33-50.

Ádány, S., Dunai, L. (1997a). "A modified multi-surface model for structural steel under cyclic loading", *5th International Colloquium on the Stability and Ductility of Steel Structures*, Nagoya, Japan, 841-846.

Ádány, S., Dunai, L. (1997b). "Modelling of steel-to-concrete end-plate connections under monotonic and cyclic loading", *Periodica Polytechnica, Civil Engineering*, Vol. 47, No. 1, 3-16.

Ádány, S., Dunai, L. (2004). "Finite element simulation of the cyclic behaviour of end-plate joints", *Computers and Structures*, Vol. 82, Issues 23-26, 2131-2143.

Akiyama, H. (2000). "Evaluation of the fractural mode of failure in steel structures following the Kobe lessons", *Journal of Constructional Steel Research*, Vol. 55, 211-227.

Azevedo, J., Calado, L. (1994). "Hysteretic behaviour of steel members: analytical models and experimental tests", *Journal of Constructional Steel Research*, Vol. 29, 71-94.

Ballio, G., Castiglioni, C.A. (1994). "Seismic behaviour of steel sections", *Journal of Constructional Steel Research*, Vol. 29, 21-54.

Ballio, G., Perotti, F. (1987). "Cyclic behaviour of axially loaded members; numerical simulation and experimental verification", *Journal of Constructional Steel Research*, Vol. 7, 3-41.

Beg, D., Skuber, P. (2000). "Earthquake resistance of frames with unsymmetric bolted connections", *3rd International Conference on Behaviour of Steel Structures in Seismic Areas*, Eds. Mazzolani, F.M., Tremblay, R., Montreal, Canada, 551-557.

Bernuzzi, C. (1998). "Prediction of the behaviour of top-and-seat cleated steel beam-to-column connections under cyclic reversal loading", *Journal of Earthquake Engineering*, Vol. 2, No. 1, 25-58.

Bernuzzi, C., Calado, L., Castiglioni, C.A. (1997). "Ductility and load carrying capacity prediction of steel beam-to-column connections under cyclic reversal loading", *Journal of Earthquake Engineering*, Vol. 1, No. 2, 401-432.

Bernuzzi, C., Zandonini, R., Zanon, P. (1996). "Experimental analysis and modelling of semi-rigid steel joints under reversal loading", *Journal of Constructional Steel Research*, Vol. 38, No. 2, 95-123.

Broderick, B.M., Thomson, A.W. (2000). "Cyclic testing of flush end-plate semi-rigid steel connections", *3rd International Conference on Behaviour of Steel Structures in Seismic Areas*, Eds. Mazzolani, F.M., Tremblay, R., Montreal, Canada, 135-140.

Bursi, O.S., Ballerini, M., Nemati, N., Zandonini, R. (1997). "Quasi-static monotonic and low-cycle behaviour of steel isolated Tee stub connections", *2nd International Conference on Behaviour of Steel Structures in Seismic Areas*, Eds. Mazzolani, F.M., Akiyama, H., Kyoto, Japan, 554-563.

Calado, L. (1989). *Caracterização do comportamento de estruturas metálicas sob acções sísmicas*, PhD Thesis, Technical University of Lisbon, Lisbon, Portugal.

Calado, L., Ferreira, J. (1994). "Cyclic behaviour of steel beam-to-column connections – An experimental research", *1st International Conference on Behaviour of Steel Structures in Seismic Areas*, Eds. Mazzolani, F.M., Goincu, V., Timisoara, Romania, 381-389.

Chan, S.L. (1998). "Geometric and material non-linear analysis of beam-columns and frames using the minimum residual displacement method", *International Journal for Numerical Methods in Engineering*, 1998, Vol. 26, 2657-2669.

Chasten, C. P., Fleischman, F. B., Driscoll, G. C., Lu, L. W. (1989). "Top-and-seat-angle connections and end-plate connections: behaviour and strength under monotonic and cyclic loading", *National Steel Construction Conference*, AISC, USA, 6-1 – 6-32.

Choi, C.K., Chung, G.T. (1996). "Refined three-dimensional finite element model for end-plate connection", *Journal of Structural Engineering*, Vol. 122, No. 11, 1307-1316.

Dafalias, Y.F., Popov, E.P. (1975). "A model of nonlinear hardening materials for complex loading", *Acta Mechanica*, Vol. 21, 173-192.

De Stefano, M., Astaneh, A.A. (1991). "Axial force-displacement behaviour of steel double angles", *Journal of Constructional Steel Research*, Vol. 20, 161-181.

Dunai, L. (1995). "*Behaviour of steel-to-steel and steel-to-concrete connections under monotonic and cyclic loading.*" Candidate of Science Thesis, Hungarian Academy of Sciences, Budapest, Hungary.

Dunai, L., Ádány, S., Wald, F., Sokol, Z. (1996a). "Numerical modelling of column-base connections", *Advances in Computational Techniques for Structural Engineering*, Ed. Topping, B.H.V., Civil-Comp Press, 171-178.

Dunai, L., Fukumoto, Y., Ohtani, Y. (1996b). "Behaviour of steel-to-concrete connections under combined axial force and cyclic bending", *Journal of Constructional Steel Research*, Vol. 36, No. 2, 121-147.

Dunai, L., Kovács, N., Calado, L. (2004). "Analysis of bolted end-plate joints: Cyclic test and standard approach", *5th International Workshop on Connections in Steel Structures*, Eds. Bijlaard, F.S.K, Gresnigt, A.M, van der Vegte, G.J, Amsterdam, The Netherlands, AISC - ECCS, 190-200.

Dunai, L., Lu, L.W. (1991a). "Analytical studies of monotonic and cyclic behaviour of flexible connections with bolted angles", *Annual Technical Session of Structural Stability Research Council*, Chicago, USA, 335-343.

Dunai, L., Lu, L.W. (1991b). "Analytical modelling of cyclic behaviour of bolted semi-rigid connections", *2nd International Workshop on Connections in Steel Structures II: Behaviour,*

Strength, and Design, Eds. Bjorhovde, R., Colson, A., Haaijer, G., Stark, J.W.B., AISC, Pittsburgh, USA, 354-360.

Dunai, L., Ohtani, Y., Fukumoto, Y. (1994). "Experimental study of steel-to-concrete end-plate connections under combined thrust and bending", *Technology Reports of the Osaka University*, Vol. 44, No. 2197, 307-320.

ECCS (1986). *Recommended testing procedure for assessing the behaviour of structural steel elements under cyclic loads.* Technical Committee 1, TWG 1.3 – Seismic Design, No. 45.

Elnashai, A.S., Elghazouli, A.Y. (1994). "Seismic behaviour of semi-rigid steel frames", *Journal of Constructional Steel Research*, Vol. 29, 149-174.

EN 1990 (2001). *Eurocode: Basis of structural design.*

EN 1993-1-1 (2004). *Eurocode 3: Design of steel structures – Part 1-1: General rules and rules for buildings.*

EN 1993-1-5 (2005). *Eurocode 3: Design of steel structures – Part 1-5: Plated structural elements.*

EN 1993-1-8 (2004). *Eurocode 3: Design of steel structures – Part 1-8: Design of joints.*

EN 1994-1-1 (2004). *Eurocode 4: Design of composite steel and concrete structures – Part 1-1: General rules and rules for buildings.*

Fahny, M., Stojadinovic, B., Goel, S.C. (2000). "Hysteretic behaviour of steel moment resisting column bases", *3rd International Conference on Behaviour of Steel Structures in Seismic Areas*, Eds. Mazzolani, F.M., Tremblay, R., Montreal, Canada, 191-197.

Gebbeken, N., Rothert, H., Binder, B. (1994). "On the numerical analysis of end-plate connections", *Journal of Constructional Steel Research*, Vol. 30(2), 177-196.

Guisse, S., Vandegans, D., Jaspart, J.P. (1996). "Application of the component method to column bases – Experimentation and development of a mechanical model for characterization", *Technical Report*, MT 195, Research Centre of the Belgian Metalworking Industry, Steel Construction Department.

Jaspart, J.P. (1991). *Étude de la semi-rigidité des noeds pouter-colonne et son influence sur la résistance et la stabilité des ossatures en acier*, These de Doctorat, Université de Liege, Faculté des Sciences Appliquées.

Jaspart, J.P. (2000). "General report: session on connections", *Journal of Constructional Steel Research*, Vol. 55, 69-89.

Karsan, I.D., Jirsa, J.O. (1969). "Behaviour of concrete under compressive loading", *Journal of the Structural Division*, ASCE, 95(2).

Kasai, K., Xu, Y., Mayangarum, A. (2000). "Experimental analysis of bolted semi-rigid beam-column connections. Part I. Cyclic loading experiment", *3rd International Conference on Behaviour of Steel Structures in Seismic Areas*, Eds. Mazzolani, F.M., Tremblay, R., Montreal, Canada, 199-206.

Kato, B., Aoki, H., Yamanouchi, H. (1990). "Standardised mathematical expression for stress-strain relations of structural steel under monotonic uniaxial tension loading", *Material Structures*, RILEM, No. 23, 47-58.

Kishi, N., Komuro, M., Chen, W.F. (2004). "Four-parameter power model for M-Θ curves of end-plate connections", *5th International Workshop on Connections in Steel Structures*, Eds. Bijlaard, F.S.K, Gresnigt, A.M, van der Vegte, G.J, Amsterdam, The Netherlands, AISC – ECCS.

Kovács, N. (2005). *Cyclic behaviour of end-plate joints of steel and composite structural elements*, PhD Thesis, Budapest University of Technology and Economics, Faculty of Civil Engineering, Budapest, Hungary; Supervisors: Dunai, L., Calado, L. (Tech. Univ. of Lisbon)

Kovács, N., Calado, L., Dunai, L. (2002). "Behaviour of bolted composite joints; Experimental study." *Journal of Constructional Steel Research*, Vol. 32, Issues 3-5, 725-738.

Kovács, N., Dunai, L., Calado, L. (2004). "Local instability phenomena of steel and composite joints under cyclic loading", *4th International Conference on Coupled Instabilities in Metal Structures*, Rome, Italy, 391-400.

Kulak, G.L., Fisher, J.W., Struik, J.H.A. (1987). *Guide for design criteria for bolted and riveted joints*, Second Edition, John Willey & Sons, New York.

Kukreti, A.R., Abolmaali, A.S. (1999). "Moment-resistance hysteresis behaviour of top and seat angle frame connections", *Journal of Structural Engineering*, Vol. 125, No. 8, 810-820.

Lee, G.C., Lee, E.T. (1994). "Local buckling of steel sections under cyclic loading", *Journal of Constructional Steel Research*, Vol. 29, 55-70.

Maggi, Y.I., Gonçalves, R.M., Calado, L. (2003). "Numerical and experimental behaviour of beam-to-column extended end plate connections", *4th International Conference on Steel Structures in Seismic Areas*, Ed. Mazzolani, F.M., Naples, Italy, 343-349.

Mazzolani, F.M. (1988). "Mathematical model for semi-rigid joints under cyclic loading", *Connections in Steel Structures*", Ed. Chen, W.F., Elsevier, 112-120.

Mazzolani, F.M. (2002). "The 'Recos' research project", *12th European Conference on Earthquake Engineering*, London, UK, (published on CD).

Mazzolani, F.M., Piluso, V. (1993). *ECCS manual on design of steel structures in seismic zones*, TC 13 Seismic design.

Murray, T.M. (1988). "Recent development for the design of moment end-plate connections", *Journal of Constructional Steel Research*, Vol. 10, 133-162.

Nemati, B.N., Le Houedec, D. (1996). "The analysis and the 3D finite element simulation of the steel bolted end-plate connections", *Advances in Computational Techniques for Structural Engineering*, Ed. Topping, B.H.V., Civil-Comp Press, 179-187.

Nethercot, D.A. (1985): *Steel beam-to-column connections − A review of test data*, CIRIA Project No. 338, London, UK.

Popov, E. P., Petersson, H. (1978). "Cyclic metal plasticity: experiments and theory." *Journal of Engineering Mechanics Division*, ASCE, Vol. 104(6), 1371-1388.

Shen, J., Astaneh, A.A. (2000). "Hysteretic model of bolted-angle connections", *Journal of Constructional Steel Research*, Vol. 54, 317-343.

Shi, Y.J., Chan, S.L., Wong, Y.L. (1996). "Modelling for moment-rotation characteristics for end-plate connections", *Journal of Structural Engineering*, Vol. 122, No. 11, 1300-1305.

Simões da Silva, L., Coelho, A.G. (2001). "A ductility model for steel connections", *Journal of Constructional Steel Research*, Vol. 57, 45-70.

Thomson, A.W., Broderick, B.M. (2002). "Cyclic testing and analysis of semi-rigid flush end-plate joints", *12th European Conference on Earthquake Engineering*, London, UK, (CD).

Usami, T., Ge, H. B., Saizuka, K. (1997). "Behaviour of partially concrete-filled steel bridge piers under cyclic and dynamic loading", *Journal of Constructional Steel Research*, Vol. 41, No. 2, 121-136.

Vandegans, D. (1997). *Column bases: Experimentation and application of analytical models*, Technical Report, MT 196, Research Centre of the Belgian Metalworking Industry, Steel Construction Department.

Wald, F. (1993). *Column-base connections; a comparative state-of-the-art review*, COST C1 Project, CIPE 3510 PL 20143, Technical University of Prague, Czech Republic.

Wald, F., Steenhuis, M. (1992). "The beam-to-column bolted joint stiffness according to Eurocode 3", Cost project C1, Semi rigid behaviour of civil engineering structural connections, *1st State-of-the-art workshop*, Strasbourg, France, 503-516.

Xu, Y., Kasai, K. (2003). "Cyclic behaviour of low-cycle fatigue of semi-rigid connections, Part II. bolted T-stub connections", *4th International Conference on Steel Structures in Seismic Areas*, Ed. Mazzolani, F.M., Naples, Italy, 321-327.

Yao, T., Nikolov, P.I. (1992). "Numerical experiments on buckling/plastic collapse behaviour of plates under cyclic loading", *Stability and Ductility of Steel Structures under Cyclic Loading*, Eds. Fukumoto, Y., Lee, G., CRC Press, USA, 203-214.

CHAPTER 4

ANSYS (2001). *Structural Analysis Program*, Ver. 7.0.

Cholnoky, P., Dunai, L., Horváth, L. (2006). "Development of new generation of natural draughed steel cooling towers", *IABSE Symposium*, Budapest, Hungary, Report, Vol. 92, IABSE publisher, 168-169 (on CD 8 pages).

Dunai, L. (2006). "Advanced stability analysis and design of a new Danube arch bridge", *6th European Solid Mechanics Conference*, Budapest, Hungary, extended abstract, p. 2.

Dunai, L., Horváth, L., Tóth, J., Vigh, L.G. (2002). "Experimental and numerical studies on joints of steel cooling tower", *3rd European Conference on Steel Structures*, Coimbra, Portugal, Eds. Lamas, A., Silva, L.S., CMM Publisher, 1111-1120.

Dunai, L., Joó, A.L., Kaltenbach, L., Kálló, M., Köröndi, L. (2004). *Experimental study on the stability of a tied arch bridge model*, Report, Department of Structural Engineering, Budapest University of Technology and Economics.

Dunai, L., Joó, A.L., Szatmári, I., Vigh, L.G. (2006a). *Strength of the Dunaújváros Danube bridge during erection*, Report, Department of Structural Engineering, Budapest University of Technology and Economics.

Dunai, L., Joó, A.L., Vigh, L.G. (2006b). "Advanced stability analysis and design of a new Danube arch bridge", *6th European Solid Mechanics Conference*, Budapest, Hungary, presentation material.

EN 1990 (2001). *Eurocode: Basis of structural design.*

EN 1993-1-1 (2004). *Eurocode 3: Design of steel structures – Part 1-1: General rules and rules for buildings.*

EN 1993-1-5 (2005). *Eurocode 3: Design of steel structures – Part 1-5: Plated structural elements.*

EN 1993-1-6 (2005). *Eurocode 3: Design of steel structures – Part 1-6: Strength and stability of shell structures.*

EN 1993-1-8 (2004). *Eurocode 3: Design of steel structures – Part 1-8: Design of joints.*

EN 1993-2 (2005). *Eurocode 3: Design of steel structures – Part 2: Steel bridges.*

Goricsán, I., Balczó, M., Lajos, T. (2005). "Aerodynamic investigation of the Dunaújváros Danube bridge by wind tunnel tests", *Scientific Publications of the Department of Structural Engineering, BME*, 65-76. (in Hungarian)

Hegedűs, I. (2005). "Problems related to the effect of wind for the design of large span arch bridges", *Scientific Publications of the Department of Structural Engineering, BME*, 41-56. (in Hungarian)

Honfi, D., Joó, A.L., Dunai, L., Ádány, S. (2005). "Parametric study on the structural versions of the Danube bridge in Dunaújváros", *Scientific Publications of the Department of Structural Engineering, BME*, 9-18. (in Hungarian)

Horváth, A., Dunai, L., Nagy, Zs (2006). "Dunaújváros Danube bridge: construction, design and research", *Structural Engineering International*, Journal of the International Association for Bridge and Structural Engineering (IABSE), Vol. 16, No. 1, 31-35.

HS (2002). *Design of Highway Bridges: III. Specifications for Steel Bridges.* ÚT 2-3.413 Hungarian Standard.

JHSB (1994). *Specifications for Highway Bridges, Part II. Steel Bridges*, Japan Road Association.

Joó, A.L., Dunai, L. (2005). "Strength of an arch bridge model: experiment and design methods", *4th European Conference on Steel and Composite Structures*, Maastricht, The Netherlands, Eds. Hoffmeister, B., Hechler, O., Druck und Verlaghaus Mainz Publisher, Vol. B, 4.7-49 – 4.7-56.

Joó, A.L., Dunai, L., Kálló, M., Kaltenbach, L., Köröndi, L. (2005). "Experimental analysis of a Nielsen-type bridge model", *Materials Engineering*, Vol. 12, No. 1, 1-6.

Kitada, T., Nakai, H., Sugiyama, I., Kurimoto, H., Sakano, M. (1989). "An experimental study on ultimate strength of arch ribs in Nielsen-Lohse bridge with basket-handle type", *Journal of Structural Engineering*, Vol. 35 A, JSCE, 155-164.

Mihálffy, A., Joó, A.L., Dunai, L., Szatmári, I. (2005). "Fatigue analysis of orthotropic bridge decks", *Scientific Publications of the Department of Structural Engineering, BME*, 65-76. (in Hungarian)

Nakai, H., Kitada, T, Kunihiro, M., Kitazawa, M., Hasino, F. (1995). "Proposition of methods checking the ultimate strength of arch ribs in steel Nielsen-Lohse bridges", *Stahlbau*, 64, H 5.

Tóth, J. (2003). *Design methods for bolted end-plate connections of tubular structural members*, Student scientific research work (TDK), Department of Structural Engineering, Budapest University of Technology and Economics, Advisors: Dunai, L., Horváth, L. (in Hungarian)

Vigh, L.G. (2006). *Virtual and real test based analysis and design of non-conventional thin-walled metal structures*, PhD Thesis, Faculty of Civil Engineering, Budapest University of Technology and Economics, Budapest, Hungary; Supervisors: Dunai L., Okura, I. (Osaka University).

Vigh, L.G., Dunai, L. (2004). "Finite element modelling and analysis of bolted joints of 3D tubular structures", *Computers and Structures*, Vol. 82, 2173-2187.

Vigh, L.G, Dunai, L., Kollár, L. (2006). "Numerical and design considerations of earthquake resistant design of two Danube bridges", *1st European Conference on Earthquake Engineering and Seismology*, Geneva, Switzerland, ID 1420 /1-10.

Yoshikawa, O., Sugiyama, I., Kurimoto, H., Aketa, H. (1993). "Construction of the Shinhamadera bridge", *Stahlbau*, Vol. 62, H. 5, S. 125-136.